MODELS FOR THE HYDROCRACKING OF FISCHER-TROPSCH DERIVED WAXES

PHILIP LE GRANGE

THESIS PRESENTED FOR THE DEGREE OF

MASTER OF SCIENCE

IN THE DEPARTMENT OF CHEMICAL ENGINEERING

UNIVERSITY OF CAPE TOWN

FEBRUARY 2009

ACKNOWLEDGEMENTS

Professor Möller, who has imparted such a wealth of knowledge and tirelessly committed himself to training his students, I have learnt so much from you.

Professor Thybaut and Dr Gisela Lozano at the University of Ghent, Belgium, for their hospitality and assistance during my stay there.

My colleagues (and friends) Michael, Jako, Ross for the assistance they gave me on this project and Mr Walter Böhringer for invaluable assistance on all things chemical.

Massive thanks to my family and friends for their continual support, to Joachim for being an excellent sounding board and Monika in Ghent for her inspiration.

To my sponsors: The University of Cape Town, C*change DST Centre for Excellence in Catalysis, German Academic Exchange Service, Ernst and Ethel Eriksen Trust and the Max and Lillie Sonnenberg Trust whose support made this research possible.

"In all you ways acknowledge Him and He will make your paths straight"
Proverbs 3:6

DECLARATION

I know the meaning of plagiarism and declare that all of the work in this thesis, sae for that which is properly acknowledged is my own.

Signed: _____ Date:_____

SYNOPSIS

A process route for the production of synthetic fuels based on the reaction of a carbon source to wax (Fischer-Tropsch) followed by the sequential conversion of wax to fuels (Hydrocracking) is becoming increasingly significant. Central to this process route is the hydrocracking reaction system.

Hydrocracking models presented in current literature are either based on fundamental chemistry and contain too many parameters for practical industrial application or are empirical in nature and should not be used outside the specific system and conditions for which they were derived, making them of limited use for design and optimisation. The need therefore exists for models based on fundamental principals which can be extrapolated yet with few enough parameters for them to be feasibly implemented.

Accolla (2006) developed the first true 'hybrid' model that meets these criteria (Model- A). This study continues the development of this model (Model-B) with significant changes being made to the phase equilibrium calculations and kinetics. The study also develops a second generation model (Model-C) that includes the isomers species, which are required for estimation of the product fuel quality.

On regression against data from literature both models B and C were able to accurately predict middle distillate yield and selectivity. Model-C was also able to provide a good approximation of the product carbon number and iso to normal paraffin ratio for the hydrocracking of several different feedstocks. It was demonstrated with Model-C that limited isomer data led the parameters to converge to incorrect values. Based on this and the number of parameters, Model-B is recommended for industrial application.

The Models have the potential to be a powerful tool in the design, optimisation and control of hydrocracking systems and could significantly increase the profitability of the process.

CONTENTS

LIST OF FIGURES

LIST OF TABLES

NOMENCLATURE

α	-	Anderson-Schulz-Flory chain growth probability
q_i	-	Loading of species i
$q_{i,sat}$	-	Saturation loading of species i
K_i	-	Seperation factor for species i
f_i	-	Fugacity of Species i
ψ	-	Vapour fraction (Rachford-Rice equation)
z_i	-	Total Species Mole Fraction (over both liquid and vapour phases)
T_r	-	Reduced Temperature
ω	-	Accentric Factor
T_C	-	Critical Temperature
P_C	-	Critical Pressure
P_{vap}	-	Vapour pressure
r_j	-	Reaction rate of species j
P	-	Pressure
P_0	-	Saturation Pressure
P_{sat}	-	Saturation Pressure
σ	-	Surface Tension
V_M	-	Liquid Molar Volume
k_A	-	Rate Constant of Type-A β-scission
k_{B1}	-	Rate Constant of Type-B1 β-scission
k_{B2}	-	Rate Constant of Type-B2 β-scission
k_C	-	Rate Constant of Type-C β-scission
C_i	-	Concentration of species i
b_{ij}	-	Peng-Robinson Equation binary interaction parameter
$C_{surface,i}$	-	Concentration of species i on the catalyst surface
$C_{bulk,i}$	-	Concentration of species i in the bulk phase
C_{max}	-	Maximum Carbon Number in Feed
m_i	-	Number of Paraffin Species in a Lump
ς_i	-	Global Symmetry Number
R	-	Universal Gas Constant (8.314..)
CN_i	-	Carbon Number of Species i

GLOSSARY

FTS	-	Fischer-Tropsch Synthesis
VLE	-	Vapour Liquid Equilibrium
CPCP	-	Corner Protonated Cyclo-Propane
CPCB	-	Corner Protonated Cyclo-Butane
CPCPe	-	Corner Protonated Cyclo-Pentane
VGO	-	Vacuum Gas Oil
SMDS	-	Shell Middle Distillate Synthesis
SEKM	-	Single Event Kinetic Model
PREOS	-	Peng-Robinson Equation of State
WHSV	-	Weight Hourly Space Velocity

1. INTRODUCTION

1.1. PREAMBLE

There is currently a growth in the global demand for high quality and environmentally friendly diesel fuels. These fuels are technically challenging to produce from traditional crude oil feedstocks and will become even more so with increasingly stringent environmental legislation and the depletion of many of the sources of high quality crude oil.

Synthetic fuels produced from alternative carbon sources via the Fischer-Tropsch Synthesis (FTS) process are seen as a viable solution to this problem. In addition to being a proven technology the versatility in the choice of feedstock for FTS has major strategic value with the ability to use a range of carbon sources making it possible for a country to produce fuels independently of other nations.

The FTS process, however, produces low diesel yields (30 to 40 percent by weight) even when run under optimal diesel production conditions. However, an alternative process is made possible by the linear and pure (free of nitrogen, oxygen, sulphur and metal impurities) nature of the FTS hydrocarbon product. This process route, in which the FTS reaction is followed by a hydrocracking reaction, has approximately double the diesel yield of direct FTS (Sie et al., 1991).

This project aims to develop fundamental engineering models of the hydrocracking process. These models will be regressed against literature data to determine if they provide a satisfactory description of the process. The tools this project develops could be extremely valuable in the design and optimisation of hydrocracking processes. Additionally models could be used to determine kinetic parameters of this complex process from experimental data. There is the potential for application in the model predictive control of industrial hydrocracking reactors and in the training of plant operators.

1.2. BACKGROUND

Hydrocracking is a process whereby long carbon chain length hydrocarbons are 'cracked' via a complex kinetic pathway down to lower carbon chain length hydrocarbons. In a traditional petrochemical refinery hydrocracking is used to convert heavy products (e.g. heavy gas-oil) from distillation into lighter more useful products such as diesel and kerosene. This technology is well developed for the processing of regular, impure, refinery streams.

In recent years however, wax hydrocracking has gained significant attention as an alternative FTS process route. Direct FTS has a low diesel yield (middle distillates in figure 1.1) even when run under optimal diesel production conditions. A more selective process route to diesel production is to run the FTS process till a high conversion to wax is obtained ($\alpha \approx 0.95$, where α is the chain growth probability and is dependant on operating conditions; Anderson, 1984) and then hydrocrack the wax to diesel.

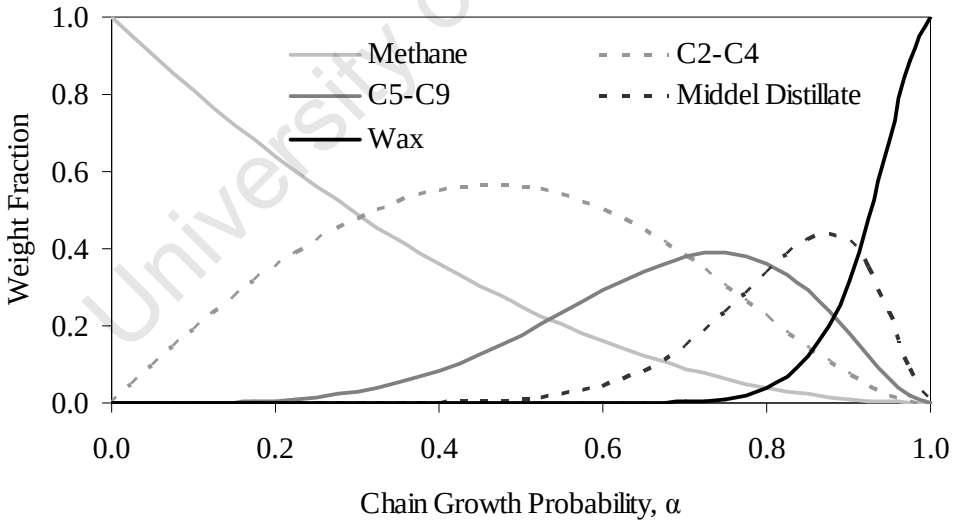

Figure 1.1: FTS Selectivity to Various Hydrocarbon Products vs. the Chain Growth Probability

Hydrocracking is the ideal technology to meet the increasing global demand for high quality and, in conjunction with natural gas based FTS, environmentally friendly

diesel. It produces fuels with a cetane number in excess of 70 (Sie et al., 1991; Leckel, 2005; Leckel et al., 2006) which is a significant improvement on current technology which typically produces diesel with a cetane number of 40 to 50. This is a result of the highly linear nature and the absence of aromatics in the FTS wax feedstock. (Scherzer & Gruia 1999)

Fuels derived from the FTS-Hydrocracking Process are essentially free of aromatic, sulphur and nitrogen impurities leading to significantly 'cleaner' combustion with these fuels. Studies by Basak et al. (2004) indicate that the saturated, aromatic free nature of the fuel allows for better combustion, thus lowering emission of NO_x and CO. The fuel is virtually free of SO_x emissions (Sie et al. 1991).

The above mentioned transportation fuel pollutants are becoming more and more stringently legislated (DieselNet Website). Hydrocracking is clearly the more efficient way of meeting legal requirements and is in stark contrast to the diesel refined from crude oil which contains large amounts of the polluting heteroatoms highlighted above, requiring extensive further processing to meet environmental specifications.

FTS as a process route (GTL, CTL, BTL) is growing globally (Table 1.1) and it is expected that as a result FTS Wax Hydrocracking will also grow industrially as a process.

Table 1.1: Proposed and New FT Plants (Adapted from Catalysis Review, Dec. 2002)

Operator	**Location**	**Capacity (10^3) Tpa**	**Planned Start Up**
SASOL/CHEVRON	Nigeria	1320	Under Construction
SASOL/QPC	Qatar	1360	Online
SHELL/PERTIMINA	Indonesia	3000	-
SHELL/EGPC	Egypt	3000	-
SHELL/NIOC	Iran	3000	-
SHELL	Qatar	Equivalent of 140000bpd	Under Construction
SHELL	Trinidad	3000	-
	TOTAL	**18680**	

SHELL has been operating a hydrocracking plant producing diesel from FT-Wax in Malaysia since 1993. SASOL and PetroSA currently operate large hydrocracking pilot plants (at Sasolburg and Mossel Bay respectively) using natural gas based FT Wax as feedstock. Additionally as a part of a joint venture between SASOL and CHEVRON a refinery based on this configuration has recently come online in Qatar and a further plant of this type is under construction in Nigeria. As a result of the large amount of development happening in this area hydrocracking technology is rapidly gaining importance internationally.

The first stage of a process Model (Model A) has already been developed (Accolla, 2006). In order to propose optimal hydrocracking conditions however, it is necessary to develop a more rigorous hydrocracking process model capable of predicting fuel properties and the unusual reactivity's observed in literature (Leckel 2005, Leckel et al., 2006).

1.3. SCOPE OF RESEARCH

It is ultimately the aim of this research to create a hydrocracking process model that is both accurate and capable of predicting the fuel quality (measured by the cetane number and cold flow properties). The latter would be of particular value in performing economic assessments.

There are a number of crucial issues that need to be addressed and extensions to model A that need to be made in order to achieve the above. The primary area to be addressed will be the reaction kinetics. These are important for the following reasons:

1. In small pore catalysts type-A β-scission is thought to be inhibited by steric constraints (see section 2.2.1). In these catalysts types B1, B2 & C β-scission, which are approximately 1000 times slower than type A, are assumed to be kinetically limiting by Model-A. However, in larger pore catalysts type-A β-scission is not inhibited and isomerisation, which is slower than type A β-scission, will be kinetically significant (see table 2.1 and Brouwer, 1980 and Martens et al., 1986). Taking isomerisation into account could significantly improve the accuracy

of the current model for large pore catalysts. It is also essential to include isomerisation into the model kinetics as knowledge of the hydrocarbons' molecular structure allows for prediction of fuel properties.

2. The rate expressions in Model-A have a direct dependence on hydrogen partial pressure rather than the inverse dependence, from the dehydrogenation equilibrium, that the single events models have (Baltanas et al., 1989). Thus Model-A predicts the converse effect of varying the hydrogen partial pressure to that found in literature (Martens & Marin, 2001). Additionally the olefin to paraffin equilibrium ratio varies with carbon number. As such, incorporating the equilibrium between the olefins and paraffin's may play a important role in accurate prediction of the product distribution.

3. The Vapor Liquid Equilibrium (VLE) plays a central role in determining the selectivity of the hydrocracking process (Accolla, 2006). Thus accurate prediction of the vapour liquid equilibrium is vital. The Peng-Robinson equation of state (Peng and Robinson, 1976) currently used was derived using hydrocarbons with less than 10 carbon atoms and may not extrapolate well to heavy paraffinic waxes and a new approach to the VLE is required.

From the above points it is clear that extending the current kinetic scheme to include isomerisation, olefin to paraffin equilibria (including correcting the kinetic dependence on hydrogen) and accurate prediction of the VLE should improve on the accuracy of Model-A and provide a model with greater product information.

The purpose of this thesis is to mathematically model the kinetics based on fundamental theory. The resulting model will be tested by comparison to industrial type hydrocracking data (Leckel, 2005; Leckel et al., 2006; Pellegrini et al., 2008 and Sie et al., 1991).

2. LITERATURE REVIEW

2.1. CHEMISTRY OF N-ALKANE HYDROCRACKING

The hydrocracking and hydroisomerisation of an alkane using a heterogeneous bifunctional catalyst is mechanistically described by a 6 step process:

1) Dehydrogenation (alkane to olefin)
2) Protonation (olefin to carbenium ion)
3) Isomerisation
    3a) rearrangement
    3b) branching
4) Hydrocracking/β-scission (hydrocarbon 'cracked' into shorter chain hydrocarbons)
5) De-protonation (carbenium ion to olefin)
6) Hydrogenation (olefin to alkane)

The above was first formulated by Weis (1962) and Coonradt & Garwood (1964) and is generally accepted in the field (Weitkamp, 1975; Weitkamp et al., 1983; Martens et al., 1986; Scherzer & Gruia, 1996; Martens & Jacobs, 2001). This reaction scheme is depicted in figure 2.1.

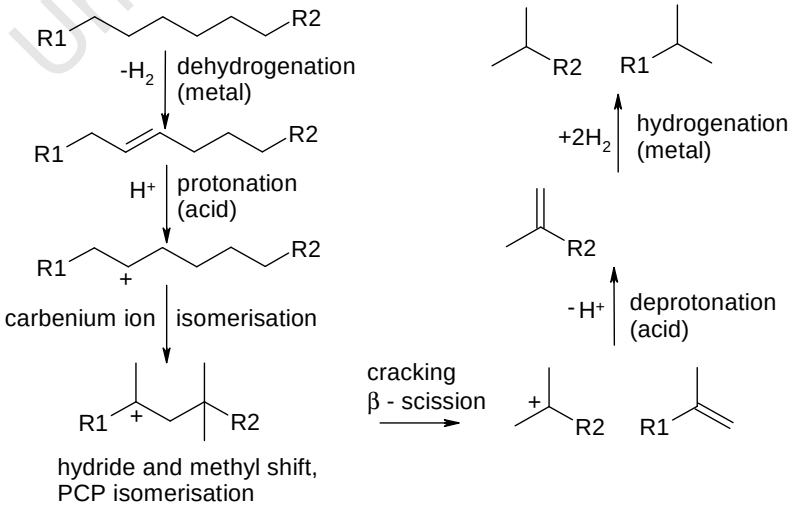

Figure 2.1: Hydrocracking Reaction Scheme

Overall reaction: $C_nH_{2n+2} + H_2 \rightarrow C_iH_{2i+2} + C_jH_{2j+2}$, where $i + j = n$ (2.1)

2.1.1 (De)Hydrogenation and (De)Protonation

Hydrogenation and dehydrogenation take place on the metal sites of the bifunctional catalyst, while protonation/deprotonation takes place on Brønsted acid sites (Maxwell, 1983). For 'ideal' bifunctional catalysts (section 2.2.3) these steps are typically assumed to be in quasi-equilibrium (Martens & Marin, 2003). This is a result of the rapid rates of these reactions which is inferred from the low quantities (non measurable actually) of alkenes and carbenium ions in comparison to the saturated species (Guillaume et al., 2003). Though direct evidence for carbenium ion intermediates is lacking their presence is logically deduced based on the type of products that result from cracking and rearrangement which follow the rules of carbenium ion chemistry (Pines, 1981; Wojciechowski et al., 1986).

2.1.2 Isomerisation

Isomerisation (also referred to as hydroisomerisation) occurs on acid catalyst sites and is divided into two mechanisms (shown in figure 2.2), type-A and type-B. The type-A mechanism results in the rearrangement of a molecule's structure via shifting of a side chains position. Type-B mechanism on the other hand does this by changing the number of side chain branches and degree of branching of these chains.

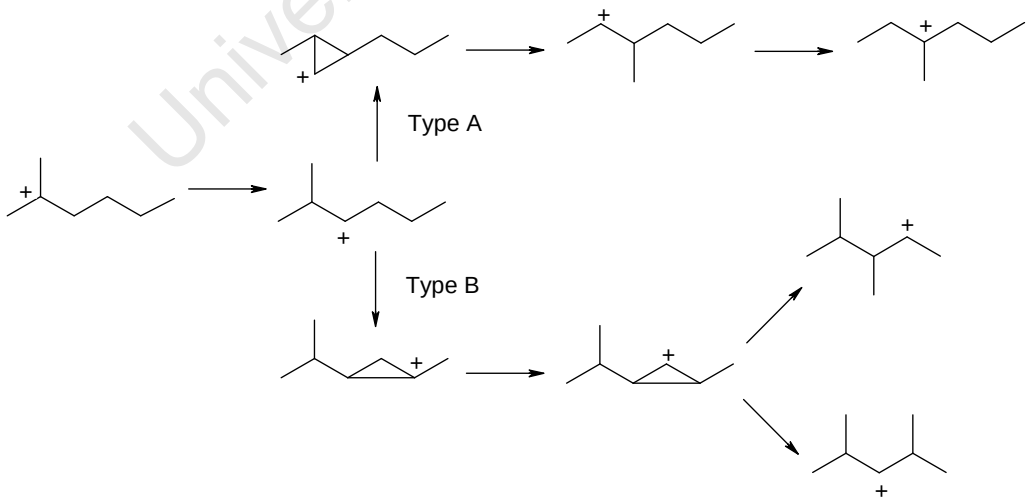

Figure 2.2: Hydroisomerisation via Protonated Cyclo-Propane

Both types A and B proceed via protonated cycloalkanes. Type-B however proceeds via a corner to corner migration of hydrogen in the cycloalkane intermediate as opposed to the 1,2 hydride shift followed by the type A mechanism (Martens & Jacobs, 1990).

Martens & Jacobs (1990) demonstrate that type-B isomerisation will always be slower than type-A (2 orders of magnitude at 400K) as the corner to corner proton jump required by type B isomerisation proceeds over a higher energy barrier.

It is generally accepted that branching isomerisation occurs sequentially on long chain n-alkanes in a series of consecutive reactions. A mono-branched isomer is reacted to form a di-branched isomer (with parallel branching) which in turn is reacted to form a tri-branched isomer and so on. This has been observed experimentally (Weitkamp, 1975; Steijns et al., 1981; Weitkamp, 1982; Vansina et al., 1983). Higher levels of branching than tri- are not observed in hydrocracking systems due to the high rate of type-A β-scission which causes tri-branched isomers to react before they can branch further (section 2.2.1 and table 2.1).

Table 2.1: Relative Rates of Decane Conversion over Pt/USY (negligible steric hindrance) Zeolite Catalyst (Martens & Jacobs, 2001)

Reaction	Relative Rate
Type-A β-scission	1050
Type-B1 β-scission	2.8
Type-B2 β-scission	1
Type-C β-scission	0.4
PCP Branching	0.8
Methyl Shift	56

The bulk of branched isomers form methyl side chains, however, ethyl and propyl side chain branching is also observed. The branch size depends on the number of carbon atoms in the protonated cycloalkane ring intermediate (Martens & Jacobs, 1990). For methyl branches the mechanism proceeds via corner protonated cyclo-propane (CPCP), as seen in figure 2.2, while ethyl branches form from a corner protonated cyclo-butane (CPCB) and propyl branches from a corner protonated cyclo-pentane (CPCPe).

The rates of branching and branch rearrangement decrease with the size of the protonated ring intermediate. The relative rates of branching were found to be independent of the chain length of the alkane under consideration with $r_{CPCP}:r_{CPCB}:r_{CPCPe}$ = 100:25:5 (Martens & Jacobs, 1990) highlighting the lack of importance of mechanisms based on protonated cycloalkane ring intermediates larger than cyclo-butane. Other mechanisms have been suggested (e.g. Lee, 1978) however the above are generally accepted as appropriate.

2.1.3 Cracking

Hydrocracking proceeds via a mechanism known as β-scission. In β-scission the carbon-carbon bond in the β-position from the carbon atom carrying the positive charge is broken, effectively 'cracking' the molecule in two. There are 5 types of β-scission: A, B1, B2, C & D (see figures 2.3a to 2.3e). These are distinguished by the number and position of side chains in the reactant and product (Table 2.2).

Type-A hydrocracking is significantly faster than types B1, B2 & C which in turn are significantly faster than type D. This is a result of the relative stabilities of the alkylcarbenium ion intermediates which decreases in the order:

Tertiary>Secondary>Primary

This explains the relative reactivaties (table 2.1) of different hydrocracking mechanisms, as those with more stable intermediates are energetically favoured.

Table 2.2 Distinctions between β-Scission Types (Martens & Jacobs, 1990)

β-Scission Mode	A	B1	B2	C	D
Minimum Carbon #	8	7	7	6	4
Feed Ion	Tertiary	Secondary	Tertiary	Secondary	Secondary
Product Ion	Tertiary	Tertiary	Secondary	Secondary	Primary
Minimum Branching	Tri-	Di-	Di-	Mono-	None
Branching Position	α, γ, γ	γ, γ	α, γ	γ	-
Product Branching	Alkyl + Methyl	Alkyl + Non	Methyl + Non	Non + Non	Non + Non

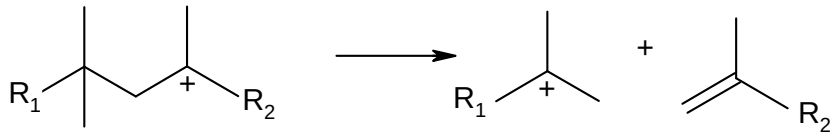

Figure 2.3a: Type-A β-scission (Tertiary to Tertiary Carbenium Carbocation)

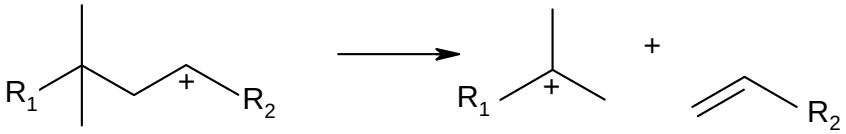

Figure 2.3b: Type-B1 β-scission (Secondary to Tertiary Carbenium Carbocation)

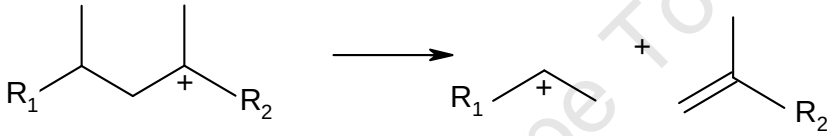

Figure 2.3c: Type-B2 β-scission (Tertiary to Secondary Carbenium Carbocation)

Figure 2.3d: Type-C β-scission (Secondary to Secondary Carbenium Carbocation)

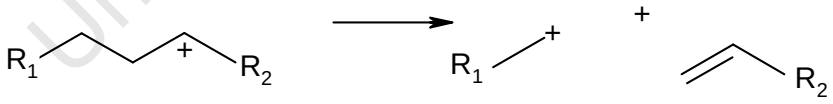

Figure 2.3e: Type-D β-scission (Secondary to Primary Carbenium Carbocation)

2.2. HYDROCRACKING

2.2.1 Catalyst Class

Zeolites (crystalline aluminosilicates) such as ZSM-5 and Zeolite Y are commonly used as hydrocracking catalysts in preference to their amorphous counterparts for the following reasons (Scherzer & Gruia, 1996):

1. Higher thermal stability
2. Lower coking tendency
3. Stronger resistance to catalyst poisons
4. Easier to regenerate
5. Greater cracking and isomerisation activity due to higher acidity (quantified in both strength and number of acid sites)

They also exhibit ion exchange, sorption and molecular sieve properties (Weitkamp et al., 1983; Scherzer & Gruia, 1996).

In medium pore catalysts (e.g. ZSM-5) type-A β-scission is inhibited by steric constraints (Weitkamp et al., 1983). Essentially the catalyst's pores are not large enough to contain the tri-branched isomers that are the reactants for type-A β-scission. In these catalysts types B&C β-scission, which are several orders of magnitude slower than type-A, are assumed to be limiting (Model-A). However, in larger pore catalysts (e.g. zeolite Y) type-A β-scission dominates under most conditions and in this situation branching isomerisation is slower than β-scission (Martens et al., 1986; Brouwer, 1980).

The product of single phase hydrocracking kinetics at a constant space velocity is primarily dependent on reaction temperature and the relationship between the acid site reactions and the metal site hydrogenation and dehydrogenation activity (Coonradt and Garwood, 1964).

2.2.2 Effect of Temperature on Catalyst Class

The effect of temperature on hydrocracking is strongly dependent on the type of catalyst used. Due to their higher acidity zeolite catalysts require a lower temperature to achieve the same conversion of feed as their amorphous counterparts. However it has been found that at higher temperatures the amorphous catalysts have a greater selectivity towards diesel than their zeolite counterparts (Scherzer & Gruia, 1996).

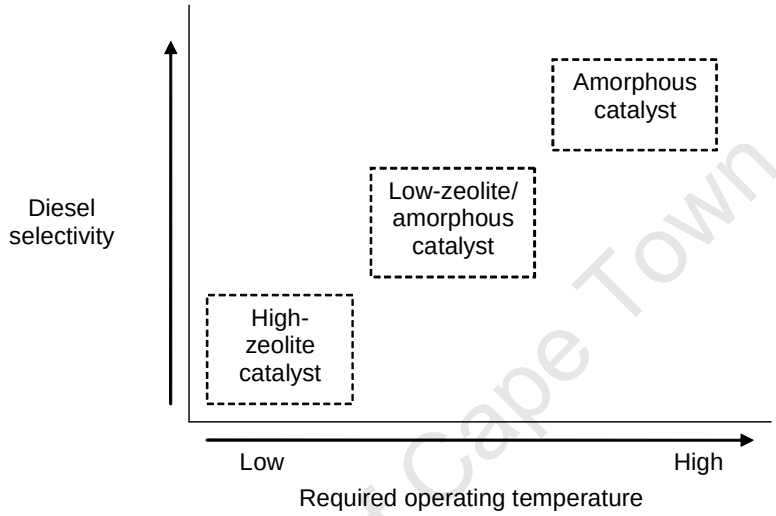

Figure 2.4a: Catalyst Class - Temperature vs. Diesel Selectivity, where High- and Low- denote the level of zeolite acidity (Scherzer & Gruia, 1996)

The selectivity in figure 2.4a was obtained at a constant conversion. Scherzer and Gruia (1996) report that for the hydrocracking of a light Arabian vacuum gas oil (VGO) the zeolites produce a superior quality fuel to that of an amorphous catalyst in terms of cetane number and pour point. This is due to the higher hydrogen consumption of the reaction as a result of the zeolite catalyst, leading to a more hydrogenated product. As VGO contains a larger percentage of non-linear hydrocarbons (aromatics etc) it is uncertain whether this result is applicable to the predominantly linear FTS waxes.

Schulz and Weitkamp (1972) published more specific data on the reaction temperature dependence of different catalyst types, see figure 2.4b. This figure clearly demonstrates the higher reaction temperatures of amorphous catalysts in comparison to their zeolite counterparts. However, the zeolite data in figure 2.4b was determined

from the cracking of n-dodecane while that for the amorphous catalysts was obtained from n-hexadecane. While the temperature range over which a catalyst is active for hydrocracking is in all likelihood similar for both compounds it does make the prediction of qualitative trends impossible.

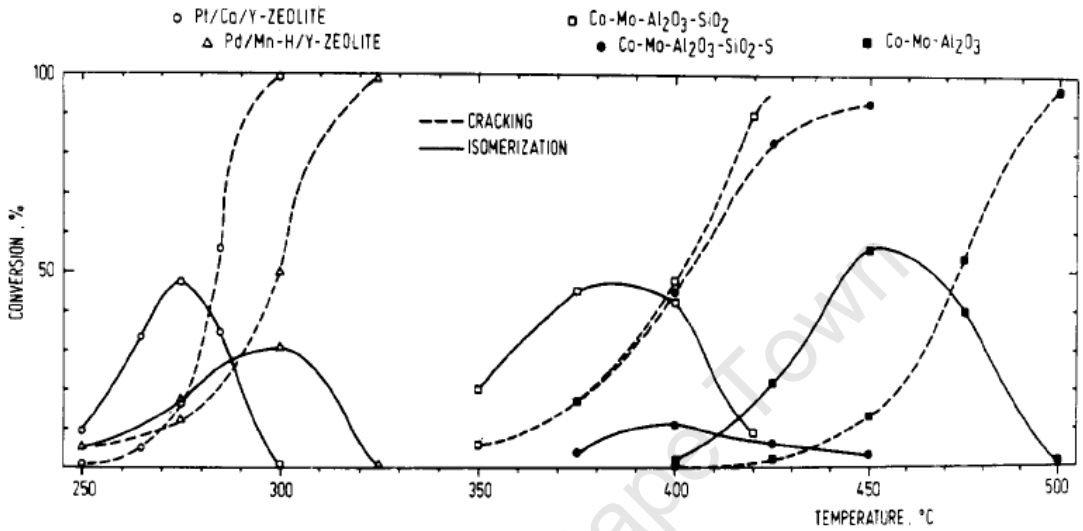

Figure 2.4b: Hydroconversion dependence on reaction temperature for different bifunctional catalysts (Schulz & Weitkamp, 1972)

2.2.3 Bifunctional Catalysts & Ideal Hydrocracking

Bifunctional catalysts are acid catalysts onto which a metal phase is deposited. The metal serves to catalyse hydrogenation/dehydrogenation reactions. It is evident that hydrocracking requires a bifunctional catalyst (see table 2.3 for typical acid and metal functions).

In most industrial hydrocracking bifunctional catalysts the metal sites have a higher activity to that of its acid sites. This lends itself to the classical hydrocracking mechanism often referred to as ideal hydrocracking. In ideal hydrocracking the hydrogenation/ dehydrogenation steps are taken to be in equilibrium with the rate determining steps being the acid surface reactions. The bifunctional reaction mechanism shown in figure 2.1 is favoured by this type of catalyst (Weitkamp et al., 1978; Martens & Jacobs, 1990; Guillaume et al., 2003).

Table 2.3: Bifunctional hydrocracking catalysts (adapted from Martens, 2000)

	Hydrogenation function	Acidic function (support)	
Increasing hydrogenation activity ↓	Ni/Mo	Al_2O_3	↓ Increasing acidity
	Ni/W	Al_2O_3/halogen	
	Pt/Pd	SiO_2/Al_2O_3 (e.g. zeolites)	

This is obviously not the case for nonideal hydrocracking. Nonideal hydrocracking is favoured under conditions of high temperature and low pressure. It has also been found to become more pronounced at long carbon chain lengths (Debrabandere & Froment, 1997; Thybaut et al., 2005). Thybaut et al. (2005) report that for the hydrocracking of octane on 0.5%Pt loaded USY zeolite the activation energy of dehydrogenation (60kJ/mol) is half that of cracking and isomerisation (120kJ/mol and 118 kJ/mol respectively).

There are essentially two types of nonideal behaviour. The first is where the metal function activity is greater than the acid function activity. In this instance metallic hydroconversion mechanisms will compete with, or dominate over, the ideal hydrocracking reaction mechanism. Conversely the second type of non-ideal behaviour is where the metal function is much weaker than the acid function. In this case we can no longer assume that the hydrogenation/dehydrogenation reactions are in equilibrium and need to treat them as potentially limiting reactions.

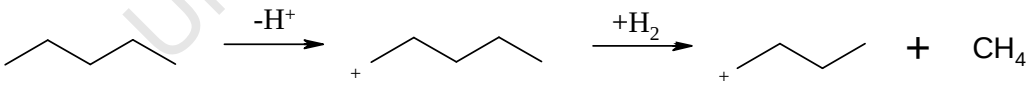

Figure 2.5: Reaction pathways for hydrogenolytic demethylation (adapted from Bohringer et al., 2007)

Bohringer et al. (2007) report on reaction mechanisms that may be competitive with hydrocracking at certain reaction conditions. Of particular interest is the mechanism of successive hydrogenolic demethylation which produces the methane which is not a possible product of the classical hydrocracking mechanism but is however present in the product of FTS wax hydrocracking (Leckel, 2005; Pellegrini et al., 2008).

2.2.4: Effect of the Metal Function

An advantage of the metal function is that it allows operation at approximately 100K lower than would normally be necessary in an acid zeolite. However, significant amounts of hydrogen are required in the feed in order to ensure high selectivity and good time on stream of the metal function. As a result of these factors, the choice of metal function can have a large impact on the process economics.

A high hydrogenation/dehydrogenation activity is desired for the metal function. Scherzer & Gruia (1996) state that this activity decreases in the order:

Noble Metal> Sulphided Transitional Metal >>Sulphided Nobel Metals

Non-noble transition metal functions in sulphided form are used when feedstocks contain high concentrations of sulphur as they have a higher resistance to the sulphur poisoning that rapidly deactivates noble metal functions.

2.2.5: Effect of the Acid Function in Zeolites

The acidity of a zeolite catalyst depends on the number and strength of catalyst acid sites which are determined by the SiO_2/Al_2O_3 ratio of the catalyst framework (Martens & Jacobs, 1997).

Rastelli et al. (1982) demonstrate that at low Al/(Al+Si) ratios (high SiO_2/Al_2O_3 ratios) the acid sites posses a high individual acidity, however, there are few of them, which leads to a low overall catalyst acidity. The converse was found to be true at high Al/(Al+Si) ratios (low SiO_2/Al_2O_3 ratios) where there are many weak acid sites, also leading to a low catalyst acidity. Data from Rastelli et al. (1982) indicates that the overall catalyst acidity reaches a maximum at a Al/(Al+Si) ratio of 0.1 (see figure 2.6).

Park and Ihm (2000) related the zeolite acidity to the activity of the bifunctional catalyst in the hydrocracking and hydroisomerisation of hexadecane, confirming the effect deduced by Rastelli et al. (1982).

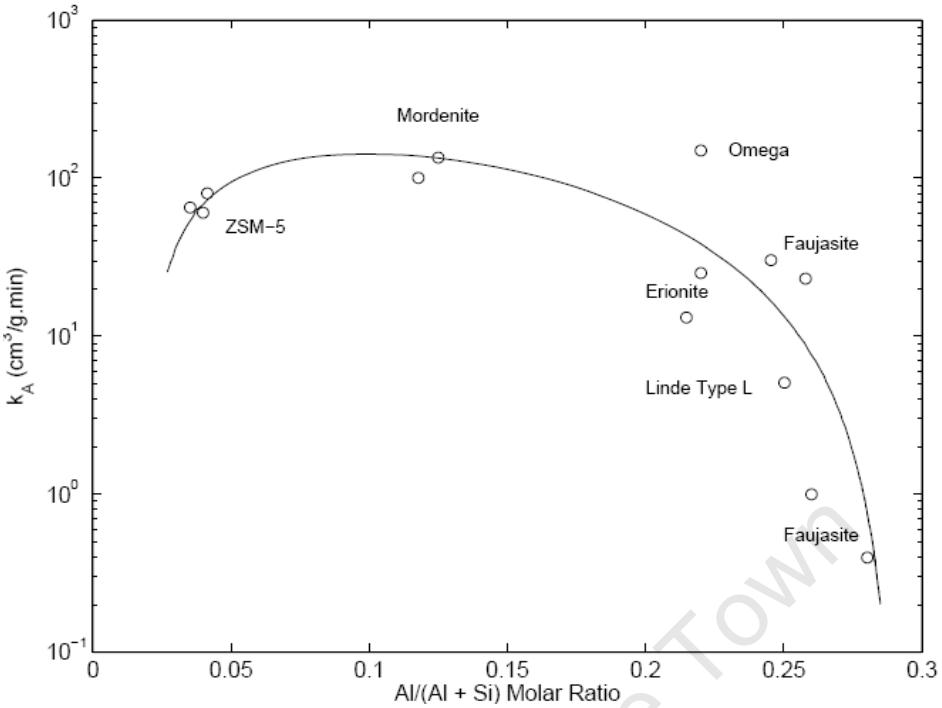

Figure 2.6: Cracking of n-butane, pseudo 1st order rate constant vs. zeolite aluminium content (adapted by Kukard, 2009 from data of Rastelli et al., 1982)

2.3. PROCESS ROUTES

Hydrocrackers are traditionally fixed bed reactors configured in trickle bed mode (Scherzer & Gruia, 1996). This is thought to be the case in the majority of modern industrial FTS hydrocracking configurations however this is only based on the one source available in open literature Sie et al. (1991) which talks about the Shell Middle Distillate Synthesis (SMDS) process. The fact that virtually all of the lab and bench scale research results published by the large fuels companies pertain to trickle bed reactors is indicative that their industrial scale operations utilise this reactor type.

The SMDS process route is a modified FTS process that focuses on maximising the yield of middle distillates, specifically gas oil (diesel) and kerosene (basis of jet fuel), instead of gasoline (which is the traditional focus of FTS). This process consists of two main processing stages: the conversion of synthesis gas into wax via FTS and the subsequent hydrocracking of FTS wax into diesel.

The first stage is low temperature FTS with a high chain growth probability ($\alpha > 0.9$), so as to maximise the production of heavy hydrocarbons and limit the formation of light gas products. The second stage is the mild hydrocracking (300-350ºC, 30-50bar with a proprietary Shell catalyst) of the FTS product to diesel in the middle distillate range (C_{10} - C_{20}) in a trickle bed reactor. The heavy product from distillation is recycled back to the hydrocracking unit, figure 2.7a (Sie et al., 1991).

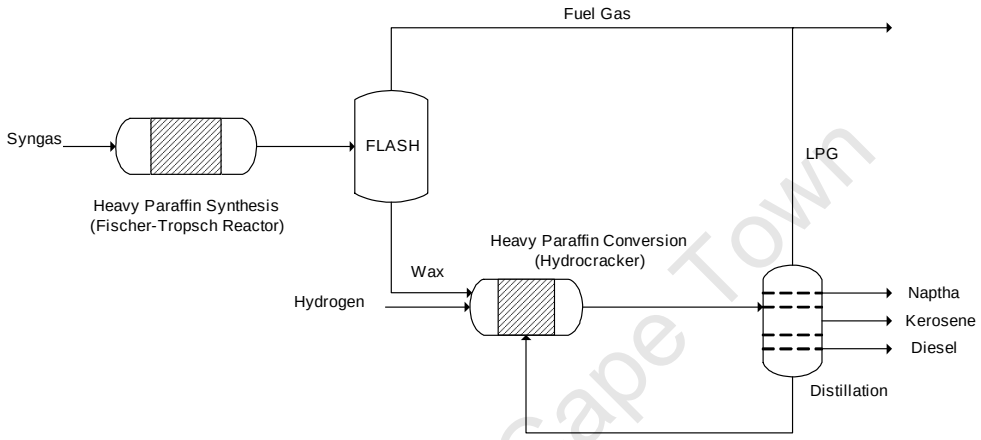

Figure 2.7a: Shell Middle Distillate Synthesis Process (Adapted from Sie et al., 1991)

Flexibility in the SMDS product is made possible by manipulation of the single pass conversion through the hydrocracker. This allows for a myriad of possible product compositions including the maximum gas oil mode and maximum kerosene mode depicted in figure 2.7b (Sie et al., 1991).

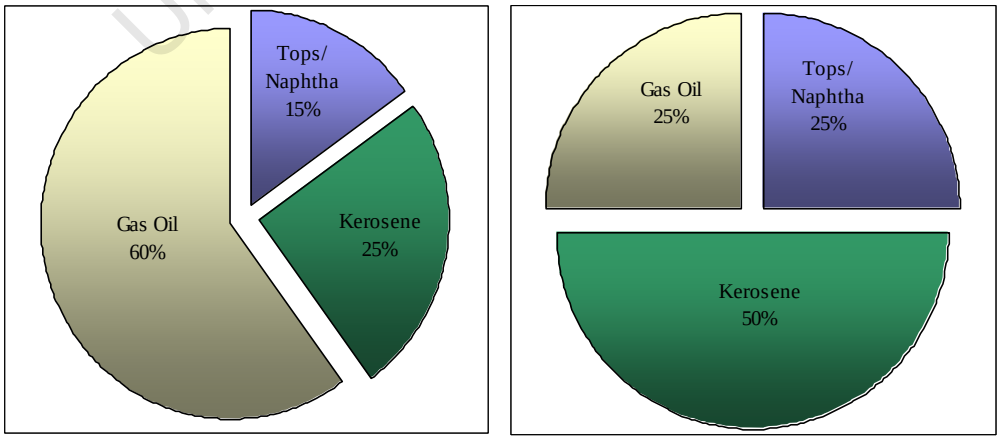

Figure 2.7b: Variation in Product Yield between Maximum Gas Oil & Kerosene Modes of Operation for SMDS Process (Adapted from Sie et al., 1991)

2.4. THE INFLUENCE OF VAPOUR-LIQUID EQUILIBRIUM

Work on the Shell Middle Distillate Synthesis (SMDS) process led Sie and co-workers (Sie et al., 1991) to conclude that dual phase behaviour in industrial hydrocrackers plays a crucial role in optimising the process. They found that under dual phase conditions heavier hydrocarbons would preferentially adsorb/condense in the catalyst pores. This is depicted as the degree of adsorption in figure 2.8.

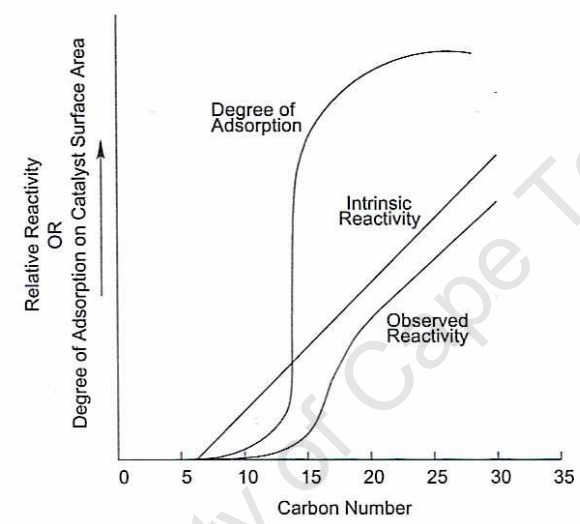

Figure 2.8: n-Paraffin Reactivity as a Function of Carbon Number (Sie et al., 1991)

Experimental work by Laxmi Narasimhan et al. (2006) demonstrates that there is no preferential adsorption of hydrocarbons from the liquid phase, figure 2.10. Thus the dual phase behaviour reported by Sie et al. (1991) is due to VLE between the gas and liquid phases rather than adsorption between the liquid and surface phase. As the two types of equilibria have similar effects it may be possible for one to mimic another.

The observed reactivity clearly differs from the intrinsic reactivity predicted by Archibald's heuristic rules (section 2.5.1). The important difference between the system studied by Sie et al. (1991) and that used by Archibald is the number of phases present in the system. Archibald's approach applies to single phase hydrocracking and fails to take into account the dual phase behaviour which causes the enhanced adsorption and residence time of heavier hydrocarbons ($>C_{16}$).

The dual phase behaviour is responsible for the S-shape in the observed reactivity and also explains the difference between the reactivity predicted by Archibald and that observed by Sie. Incidentally this behaviour explains the high selectivity towards a diesel product (C_{10} to C_{20}) displayed by the hydrocracking process, as middle distillates evaporate from the liquid phase before they can crack into lighter products.

The rapid increase in reactivities from C_{10} to C_{17}, shown in figure 2.9, reflects the both phase equilibrium and the number of active carbon centres. Constant gradients in the reactivity-temperature plots (figure 2.9) reveal a constant activation energy for the different hydrocarbons, which is indicative of a single kinetic step being rate limiting.

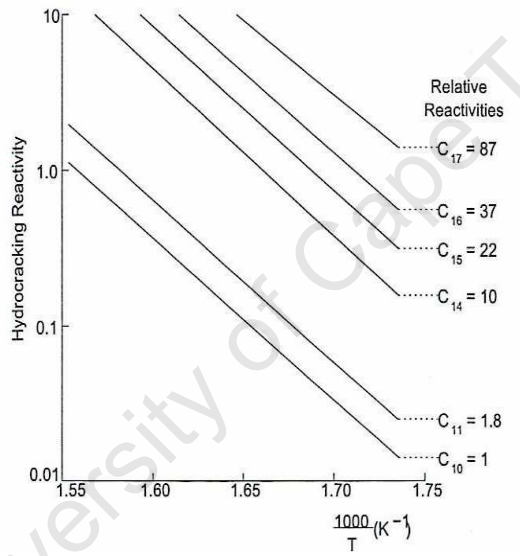

Figure 2.9: Reactivity different n-Paraffin's (Sie et al., 1991)

Thybaut et al. (2006) performed modelling and experiments on different stirred reactor systems in order to 'bridge the gap' between laboratory and industrial hydrocracking. They concluded that there was preferential conversion of the heavier hydrocarbons in both the liquid and vapour phases.

The liquid phase system used consisted of a liquid phase with gas bubbles dispersed through it. This is different from an industrial reactor in which a thin liquid layer flows over the catalyst particles in an otherwise gaseous system.

The degree of adsorption reported by Sie et al. (1991), Figure 2.8, is seen to increase rapidly in a spike at approximately $C_{14.}$ As all the hydrocarbon feeds used by Thybaut have a carbon number lower than this (parapur feed, C_9-C_{13}) it is possible that there could be a liquid phase adsorption effect which was not detected. Though the conclusions reached by Thybaut et al. are no doubt valid for their systems it is uncertain whether they can be generalised to industrial situations.

2.5. ALKANE HYDROCRACKING MODELS

There are five distinct types of models, namely:

1. Heuristic models (Archibald's Rules)
2. Discrete pseudo-component lumped models
3. Continuum lumping models
4. Single events kinetic models (based on Archibald's Rules)
5. Hybrid Models

2.5.1 Archibald's Rules

Archibald et al. (1960) were the first to propose a 'model' for hydrocracking. It consists of four fundamental rules that describe the process of hydrocracking:

1. The n-paraffin will react to form a secondary carbenium ion at any secondary carbon atom molecule.
2. Cracking will occur at the C-C bond in the β-position to the carbenium carbon atom, to yield an alkene and a smaller secondary or tertiary carbenium ion.
3. Alternate β –bonds in the carbenium ion will crack with equal probability as long as the resulting alkene cracked product is C_3 or larger in carbon number and the accompanying carbenium ion is C_4 or larger. It is important to note that the cracking of β –bonds to give C_3 or smaller carbenium ion fragments will not occur.
4. Carbenium ions from the initial cracking step have the possibility to crack further in the reaction network until they are reduced to C_7 fragments or smaller, yet it must occur in accordance with rule 3 above.

Based on rules 3 and 4 above it is predicted that the reactivity of a linear hydrocarbon will increase linearly with chain length from C_7 onwards (see the intrinsic reactivity in figure 2.8).

2.5.2 Discrete Pseudo-Component Lumping

These models divide the reaction mixture into discrete pseudo-components based on molar mass, boiling range or groupings of carbon numbers. The first true model of this type was developed by Stangeland (1974) and was evolved from the hydrocracking rules proposed by Archibald et al. (1960) (see section 2.5.1).

Stangeland proposed that the change in a particular lump would be entirely dependent on its own rate of cracking (depletion) and the contribution from the cracking of heavier components above it (formation). The driving force behind this model is thus a statistical approach in which 4 parameters are used to predict the hydrocracking yield.

The discrete lumping approach has been further developed and reworked (Krishna & Saxena, 1989; Mohanty et al., 1991) and is probably the most commonly used in industry. It has the drawback of requiring a large number of 'lumps' and thus rate constants in order to obtain resolution on the reaction network. Additionally the parameters for these types of models need to be recalculated for different feedstocks, due to compositional differences within the same lumps. Hence prediction of the products change in properties with change in feed cannot be determined without further experimentation (Basak et al., 2004).

2.5.3 Continuum Lumping

In this class of models, reaction mixtures are taken to be a continuum with respect to a certain property of the mixture. Laxmi Narasimham et al. (1996) took this to be the boiling point, with the system thus being quantified by a distillation curve which changes continuously as the reaction proceeds.

The chosen property is then related mathematically by a reactivity function to the reactivity of a compound of higher boiling point allowing for prediction of the hydrocracker product (Ancheyta et al., 2005). Basak et al. (2004) extended the model

of Laxmi Narasimham et al. (1996), dividing the reaction mixture into continuous mixtures of paraffinic, naphthenic and aromatic components, which required the definition of concentration, reactivity and species distribution functions for each continuous mixture as well as six product distribution functions (Ancheyta et al., 2005).

These models suffer from the same drawback as the discrete models in that the parameters vary with feedstock and hence need to be recalculated for different feeds. Basak et al. (2004) applied their model and reported improved plant performance in a number of cases. However, as their model requires 21 parameters which need to be estimated from experimental data this model could prove costly to apply and may not be scalable over the full range of operating parameters.

2.5.4 Single Events Kinetic Model

The single event kinetic model (SEKM) was developed in the mid 1980`s (Baltanas & Froment, 1985) and has been extensively developed during the last two decades. It is a structure oriented micro-kinetic model that is based on breaking up the reactions on the catalyst surface into smaller elementary steps.

In SEKM a reaction network is used to generate every possible carbocation intermediate. Each carbocation is represented by a matrix and a vector and reactions are simulated via matrix operations (Baltanas & Froment, 1985).

This approach has the advantage of being independent of the feedstock i.e. once the rates of the elementary steps have been determined further experimentation is unnecessary. However, there are a very large number of elementary steps; for instance the hydrocracking of n-nonadecane (C_{19}) yields: 1981 alkanes, 25 065 alkenes and 20 437 carbenium ions; with 25 065 dehydrogenations, 42 600 protonations 42 600 deprotonations, 15 970 PCP branchings and 6429 β-scissions.

It is apparent that determination of 178 486 rate constants (C_{19}) is impractical. In actual industrial feedstocks containing long chain paraffins of up to C_{120}, the number of reactions would in fact be infinitely greater as the number of possible intermediates increases exponentially with increasing chain length.

The number of rate constants can be significantly reduced if only the type of carbenium ion (primary, secondary & tertiary) is considered to be relevant to the reaction rate. This assumption neglects the impact of variations in the carbenium ions skeletal structure, with the exception of global symmetry, on the reaction rate (Martens & Marin, 2001).

The global symmetry and the molecules symmetry number are calculated from the third law of thermodynamics. When this is incorporated into transition state theory it allows the reaction rates to be written in terms of the number of elementary steps and the single event rate constant (Baltanas et al., 1989; Vynckier & Froment, 1991). This reduces the number of rate constants in the system, 24 for linear and cyclic paraffin's and 10 for a purely linear feedstock (Martins & Marin, 2001).

The following assumptions are inherent in the single event model (Martens, 2000):

1. Only secondary and tertiary carbenium ions are considered as intermediates.
2. The single-event rate coefficients are independent of the carbon number and structure of the carbenium ions involved.
3. The single-event rate coefficients for β-scission only depend on the type of the reactant and product ion and not on the olefin formed.
4. The single-event protonation rate coefficients depend only on the type of carbenium ion formed and are independent of the olefin being protonated.
5. The single event rate coefficients for deprotonation depend both on the type of deprotonated carbenium ion and on the olefin formed

Though through the above a feasible number of parameters are obtained, the reaction networks of SEKM models (in which the number of elementary reactions increases exponentially with carbon number) are far too extensive to be used in modelling the heavy hydrocarbons in industrial hydrocracking.

2.5.5 Hybrid Models

Schweitzer et al. (1999) made use of a judicious lumping scheme which combines the single events and discrete lumping approach in a hybrid type model. Species with the same carbon number and degree of branching are lumped together with the reactions between lumps described in terms of single event kinetic parameters. This lumping scheme largely prevents the variation in the composition of individual lumps and as a result the model parameters are independent of the feedstock used.

Use of this lumping scheme allows for the construction of industrial hydrocracking models with a reasonable number of reactions that do not need their parameters to be re-determined when the process feedstock is changed. As determining of the parameters requires experimental data, determining of parameters can be both expensive and time consuming.

The model posed by Schweitzer et al. (1999) however, makes use of Langmuir Adsorption to describe the interaction between the liquid phase and the catalyst surface and does not take into account the VLE. Work by Laxmi Narasimhan et al. (2006) demonstrates that the adsorption of hydrocarbons from the liquid phase is independent of carbon number (figure 2.10). In the work of Schweitzer et al. Langmuir Adsorption is in fact providing an approximation to the VLE which explains the successful results of this work in spite of the erroneous methodology.

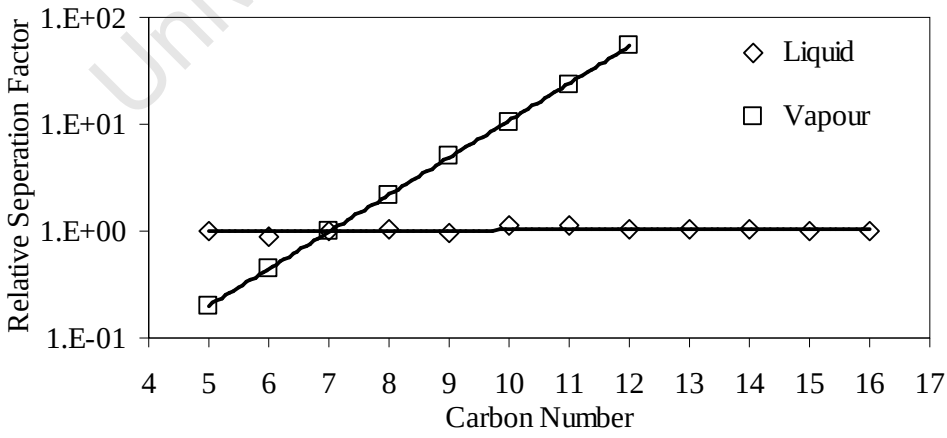

Figure 2.10: Alkane adsorption as a function of carbon number, with heptane as a reference compound (adapted from Laxmi Narasimhan et al., 2006)

Martens and Marin (2001) derived recursive formulas for the number of single events by examination of the evolution of the reaction network, incorporating SEMK into an industrial hydrocracking model that uses the same lumping scheme as Schweitzer (Schweitzer et al., 1999). They make the standard assumptions associated with ideal catalytic hydrocracking (see section 2.2.3) and use fugacities, calculated from the Peng-Robinson (1976) equation of state (PREOS), to transform the gas phase reaction rates and Henry constants estimated by Vynckier & Froment (1991) into constants and reaction rates for the liquid phase.

Martens model uses linear non-interacting mass transport approximations for the mass transfer between the gas and liquid phases. Linear approximations have the major drawback of not taking into account the 'drag' experienced, due to bulk flow through the gas and liquid films, by the molecules entering the liquid phase e.g. drag on H_2 entering the liquid phase from the $C_3 - C_6$ hydrocarbons exiting it. If hydrogen is in excess, as is mostly the case in hydrocracking, then this approximation is reasonable.

The Langmuir Adsorption isotherm (equation 2.2) is used for the adsorption of the molecules onto the catalysts surface. Generally q_{sat} is determined by the condition $q=q_{sat}$ when $P=P_{sat}$ however for supercritical species P_{sat} does not exist and the fluid remains compressible. Thus q_{sat} is variable and this equation is no longer applicable.

$$\textit{Langmuir Adsorption Isotherm: } \frac{q_i}{q_{i,sat}} = \frac{K_i . f_i}{1 + \sum K_j . f_j} \qquad (2.2)$$

Parameters for the model were obtained by regressing gas phase data for various short carbon-chain length compounds (octane, decane, dodecane, methyl-cyclohexane, ethyl-cyclohexane and n-butyl-cyclohexane). The parameters were then used to simulate a hypothetical VGO feed. The model results revealed that mass transfer played a relatively minor role, however as the simulations are not compared to real data it is uncertain if this finding is applicable to real systems. In spite of the above criticisms, it should be noted that the model of Martens and Marin (2001) is the most advanced of its type and one of the few which currently attempts to account for mass transfer in any way.

Pellegrini et al. (2008) have published a model that uses a species lumping scheme based on species carbon number and whether the species in question is a normal-paraffin or iso-paraffin. They use the Soave-Redlich-Kwong (SRK) equation, applying simplistic regressions based on short chain lengths ($<C_{12}$) to obtain isomer properties all the way up to C_{70}.

Additionally the VLE is not imbedded within the kinetics and is assumed to remain constant across integration steps. The model fails to treat the β-scission reactions correctly with cracking only being possible on the central carbon-carbon bond, neglecting the majority of the β-scission reactions. Thus C_9 can only be formed from the cracking of C_{17} to C_{19} and not C_{12} or any other hydrocarbons.

The model does not attempt to approximate the fundamental kinetics and fits the rates to a probability function which can not be extrapolated to other feedstocks on the same catalyst with any degree of certainty. Langmuir adsorption in used within the kinetics for both liquid and vapour phase reactions and the constants for this are also obtained as part of the model regression. Unfortunately the authors have failed to realise that adsorption does not vary with carbon number in the liquid phase (figure 2.10) and thus have obtained an unrealistic picture of the liquid phase adsorption. This in turn renders all other parameters obtained from regression incorrect and is possibly the reason they need to apply *"different multiplying factors"* (Pellegrini et al., 2008) to the vapour and liquid phases and obtain low accuracy at high conversions ($X > 0.7$).

It should be noted that both Martens and Marin (2001) and Pellegrini et al. (2008) make use of correlation based estimates for the binary interaction parameters in their equation of state. To the best of the author's knowledge correlations of this sort have never been derived using binary interaction parameters for hydrocarbons with a chain length of greater than twenty. It is doubtful that the use of these correlations would be valid for the heavy waxes used in hydrocracking, see section 3.4.

Model-A developed by Accolla (2006) takes a top down approach and combines a lumping scheme based on individual carbon numbers (isomerisation is not considered in this model) with a simple kinetic scheme based on β-scission being the rate limiting

step within the hydrocracking reaction mechanism. From this assumption about the kinetics the reaction rates are built up based on an equal possibility of cracking at any carbon-carbon bond that can undergo a specifc type of β-scission. Thus the more carbon-carbon bonds a species has the more reactive it is in the model kinetics and the model reaction rate varies linearly with the number of carbon-carbon bonds at which cracking can occur.

Vapour Liquid Equilibrium (VLE) for the system is calculated using PREOS which is embedded in the model kinetics. As a result of this hybrid approach, parameters for this model are independent of feedstock. Model-A is able to predict reactor size and product selectivity using only 2 rate constants (one for type-A β-scission and a pseudo-global rate for types B1, B2 and C).

While parameters are required to perform reactor sizing, the carbon number distribution is intrinsic and may be obtained without parameter estimation provided high resolution is not required in the $C_3 - C_7$ product range. The carbon number distribution of the product of the SMDS process was obtained in this way, figure 2.11.

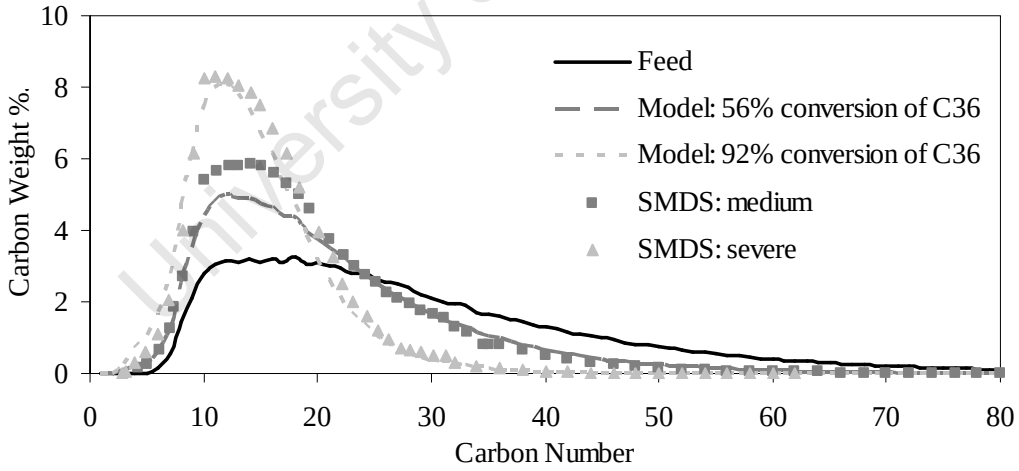

Figure 2.11: Model-A Prediction of the Product from the SMDS Process

It can be seen from figure 2.11 that a relatively good fit to the industrial data is obtained. There are however a number of limitations to this model:

1. It fails to predict the product from feedstocks below C_{20} accurately. This is probably due to an incomplete description of the system kinetics.
2. Does not incorporate isomerisation and therefore no indication of the product quality (cetane number, cold flow etc) can be obtained.
3. The non-ideal nature of the liquid mixture is not accounted for.
4. Mass Transfer between the phases is not accounted for.
5. The reaction is constrained to the VLE predicted liquid phase with gas phase reaction not being accounted for.
6. The non-ideal flow dynamics of the reactor are ignored with maldistribution of liquid within the reactor not been accounted for.

2.6. PROJECT GOALS

1. To investigate the effect of VLE on the system and apply a more robust equation of state than the PREOS. (Model-B)

2. To test the accuracy of Model-B in a rigours manner, using the industrial data from the SMDS process (Sie et al., 1991) as well as heavier, coal-based, FTS wax cracking data (Leckel, 2005; Leckel et al., 2006; Pellegrini et al., 2008).

3. From the results of testing Model-B make the required improvements to the model kinetics and distinguish between different degrees of species isomer branching within the model for the purposes of fuel quality prediction (Model-C).

4. Rigorously test Model-C against the same data mention in point two, including testing the models ability to predict the iso-paraffin/n-paraffin ratio in the product stream (data from Pellegrini et al., 2008).

5. Draw conclusions on models applicability in real industrial applications.

3. METHODOLOGY MODEL-B

3.1. ASSUMPTIONS

1. The reactor is isothermal and isobaric.

2. The adsorption selectivity of hydrocarbons from the liquid phase is unity (Laxmi Narasimhan et al., 2006) and thus the liquid and adsorbed reaction phase can be treated as one pseudo reaction phase, figure 3.1.

3. Ideal co-current trickle bed reactor system in which the catalyst always remains homogeneously wetted, i.e. all reaction occurs in the 'pseudo reactive' liquid phase and no reaction occurs over the catalyst in the gaseous state.

4. The vapour and liquid phases are in equilibrium, which is adequately described by the Twu, Coon and Cunningham (1995) modification of the Peng-Robinson equation.

5. No mass transfer limitations across the phase boundary or in the catalyst pores.

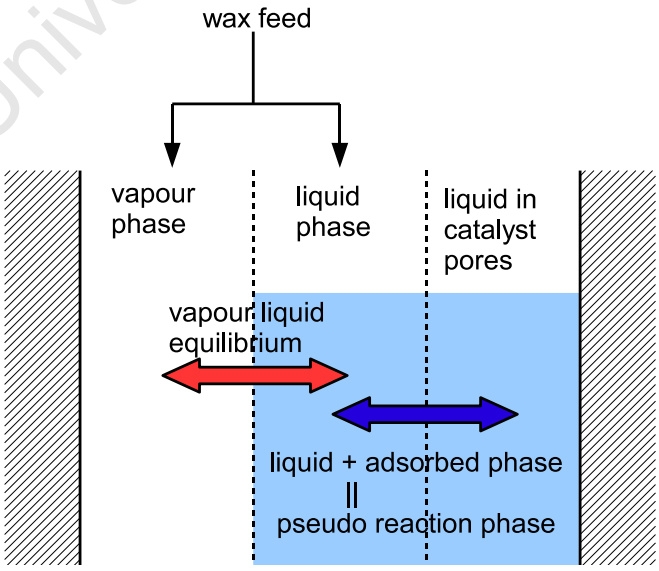

Figure 3.1: Model Hydrocracking Reactor

6. The β-scission (cracking) step in the hydrocracking mechanism is rate controlling.

7. Reactions are 1st order with respect to the liquid phase hydrocarbon concentrations and are inversely proportional to the liquid phase hydrogen concentration.

8. Linear increase in hydrocarbon cracking reactivity with carbon number.

3.2. ALGORITHM

The reactor model was integrated across both phases, where the concentrations in the kinetic rate expression were based on the liquid phase. Vapour and liquid flow rates were obtained via a flash mass balance. The algorithm can be seen in figure 3.2.

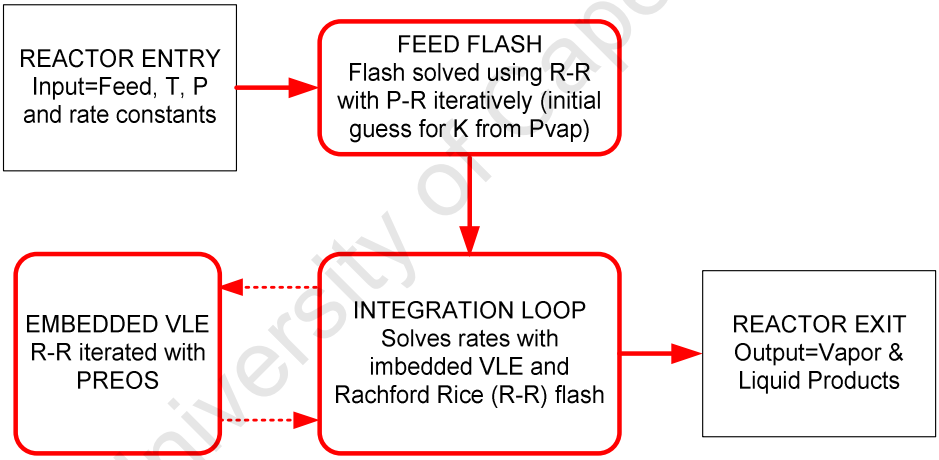

Figure 3.2: Model-B Algorithm

VLE calculation is embedded in the reactor integration and is evaluated with each call to the model. FORTRAN90 was used for the modelling. In all cases the model solved in under a minute on a modern computer. The LSODE integrator (Hindmarsh, 1983) was used for the reactor integration. The DFZERO routine (Dekker, 1969; Shampine & Watts, 1970) performed the Rachford-Rice flash calculations and RPOLY (Jenkins & Traub, 1970) was used to solve the cubic Peng-Robinson equations.

3.3. EQUATION OF STATE

Zabaloy and Vera (1998) have shown that the form of the Peng-Robinson Equation of State, originally proposed by Peng and Robinson (1976), is superior in terms of predictive capability to other equations of state of similar simplicity (specifically the Soave-Redlich-Kwong, Van der Waals and slightly more complex MCSV equations) for non-polar molecules.

Numerous modifications to the Peng-Robinson equation of state have been proposed. These are generally implemented through alterations to the attractive term which is described via the alpha function in the equation of state. Mostly this is done by replacing the 4^{th} order polynomial in accentricity describing the alpha function in the original Peng-Robinson Equation of State with a 6^{th} order polynomial, as proposed by Stryjek and Vera (1986). Polynomial equations do not extrapolate well beyond the data range from which they are regressed. As experimental data for species with high carbon numbers is unavailable, regressions will not be able to accurately describe these species properties.

Twu, Coon and Cunningham (1995) have developed an alpha function for the PREOS that is a linear function of the accentric factor. The advantage of this is clear in extrapolating data to heavy hydro-carbons. They demonstrated that this form of the alpha function showed significantly greater accuracy than that of Stryjek and Vera in predicting hydrocarbon vapour pressure from triple to critical point.

The alpha functions for the three different formulations are plotted at 600K for hydrocarbons in the range C_1 to C_{160} in figure 3.3. For light hydrocarbon species, with less than 30 carbon atoms, very little difference is observed between the different alpha function formulations. From figure 3.3 it is clear that Peng-Robinson in its original form should not be used for waxes as it reaches a maximum value at C_{70} and then decreases, which is qualitatively incorrect behaviour.

The Mathias et al. (1989) utilises the 6^{th} order polynomial (see figure 3.3) to extend the applicability of Peng-Robinsons equation to compounds with an accentricity of

greater than 0.5, including volume translation for accurate liquid phase density estimation applying the approach of Peneloux (1982). The equation is similar in form to that proposed by Stryjek and Vera (1986), however it does not make use of the additional three component specific parameters proposed by Stryjek and Vera which would need to be determined experimentally for each hydrocarbon.

At high carbon chain lengths the polynomial based value of this alpha function starts to increase exponentially. Qualitatively this also does not sensibly describe the attraction term and will cause problems at the very high carbon numbers that occur in extremely heavy waxes. The form proposed by Twu, Coon and Cunningham (1995) gives a qualitatively reasonable prediction of the attractive term.

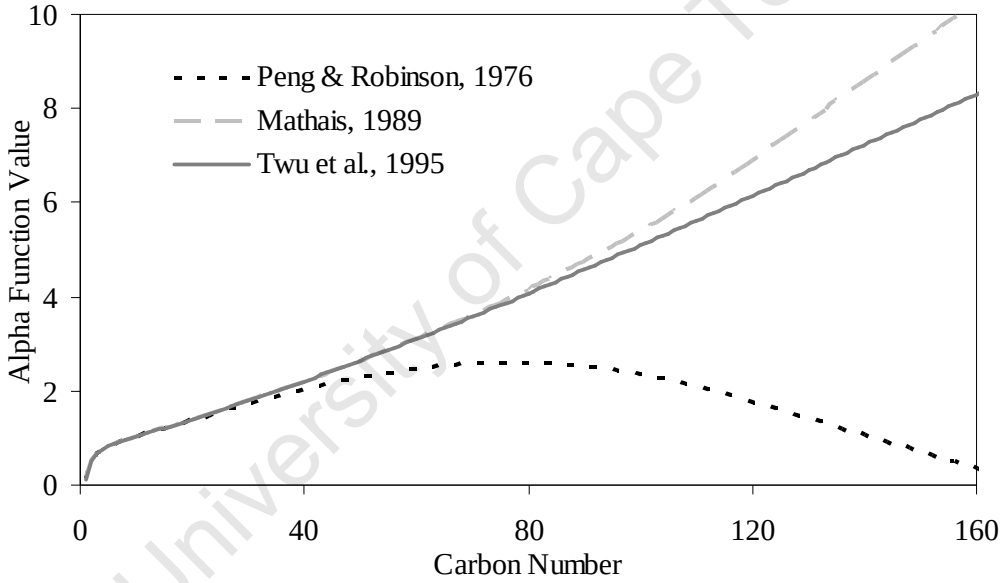

Figure 3.3: Alpha Function Value vs. Carbon Number

Twu, Coon and Cunningham have also proposed a new cubic equation of state (Twu, Coon and Cunningham, 1995). It is more complex than Peng-Robinson however it is capable of predicting liquid phase densities more accurately. The additional complexity was not deemed to be worthwhile, primarily because the parameters for such a new equation are not readily available. It was decided that for this work the Peng Robinson form of the equation would be used with the Twu, Coon and Cunningham modified alpha function.

Table 3.1: Alpha functions for versions of the PREOS

Expression	Function
Peng & Robinson (1976)	$\alpha(\omega,T_r)=[1+(0.37464+1.54226\omega-0.26992\omega^2).(1-T_r^{0.5})]^2$
Mathias et al. (1989)	Same as Peng-Robinson for ω<0.5 else: $\alpha(\omega,T_r)=[1+(0.3796+1.485\omega-0.1644\omega^2+0.01666\omega^3).(1-T_r^{0.5})]^2$
Twu,Coon & Cunningham (1995)	$\alpha(\omega,T_r)=\alpha^0+\omega.(\alpha^1-\alpha^0)$ $\alpha^0=T_r^{-0.171813}e^{0.125282(1-T_r^{1.77634})}$ $\alpha^1=T_r^{-0.607352}e^{0.511614(1-T_r^{2.20517})}$

3.4. NON-IDEAL FLUID MIXING IN THE VLE

Due to the large number of components in this mixture, estimation of the binary interaction parameters is not a simple matter. Most correlations for prediction of binary interaction parameters are based on the ratios of the critical volumes of the mixture and not derived for hydrocarbons with a chain length greater than C_{20} (Hudson & Mc Coubrey, 1960; Nishiumi et al., 1988; Tsonopoulos et al., 1989).

Nishiumi et al. (1988) proposed two relations, one derived from data for carbon numbers of less than 16 (Nishiumi-1) and the other form carbon numbers between C_{18} and C_{20} (Nishiumi-2). The latter relation of Nishuimi et al. was excluded as a result of the limited range of alkanes for which it was derived. For the experimental data available the most accurate alkane-alkane binary estimation was determined to be the first equation of Nishiumi et al. (Nishiumi-1). However, as this relation does not extrapolate well to high carbon numbers (figure 3.4b) or account for hydrogen-hydrocarbon interactions the relation of Tsonopoulos et al. (which does account for the important hydrogen-hydrocarbon interactions) was deemed to be the most appropriate for use. The Hydrogen solubility approach was not considered as EOS provide a more general description of the VLE.

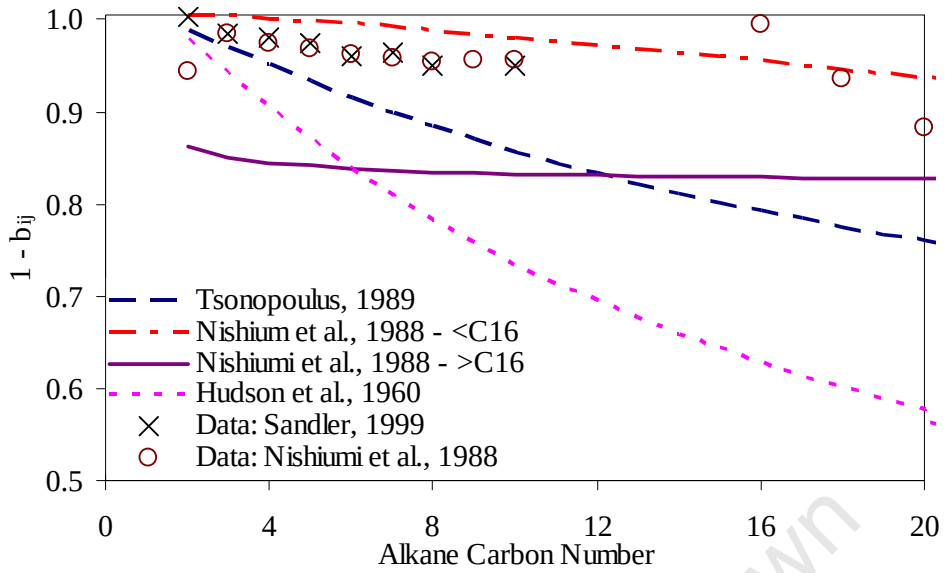

Figure 3.4a: Binary Interaction Parameters (1-b_{ij}) for Methane-Alkane pairs

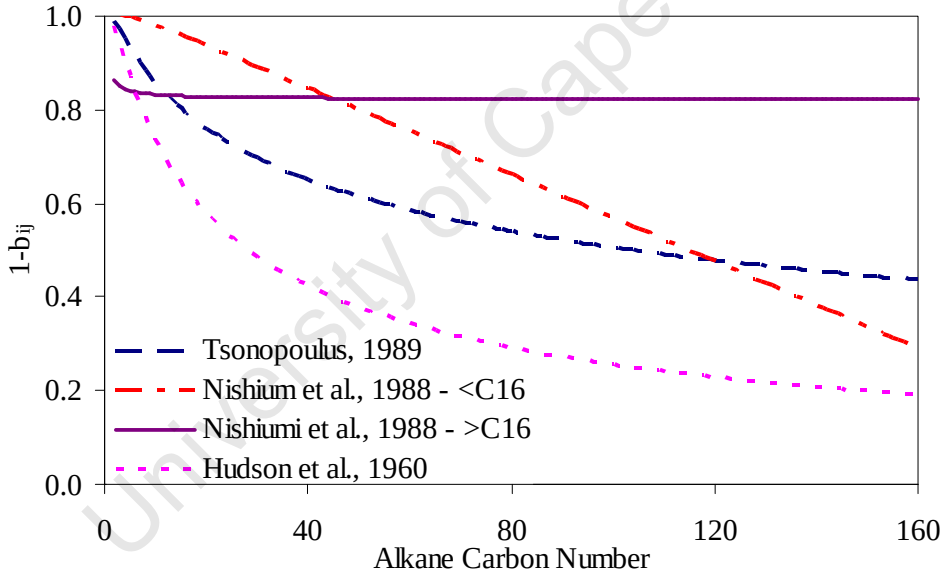

Figure 3.4b: Binary Interaction Parameter (1-b_{ij}) Extrapolation for Methane-Alkane pairs

Extrapolation using the correlations to heavy hydrocarbons generally resulted in excessive values of binary interaction parameters (figure 3.4b). A theoretical basis exists for calculation of the binary interaction parameters in the form of Gibbs Excess Models which combine equation of state and activity coefficient models. Several such models have been proposed for instance the Wong-Sandler (Wong and Sandler, 1992; Orbey and Sandler 1995; Orbey and Sandler, 1998) and MHV1 (Michelson, 1990a,

1990b; Dahl and Michelsen, 1990). Twu et al (1997) have developed a mixing rule based on incorporation of the NRLT activity model. Unlike the Wong-Sandler approach, it is able to accurately match the Gibbs Excess of the activity model and that derived from the equation of state. It has also been shown to produce more accurate results for highly non-ideal solutions than either the Wong-Sandler or MHV1 approaches (Twu et al., 1997). A Gibbs Excess Model was deemed to be beyond the scope of the modelling to be performed in this work and may be the subject of future investigations.

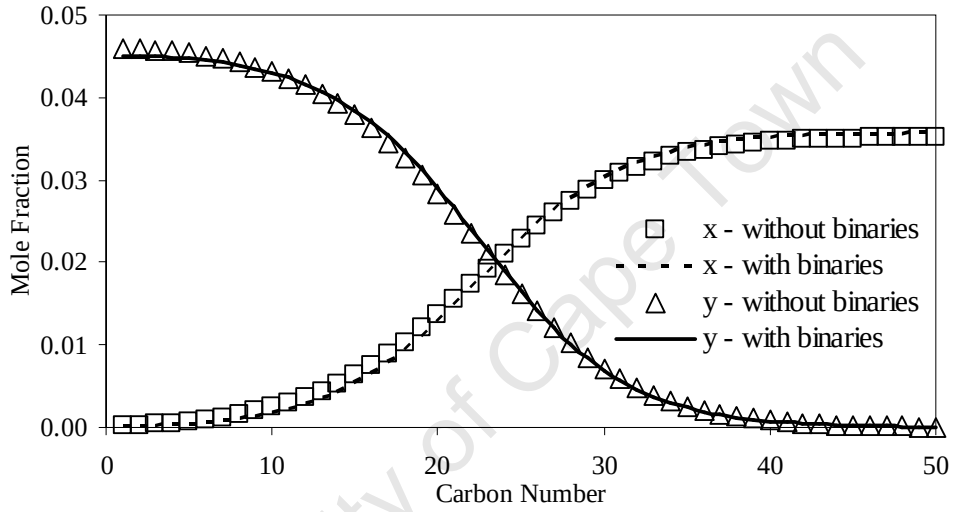

Figure 3.5: Comparison of VLE with and without binary interaction parameters of Tsonopoulos et al. (1989): equimolar hydrocarbon feed: 650K, 50bar and 20:1 hydrogen to wax molar ratio; x - denotes liquid phase and y – denote vapour phase

The correlation of Tsonopoulos et al. (1989) made minimal difference to the VLE predictions, e.g. figure 3.5. It is the opinion of the author that correlations for binary interaction parameters are not sufficiently developed for hydrocarbons heavier than C_{16} to be applied in the modelling of wax hydrocracking. As a result the binary interaction parameters were assumed to be zero, as per recommendation by Sandler (1989) for the situation in which an accurate binary interaction parameter is unavailable.

The reactor model is structured such that binary interaction parameters may be easily incorporated when reliable relations for waxes become available in literature.

3.5. RACHFORD – RICE FLASH ALGORITHM

Unlike the model of Accolla (2006) the Rachford-Rice algorithm (Rachford and Rice, 1952) was used to perform all flash calculations not just the initial feed flash. The number of non-linear equation within the flash routine was thus reduced from hundreds of equations (twice as many equations as lumped species) to one, speeding up the solution time of the flash routine by several orders of magnitude.

$$\text{Rachford-Rice Equation: } \sum_{i=1}^{Nsps} \frac{(K_i - 1)z_i}{\psi(K_i - 1) + 1} = 0 \qquad (3.1)$$

where ψ is the vapour phase fraction, K_i and z_i are respectively the separation factor and mole fraction for species *i* in the mixture.

The flash calculation is embedded within the kinetic function, see figure 3.2, and is called with all integration iterations, making it the most utilised routine within the program. Using the Rachford-Rice algorithm to increase the flash calculation efficiency thus leads to a dramatically decrease in overall model solution time.

3.6. KINETICS

Sie et al. (1991) reported that when hydrocracking with carbon numbers between C_{10} and C_{17} similar activation energies and increasing intrinsic reaction rates were observed, refer to section 2.4. This indicates that as an approximation hydrocracking can be described by a single event. It has been assumed in this model that β-scission (cracking) step is rate controlling. The other kinetic steps are assumed to be fast or at equilibrium which seems to be the case for longer chain hydrocarbons (Weitkamp, 1975; Wietkamp et al., 1983; Martens et al., 1986; Martens & Jacobs, 2001). While isomerisation can strongly influence the concentrations of carbenium ions at carbon numbers less than C_{16}, this work focuses predominantly on heavy industrial hydrocarbons and as a result this influence is neglected.

Table 3.2 depicts the 4 types of β-scission that a carbenium ion can undergo. A statistical description of the kinetics was developed based on the number of possible carbon sites at which β-Scission could occur, table 3.3. The rate of cracking is modelled as linearly increasing as the number of possible β-scission steps increases with increasing carbon number.

Table 3.2: Secondary & tertiary carbenium ion β-scission (Martens & Jacobs 2001)

Cracking Type	Ions Involved	Example	Min Carbon Number of Feed	Smallest Product Fragments
A	3°→3°	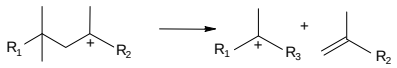	8	4
B1	2°→3°	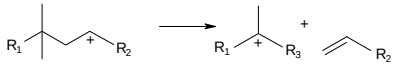	7	3
B2	3°→2°	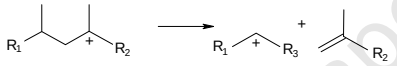	7	3
C	2°→2°	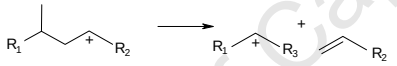	6	3

Due to the lumping by carbon number reaction, types B1 and B2 are indistinguishable in the mechanism. Therefore only three parameters are needed to fully determine the kinetics in this model. Looking at the derived rate expressions it can be seen that there are two main groups of variables: $(2k_A + 2k_{B1} + 2k_{B2} + 2k_C)$ and $(k_{B1} + k_{B2} + 2k_C)$. The type C mechanism is only found outside of these groups in the r_3 and r_6 equations and could possibly be neglected at intermediate conversions for many catalysts, as type C cracking is significantly slower than other types of β-scission. Thus potentially only two parameters are needed to characterise the kinetics for Model-B at low and intermediate conversions.

Table 3.3: Rate expressions developed to describe the hydrocracking kinetics.

C Number	Rate
j =1,2	$r_j = 0$
j=3	$r_j = (k_{B1} + k_{B2} + 2k_C).\sum_{i=7}^{n} C_i + 2.k_C.C_6$
j=4,5	$r_j = 2.(k_A + k_{B1} + k_{B2} + k_C).\sum_{i=j+4}^{n} C_i + (k_{B1} + k_{B2} + 2.k_C).C_{j+3}$
j=6	$r_j = 2.(k_A + k_{B1} + k_{B2} + k_C).\sum_{i=j+4}^{n} C_i + (k_{B1} + k_{B2} + 2.k_C).C_{j+3} - k_C.C_j$
j=7	$r_j = 2.(k_A + k_{B1} + k_{B2} + k_C).\sum_{i=j+4}^{n} C_i + (k_{B1} + k_{B2} + 2.k_C).C_{j+3} - (k_{B1} + k_{B2} + 2.k_C).C_j$
j=8..n-4	$r_j = 2.(k_A + k_{B1} + k_{B2} + k_C).\sum_{i=j+4}^{n} C_i + (k_{B1} + k_{B2} + 2.k_C).C_{j+3}$ $-((j-7)(k_A + k_{B1} + k_{B2} + k_C) + (k_{B1} + k_{B2} + 2.k_C)).C_j$
j=n-3	$r_j = (k_{B1} + k_{B2} + 2.k_C).C_{j+3} - ((j-7)(k_A + k_{B1} + k_{B2} + k_C) + (k_{B1} + k_{B2} + 2.k_C)).C_j$
j=n-2, n-1, n	$r_j = -((j-7)(k_A + k_{B1} + k_{B2} + k_C) + (k_{B1} + k_{B2} + 2.k_C)).C_j$

4. RESULTS, MODEL B

4.1. MODEL VALIDATION

In order to determine the applicability of the model to coal derived Fischer-Tropsch wax streams, the feeds for the conditions and conversions of Leckel (2005), Leckel & Liwanga-Ehumbu (2006) and Pellegrini et al. (2008) were simulated and compared to the products that they obtained.

The conversion in this work is defined to be the reaction of hydrocarbons with 23 or more carbon atoms into hydrocarbons containing less than 23 carbon atoms. This definition of conversion is commonly used in literature and values for the conversion are reported for feeds analysed in this section. Conversion by this definition is a lumped parameter and thus can disguise the systems intrinsic behaviour.

Due to the information required to perform reactor sizing calculations being unavailable, conversion is used as the reaction co-ordinate. As a result only relative ratios of kinetic parameters may be determined. The product spectrum produced by different β-scission types does not vary greatly, with large variations in the ratios of the kinetic parameters producing significant changes only at the ends of a distribution (Accolla, 2006). As a result of this minimising the error in the kinetic parameters was not deemed worthwhile. The model can thus provide an intuitive, no parameters required, estimation of hydrocracker selectivity.

Figure 4.1 depicts a Model-B simulation of figure 2.8 (from Sie et al., 1991) for an equimolar feed of hydrocarbons. The intrinsic rate in figure 4.1 is the initial rate that would be obtained if the hydrocracking was taking place in a single homogenous phase. The liquid to feed ratio of the model VLE is more gradual than that proposed for the degree of adsorption by Sie and co-workers. The observed reactivity is similar to that observed by Sie et al. (1991) in their work on the SMDS process. Model-B can be seen to successfully approximate, using VLE, the general trends in phase behaviour and reactivity observed by Sie et al.

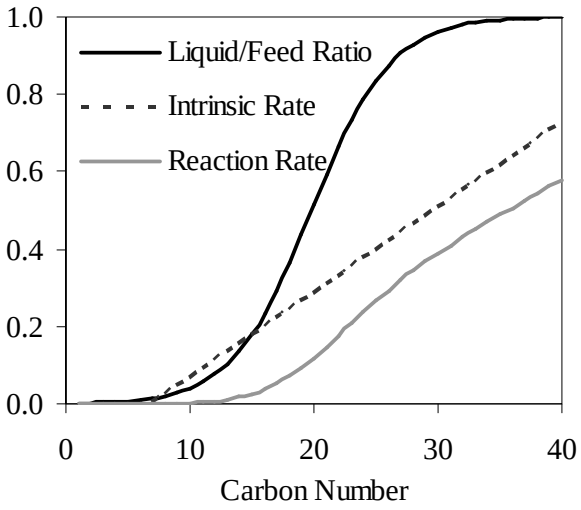

Figure 4.1: Model VLE and Reactivity's at 300˚C, 30bar, 30:1 hydrogen:wax (molar)

4.2. IRON FISCHER-TROPSCH WAX FRACTION ($C_{10}H_{22} - C_{50}H_{52}$)

Low temperature Fischer-Tropsch (LTFT) wax was hydrocracked by Leckel & Liwanga-Ehumbu (2006) using unsulphided Pt/SiO_2-Al_2O_3 modified with MoO_3, figure 4.2.

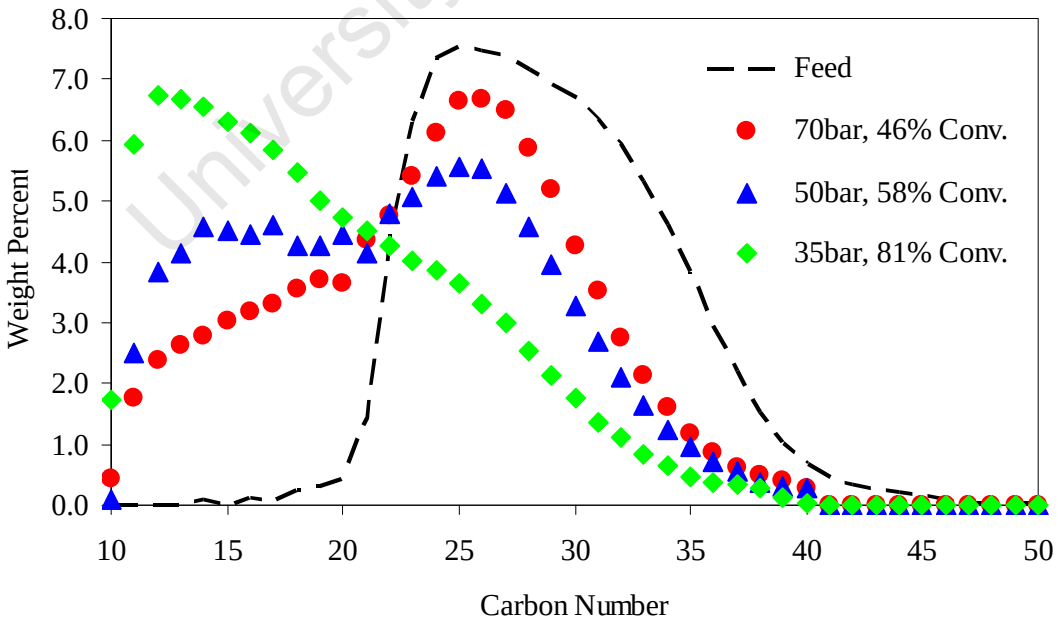

Figure 4.2: Sasol M5 wax hydrocracking carbon distribution at various conversions, 370ºC, 1.0 h-1 WHSV and 21:1 molar hydrogen-to-wax ratio. (Leckel et al., 2006)

Table 4.1: Sum of Squared Error in Model Predictions

Experimental Conditions		Sum of Squared Error			
C23+ Conv.	Pressure (bar)	1xPressure	2xPressure	4xPressure	8xPressure
0.46	70	12.23	11.62	11.45	10.38
0.58	50	12.07	7.269	6.152	4.863
0.81	35	30.19	16.46	10.405	6.614

At the reported pressure the model most accurately matches the experiment data at high pressure and low conversion conditions, table 4.1. This is a result of the unusual reactivity of the hydrocarbons. In figure 4.2 it can be seen that for the low conversion experimental runs shorter hydrocarbons in the range C_{20} - C_{25} are consumed in preference to the longer chain length C_{25} - C_{50} hydrocarbons.

This is contrary to the kinetic scheme of the model, which assumes longer chain hydrocarbons crack more rapidly than shorter chain ones as a result of the greater number of carbon-carbon bonds at which cracking can potentially occur, shown by the model simulations in figures 4.3 to 4.5. As conversion increases this behaviour leads to progressively greater inaccuracies in model product prediction. Nevertheless the model demonstrates that it can provide a rough approximation of experimental results. The bumps observed in the simulation product at C_{14} and C_{16} are a result of the higher concentrations of these species in the feed (figure 4.2)

It should be noted that for the 81% conversion (35bar) run that the liquid in the feed runs out at approximately 77% conversion (figure 4.6). The reaction was not continued into the vapour phase. This is no doubt a reason for the higher value of model error for that run in table 4.1. It should be noted that the PREOS is only an approximation and in real systems the liquid phase could run out sooner or not at all.

The complete consumption of the liquid phase predicted by the model as a result of high conversion (figure 4.6) may not be present in the real reaction system as the real product can be seen to be ‘heavier’ than the simulated product due to the unusual reactivity mentioned previously. Thus while the model predicts a vapour phase reaction the ‘heavier’, real, product may still be present in both liquid and vapour phases (as the real product data is unpublished below C_{10} flashing it is not possible).

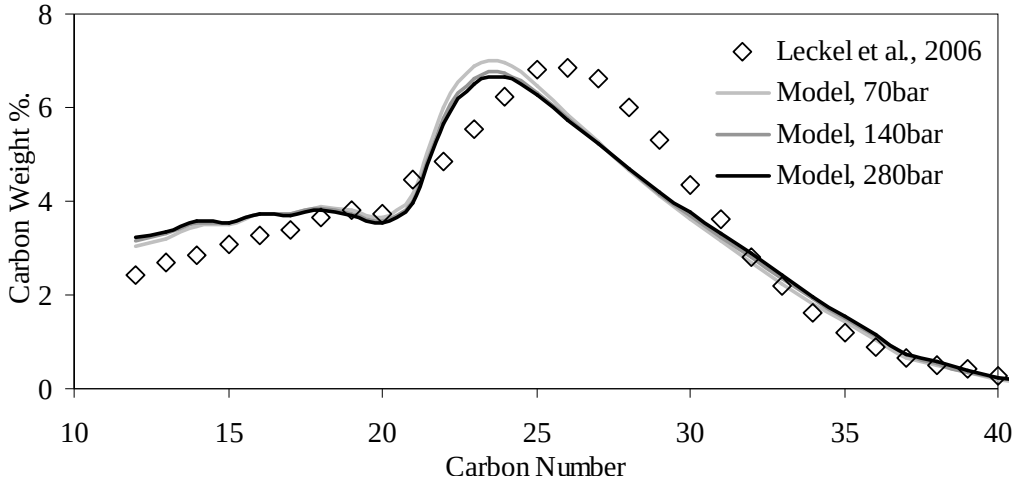

Figure 4.3: 46% Conv., 370˚C, 1hr^{-1} WHSV and 21:1 H_2:Hydrocarbon (molar)

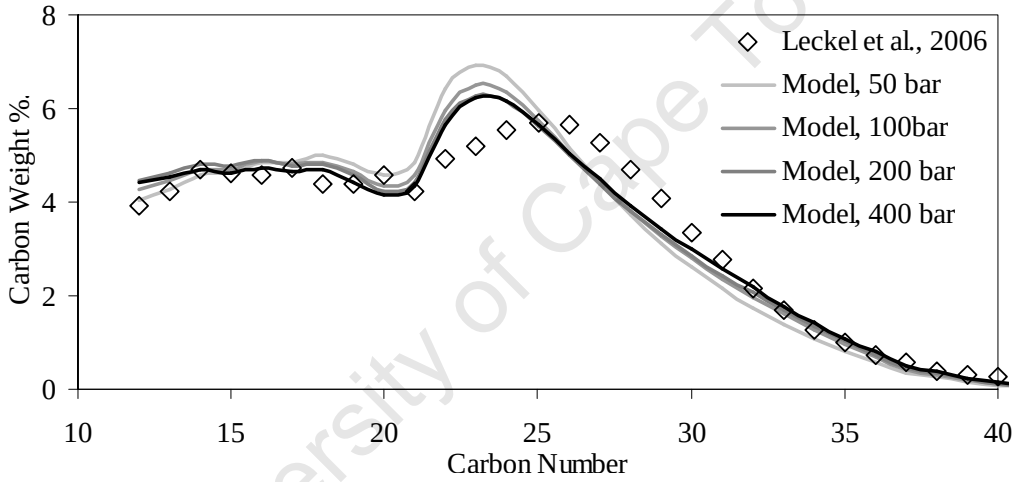

Figure 4.4: 58% Conv., 370˚C, 1hr^{-1} WHSV and a and 21:1 H_2:Hydrocarbon (molar)

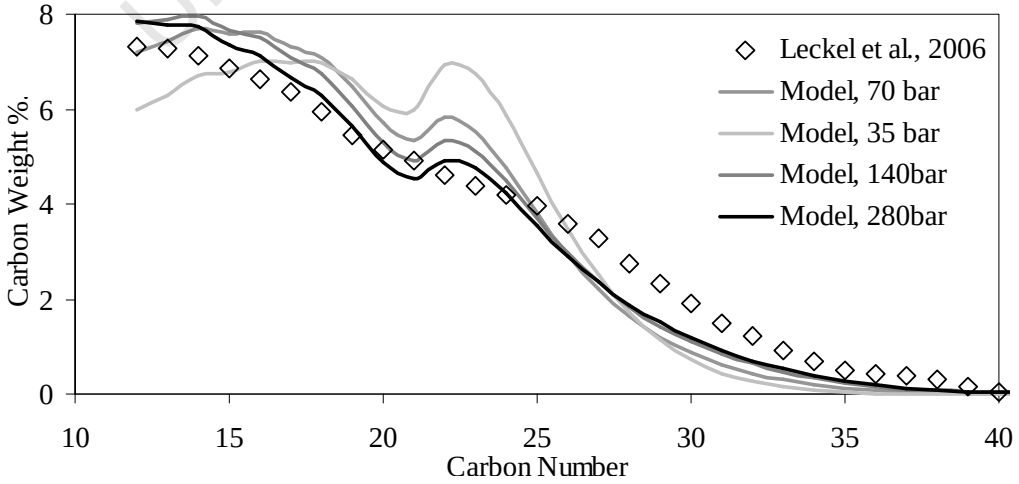

Figure 4.5: 81% Conv., 370˚C, 1hr^{-1} WHSV and and 21:1 H_2:Hydrocarbon (molar)

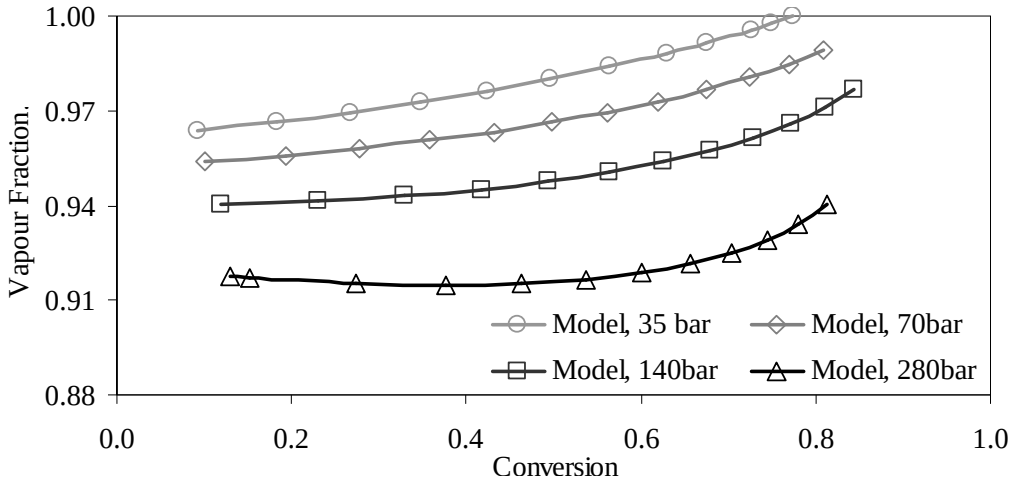

Figure 4.6: Vapour fraction vs. conversion: 370˚C, 21:1 H_2:Hydrocarbon (molar)

The initial decrease in vapour fraction for the 280bar simulation in figure 4.6 is due to the consumption of hydrogen in the hydrocracking reaction. This effect is soon outweighed by the progressive lightening of the hydrocarbons by the hydrocracking reaction.

The VLE has major a role to play with its effect being superimposed on the kinetic selectivity that is obtained. Modification of the kinetics by the VLE is greatest in the region where the phase change is located. For a binary test feed of C_{80} and H_2 this transition region was observed to move to lower carbon numbers with reduced pressure, increased temperatures and increased conversion (Accolla., 2006). However, the behaviour predicted by Model-B is fundamentally different.

This is demonstrated in figures 4.7 and 4.8; and it is clear that, in contrast to the findings of Accolla (2006), for higher pressures and lower conversions of C_{23+} the carbon number range over which transition occurs is lower. The greater amounts of light components present in the liquid phase at high pressures and low conversions lowers the liquid mixtures boiling point and thus shifts the transition region to lower carbon numbers.

The differences in behaviour observed between Model-A's C_{80} simulation and Model-B's industrial distribution of feed carbon numbers have two potential causes both stemming from the VLE. The first is the different definition of conversion used. The

C_{80} simulation uses a true conversion (based on the consumption of C_{80}) rather than the lumped measure of conversion used in industrial situations, see section 4.1. Even at very high conversions (X > 0.95) the amount of light, vapour phase, hydrocarbon produced by the C_{80} simulation was minimal. The second is the fundamental difference in feed distribution between a real industrial FTS carbon number distribution and a single C_{80} species spike input.

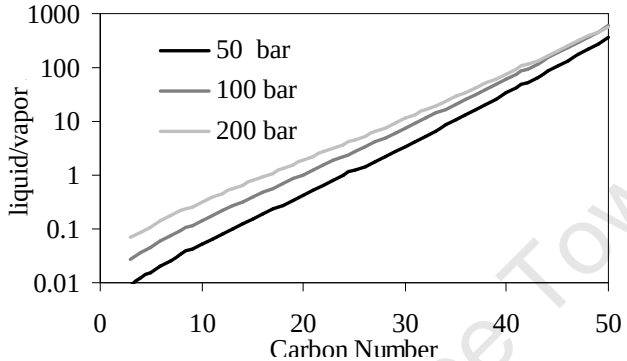

Figure 4.7: Liquid/Vapour Ratio vs.Carbon Number for Different Pressures at 58% Conv., 370˚C and 21:1 H_2:Hydrocarbon (molar)

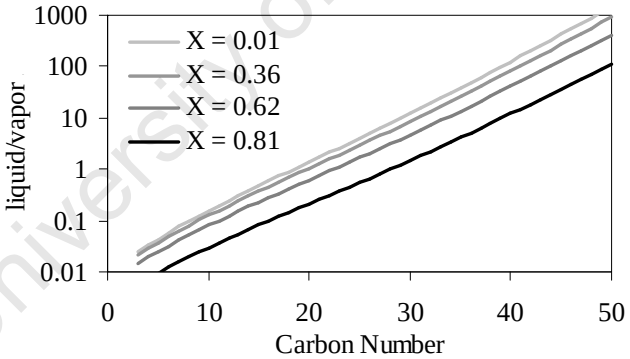

Figure 4.8: Liquid/Vapour Ratio vs. Carbon Number for Different Conversions at: 70bar, 370˚C and 21:1 H_2:Hydrocarbon (molar)

As a result of the reasons highlighted above Model-A measures the phase transition under conditions in which the effect of hydrogen consumption lowering the vapour fraction dominates over the effect of forming light hydrocarbons that can enter the gas phase and increase the vapour fraction. These competing effects were noted for the 280 bar run of figure 4.6 and are a biproduct of the hydrocracking reaction system kinetics.

Essentially the C_{80} simulations with Model-A phase look at the behaviour encountered in the low lumped conversion of a very heavy feed to middle distillates. At higher lumped conversions the opposite trends would have been observed for the C_{80} cracking. The actual phase behaviour over a longer reaction time would qualitatively be the same as that for the 280bar run of M5 wax cracking in figure 4.6.

The system kinetics and their resulting two competing effects on vapour fraction is the cause of much of the contention in literature on the hydrogen concentration dependency of hydrocracking. The relative importance of these two effects is largely dependent on the feed used and the conditions of temperature and pressure under which it is cracked.

The differences in behaviour observed between these two feeds highlights the importance of the feed distribution in hydrocracker behaviour. Trends observed for one feed and set of conditions do not necessarily apply to other feed distributions. This highlights the importance of a fundamental model.

The range of carbon numbers spanned by the transition region is proportional to the gradient of the liquid/vapour ratio lines. For this feed it can be seen from figures 4.7 and 4.8 that the transition region broadens with increasing pressure and conversion.

The unusual reactivity observed is potentially a result of several effects arising from both the VLE and the kinetics. Model B's kinetic scheme does not take into account the other rearrangements or mechanisms that occur in wax hydrocracking. Another kinetic step or combination of steps could contribute towards the unusual reactivities observed. Dehydrogenation in combination with isomerisation in particular could have a significant effect on the model product as the dehydrogenation equilibrium constant of branched species varies strongly with carbon number, section 5.7.

Total system pressure has a major effect on the model prediction of the system with significant improvements in the model accuracy being observed at higher pressure, table 4.1 and figures 4.3 to 4.5. The higher pressure may cause the VLE to simulate an effect known as capillary condensation within the catalysts pores, whereby a higher

degree of condensation is experienced within the pores. It is also possible that incomplete model kinetics create a pseudo-pressure effect that is not present in reality.

$$\textit{Kelvin Equation}: \frac{P}{P_0} = \exp\left(-\frac{2.\sigma.V_M}{R.T}.\frac{1}{r_m}\right) \qquad (4.1)$$

Capillary condensation may be described by the Kelvin Equation, equation 4.1 where σ is the surface tension, V_M the liquid molar volume and r_m the mean curvature radius.

Do (D.D Do, 1998) quantified this effect for nitrogen at 77K, for a completely no-adsorbing molecule like N_2 (i.e. doing N2-BET at 77K) micro pores are completely saturated at $P/P_{sat} > 0.1$. For macro-meso pores systems of the type used here, pores of 100A are saturated at ~ $P/P_{sat} > 0.5$. This means that if the VLE predicts no liquid phase for a mixture at a particular pressure there may still be liquid in the catalyst pores as the effective pressure experienced in the pore is higher that outside the pore. Applying the VLE to simulate this effect is a rough approximation as the actual changes in adsorbed phase concentration experienced due to capillary condensation may be different to those predicted by PREOS however qualitative trends in phase behaviour remain roughly the same.

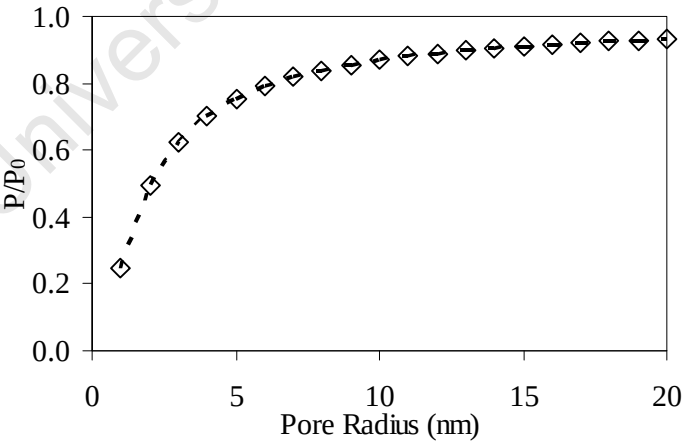

Figure 4.9: Capillary condensation of the feed as a function of pore radius at 640K

The equation 4.1 based prediction of the feed capillary pressure is depicted in figure 4.9. The DIPPR databank (Daubert et al., 1999) was used to determine the liquid molar volume and the coefficients for a surface tension correlation. The PREOS was

used to determine the composition of the liquid phase. Hydrogen, which comprised 9% on a mol basis of the feed, was excluded from the calculation as it is at super-critical conditions (no hydrocarbons are supercritical as C_{14} is the lightest hydrocarbon in the feed) and thus its surface tension is not readily apparent. It is apparent that at 10nm, such as was the case in this instance the effective increase in pressure experienced in the pores is around 15% according to Kelvin's equation.

However, equation 4.1 only accounts for surface tension forces. For adsorbing molecules like hydrocarbons there are significant forces between the molecules and the catalyst surface that are not accounted for in equation 4.1. Experience demonstrates that for adsorbing species P/P_0 can be as low as 0.001. Thus P/P_0 for hydrocarbons is almost certainly one order of magnitude lower than predicted by equation 4.1 (and potentially even three orders of magnitude lower). Implying that the effective pressure experienced is even higher than eight times the operating pressure, which is the increase used in the simulations.

In figures 4.3 to 4.5 the peak in the model predicted yield at approximately C_{23} is narrower than that observed in the experimental data. This is probably a result of the pressure effect noted previously but could also be a result of mass transfer limitations between the vapour and liquid phases in the experimental system.

Inter-phase mass transfer limitations would result in the light hydrocarbon species diffusing from the reacting (liquid) phase more rapidly than heavier hydrocarbons. Thus the cracking reaction does not proceed to the same extent as the equilibrium case as the lighter species are removed before they can crack further; resulting in a product distribution weighted more towards heavier hydrocarbons than in the equilibrium case. This could potentially explain the differences observed between the simulated and experimental data in figures 4.3 to 4.5. Such an effect if quantified could be exploited industrially to increase the selectivity towards middle distillate products.

Interestingly the carbon numbers which comprise the bulk of the vapour phases (figure 4.10) are also the carbon numbers which display the unusual reactivities noted earlier. This lends credence to the idea that mass transfer is playing a role as the greatest changes in the mass transfer driving force would occur within this region.

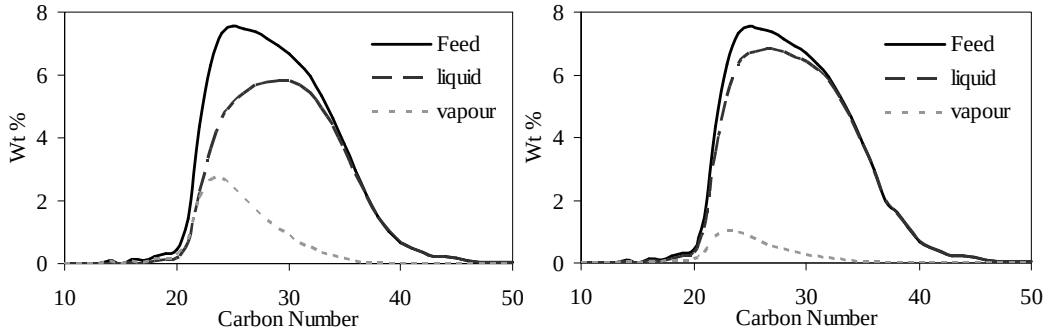

Figure 4.10: Feed flash at: 370˚C, 21 H_2/Hydrocarbon, 35bar & 140bar respectively

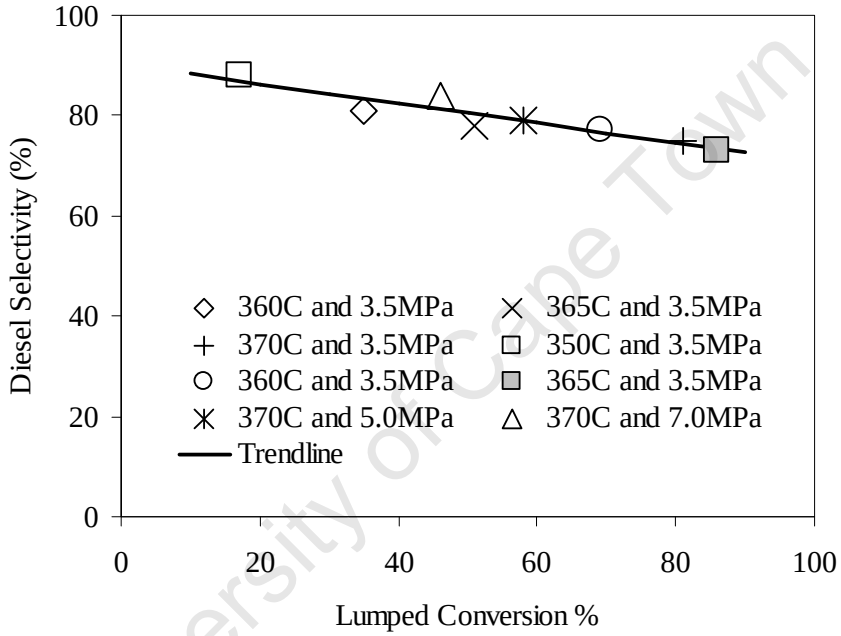

Figure 4.11: Diesel Selectivity vs. Lumped Conversion obtained from Leckel et al. (2006) data for various temperatures (350ºC – 370ºC) and pressures (35bar-70bar)

Figure 4.11 demonstrates that the hydrocracking selectivity towards the diesel fraction ($C_{10} - C_{22}$ in this instance) is a direct function of conversion and not a result of the concentration effects proposed by Leckel et al. (2006) or process conditions of temperature and pressure. A similar dependence on conversion with the opposite trend is observed for diesel yield (figure 4.12). Figure 4.13 shows that the product diesel cloud point is also affected by the conversion, while the cetane number remains approximately constant in the low seventies within experimental error. It is important to note that the trends in figures 4.11 to 4.13 are probably specific to the feed distribution and definition of conversion and should not be generalised to other feeds.

It should also be noted that inaccuracy in the model predictions may be due in a minor part to: impurities in the feed (which was 94% n-paraffin's) and errors in experimental technique (mass balance between 96% and 104% where reported).

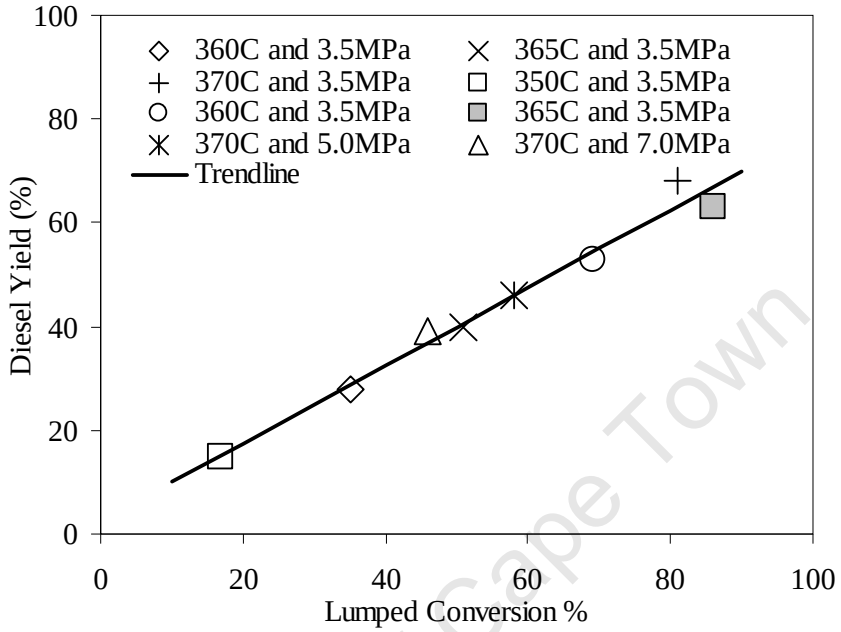

Figure 4.12: Diesel Yield vs. Lumped Conversion obtained from Leckel et al. (2006) data for various temperatures (350ºC – 370ºC) and pressures (35bar-70bar)

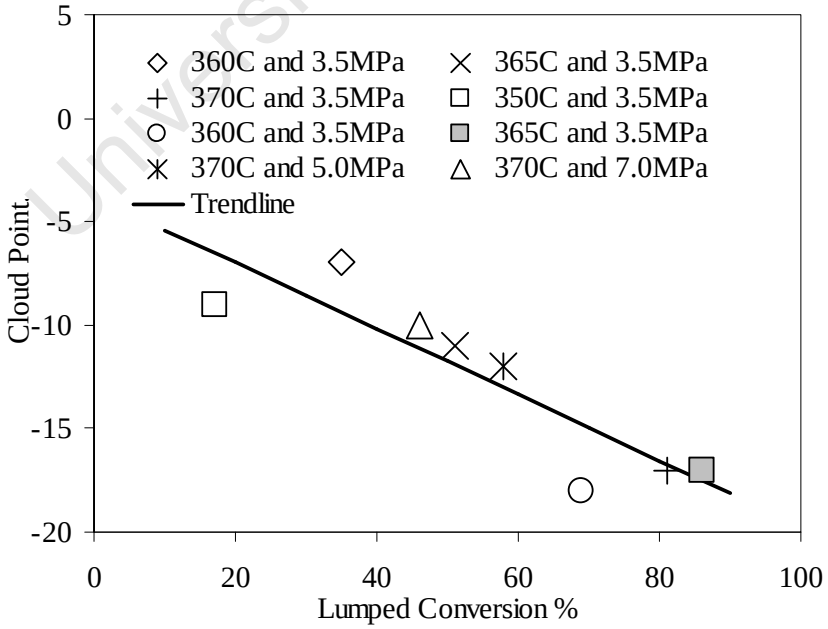

Figure 4.13: Diesel Cloud Point vs. LumpedConversion obtained from Leckel et al. (2006) data for various temperatures (350ºC – 370ºC) and pressures (35bar-70bar)

Table 4.2: Model-B vs. Real (Leckel et al., 2006) Middle Distillate Selectivity and Yield at 370ºC, WHSV = 1.0h^{-1} and H2/Hydrocarbon= 21 (Ratio Molar)

P (MPa)	X	Yield (wt%)		Selectivity (wt%)	
		Real	Model	Real	Model
3.5	81	61	63	75	80
5.0	58	46	49	79	81
7.0	46	39	41	84	82

Table 4.2 displays Model-B's accuracy in predicting the middle distillate yield (within 3wt%); middle distillate selectivity is also well predicted (within 5wt%). The closeness of the simulations to reality demonstrates the value of this model in predicting data relevant to industrial operation.

4.3. IRON CATALYSED FTS SLURRY WAX ($C_{10}H_{22} - C_{105}H_{112}$)

Sasol iron catalysed Fischer-Tropsch reactor wax was hydrocracked using a NiMo on SiO_2/Al_2O_3 catalyst by Leckel (2005). Carbon Spectra of the feed and product were reported and a full feed analysis was also done in later work by Leckel (2007). The experimental carbon product spectrum and the model predictions are shown in figures 4.14 to 4.15.

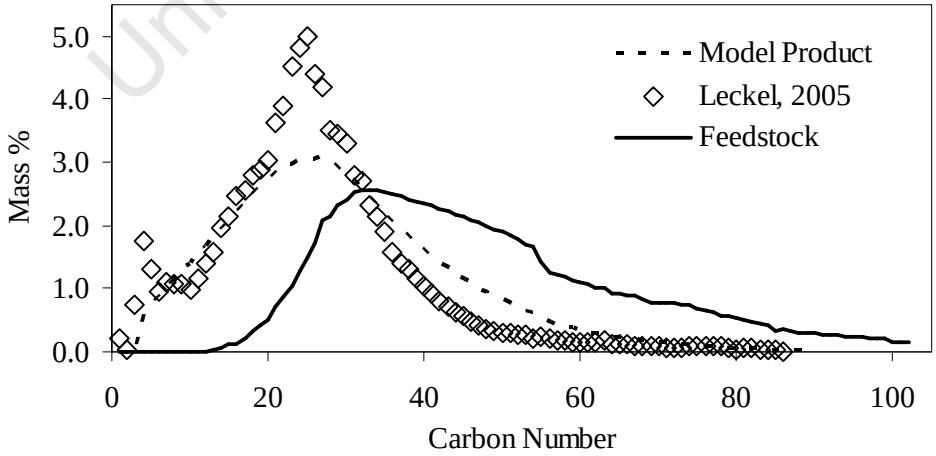

Figure 4.14: Carbon Distribution for FTS slurry Wax data (Leckel, 2005) vs. Model Predictions 35bar, 350ºC, 34% conversion with H_2:Hydrocarbon molar ratio of 38:1

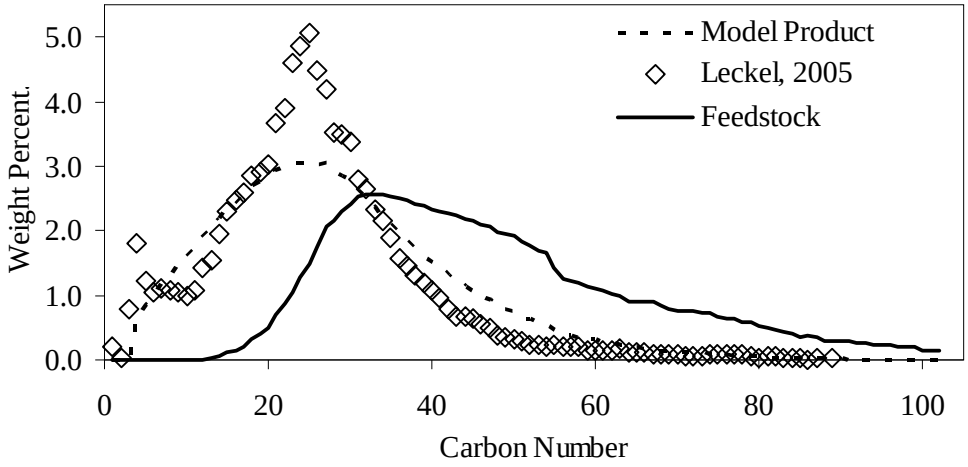

Figure 4.15: Carbon Distribution for FTS slurry Wax data (Leckel, 2005) vs. Model Prediction: 70bar, 365ºC, 37% conversion with H_2:Hydrocarbon molar ratio of 38:1

The hydrocracker product of the FT slurry wax feed shows no change with pressure (Figures 4.15 and 4.16). This is indicative of ideal hydrocracking conditions in which the dehydrogenation step is in equilibrium and in no way limiting to the overall mechanism. The sharp spikes at C_4 and C_5 are not typical of hydrocracking product spectrum. It is suspected that another mechanism is at work here, as the presence of C_1 in the product that was not in the feed should not be possible via the traditional hydrocracking reaction scheme. Two possibilities are thermal cracking and successive hydrogenolytic demethylation, see figure 2.5. These mechanisms could explain the peak observed at C_4. Successive hydrogenolytic demethylation is reported by Gates et al. (1979) as being pertinent for catalysts with a Nickel metal, as is the case here.

Comparing the model predictions to the reported experimental results it can be seen that in this instance the model under predicts the reactivity of the heavier hydrocarbons. From this, and from the unusual reactivity observed in the M5 wax cracking discussed earlier, it is evident that the reactivity of these feeds does not follow a linear dependence on carbon number, such as was used in this model.

Additionally it appears that the analysis, which was performed in 4 different segments C_1-C_4, C_5-C_9, C_{10}-C_{22} and C_{23+}, has not been normalised well between the segments.

It is observable (see figure 4.16) that in each of these segments there is a different pattern for the carbon number distribution with continuity not being maintained between the segments causing the carbon distribution to appear piecewise and leading to the conclusion that product analysis may be inaccurate.

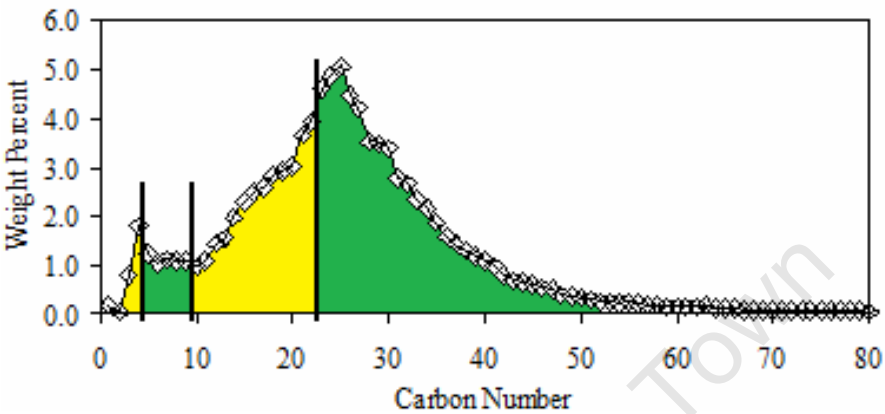

Figure 4.16: Cracked product, segmented into regions of analysis by Leckel (2005)

As in the case of the M5 wax the feed is not pure paraffin's and contains 1.5% oxygenates and 1% olefins by mass. The oxygenates would play a role in determining the product distribution (Leckel, 2007) that would not be accounted for by the model.

4.4. FTS WAX ($C_5H_{12} - C_{70}H_{142}$)

Pellegrini et al., (2008) hydrocracked an FTS wax with carbon numbers ranging from C_5 to C_{70} over an amorphous silica alumina catalyst loaded with platinum. The product is shown in figure 4.17.

The data presented by Pellegrini et al. (2008) has a feed with a similar shape to that of the FTS slurry wax (section 4.3) and hence a similar peak in the product distribution. Model-B fails to predict the sharpness of the peak observed at $C_{12}H_{26}$, however it does give a qualitative prediction of the product. Running the model at twice the operational pressure provides a slight improvement in prediction while further increase to four times the experimental pressure led to lower model accuracy.

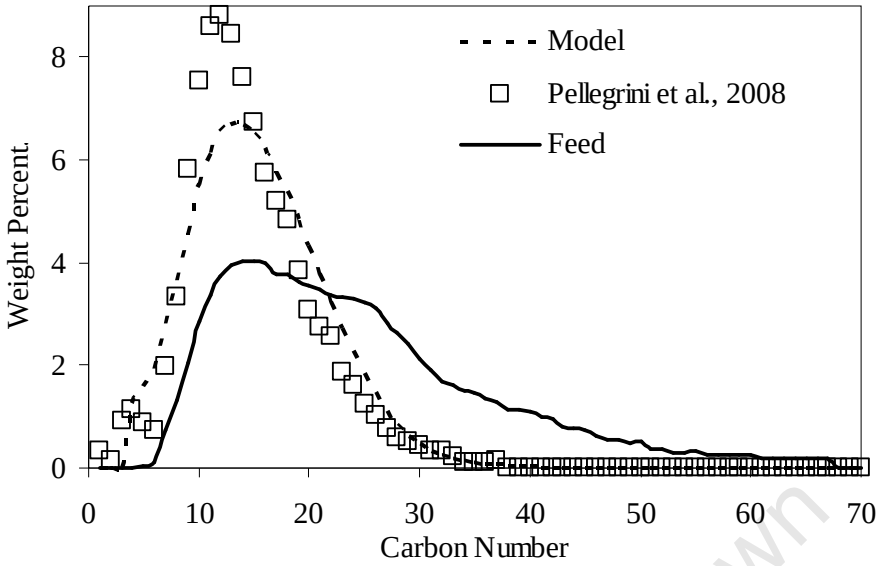

Figure 4.17: Model and experimental carbon number distribution at 367ºC, 54bar and 12:1 hydrogen:wax (molar)

The technical difficulties of analysing such a complex feed are not mentioned by the authors and the accuracy of the experimental mass balance is also not reported. It is thus difficult to obtain a measure of how reliable the experimental data is. Nevertheless model and experimental behaviour are qualitatively the same.

4.5. SUMMARY

The hydrocracking of three industrial F-T waxes has been simulated at a number of conditions. The iron catalysed FTS slurry wax was poorly predicted by the model; however this is thought to be due to inaccurate analysis of the product. The model was able to provide a qualitative prediction on the FTS wax (similar feed distribution to the iron catalysed FTS slurry wax) cracked by Pellegrini et al. (2008) but did not predict a peak of the same magnitude at $C_{12}H_{26}$.

Recently published work by van der Merwe et al. (2008) indicates the presence of a mass transfer and/or hydrodynamic effect in experiments performed at a bench or pilot scale level that are not present in industrial reactors. Bench and pilot scale reactors were operated in both up and down flow modes and on comparison the

resulting products were found to be different. Incomplete catalyst wetting in the down flow mode and mass transfer limitations in both modes can thus not be ruled out in the data used to access the models here and is potential a significant source of error.

Model prediction of the product carbon number distribution of experiments by Leckel et al. (2006) on the cracking of a SASOL M5 wax fraction was accurate for the low conversion, high pressure, runs. This was not the case at higher conversions as a result of the unusually high reactivity of the lighter hydrocarbons. The unusually high reactivity of the lighter hydrocarbons in the M5 wax is potentially due to kinetic steps, dehydrogenation etc, in the hydrocracking mechanism that have not been incorporated into the kinetic scheme. This will be investigated further in Model-C (chapters 5 & 6).

A pseudo-pressure effect whereby accuracy in product distribution prediction increases on running the model at higher than specified operational pressures is thought to be due either to incomplete model kinetics or increased condensation in the catalyst pores as a result of capillary effects. At elevated pressures conditions in the model VLE roughly approximates capillary condensation effects.

The behaviour of the VLE in the M5 wax system was found to have different trends with varying temperature, pressure and conversion to that in literature (Accolla, 2006). The different trends observed are a result of two competing kinetic effects in the hydrocracking reaction; namely the consumption of hydrogen which lowers the vapour fraction as reaction proceeds, and the reaction of heavy hydrocarbons to lighter ones which does the opposite. Thus the distribution of hydrocarbon species within the reactor, the process conditions and the way conversion is defined will determine which effect dominates the VLE in the region of interest.

Analysis of experimental data from Leckel et al. (2006) shows that product diesel selectivity, yield and cloud point are functions of conversion rather than of reactor conditions. Thus the carbon number distribution of the feed has a much greater influence on the hydrocracking product fuel than the process variables for this feed. This is thought (but not proved) to be generally true in hydrocracking reactions. Model predictions of both yield and selectivity closely matched the experimental data (table 4.2) highlighting Model-B`s usefulness to the synthetic fuels industry.

5. METHODOLOGY MODEL-C

5.1. ASSUMPTIONS

1. The reactor is isothermal and isobaric.

2. The vapour and liquid phases are in equilibrium which is adequately described by the Twu, Coon and Cunningham (1995) modification of the Peng-Robinson equation.

3. There is no preferential adsorption of hydrocarbons of different chain lengths from the liquid to the adsorbed phases and the concentration on the catalyst surface is equal to that in the bulk liquid phase, i.e. $C_{surface,i} = C_{bulk,i}$.

4. An ideal co-current trickle bed reactor system in which the catalyst always remains homogeneously wetted, i.e. all reaction occurs in the 'pseudo reactive' liquid phase and no reaction occurs over the catalyst in the gaseous state.

5. No mass transfer limitations across the phase boundary or in the catalyst pores.

6. *Ideal hydrocracking*, i.e. the dehydrogenation/hydrogenation steps are in quasi equilibrium.

7. Reactions are 1st order with respect to the liquid phase carbocation concentrations and inversely proportional to the liquid phase hydrogen concentration.

8. Protonation/deprotonation steps are in quasi equilibrium.

9. Only mechanisms involving secondary and tertiary carbenium ions are considered (type D β-scission is neglected as it is dramatically slower than other acid site steps).

10. The kinetic parameters are independent of the carbon number and structure of the carbenium ions involved.

11. *"single event protonation rate coefficients only depend on the type of carbenium ion formed and are independent of the protonated olefin."* Martens, pp 3-20 (2000)

12. *"single event rate coefficients for deprotonation depend both on the type of deprotonated carbenium ion and on the olefin formed"* Martens, pp 3-20 (2000)

13. Linear variation of kinetic constants with respect to carbon number of the reactant molecule.

14. Equilibrium within a lumped group of species is assumed.

5.2. ALGORITHM

The model algorithm may be visualise it as a program with four levels of code embedded within it, figure 5.1.

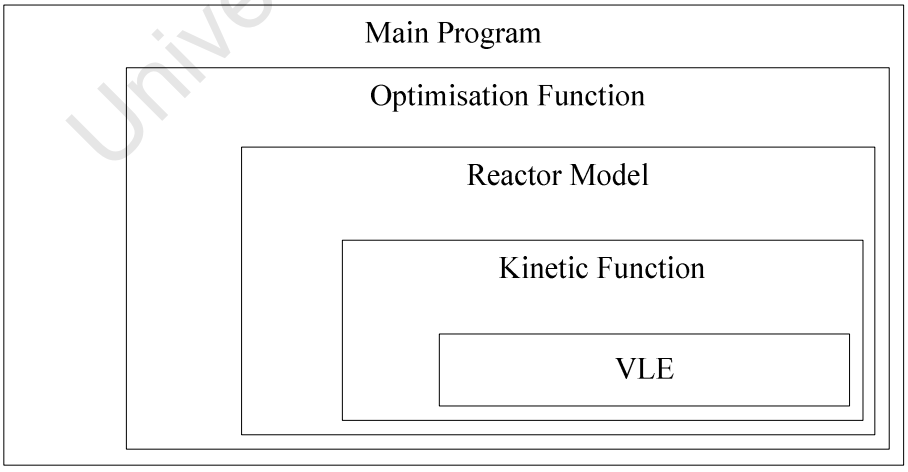

Figure 5.1: Levels of coding within hydrocracking program

The main program serves to set up the optimiser and requires an initial guess of the kinetic parameters. The optimiser function essentially calls the reactor model at different conditions of temperature, pressure and conversion and compares the results obtained with the experimental data, outputting the sum of squared error in the prediction to the optimiser routine in the main program.

As with the previous hydrocracking model, isothermal and isobaric operation are assumed (see section 3.1). This allows the coefficients used in the Peng-Robinson equation of state to be treated as constants (PR-coeff routine in figure 5.2). Correlations are used to estimate the thermodynamic properties of the species, see section 5.3. The hydrocracking model makes extensive use of global variables with temperature, pressure and species concentrations being included in the global variable module.

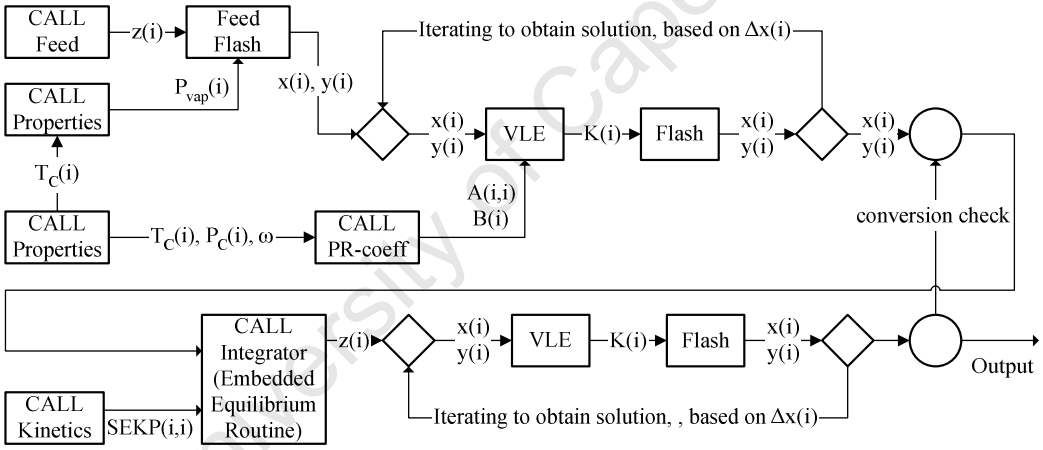

Figure 5.2: Hydrocracking Reactor Model Algorithm

Vapour pressure data (Daubert et al., 1999) is used to obtain an initial guess of the separation factor, *K(i),* between the vapour and liquid phases. The feed is then flashed using the Rachford-Rice Algorithm (section 3.5). The equilibrium is found by iterating the equation of state and the Rachford-Rice flash routine, figure 5.2. This is done again in the embedded VLE routine within the kinetics and a third time after exiting the integration routine, as the interpolative schemes used by integrators may mean that the VLE at the point of exiting the integrator may not have been computed.

As reactor sizing information is not readily available, conversion of C_{23} and higher carbon numbers into components of carbon numbers of less than 23 is used in place of the time/catalyst weight dimension. For this reason the time is looped until the correct conversion is reached (conversion check in figure 5.2). As a result the kinetic parameters obtained from the current model are ratios relative to each other. Information on the reactor dimensions and catalyst packing is required in order to obtain the actual parameter values.

The kinetic parameters are dependent only on species concentrations as a result of the assumption that the reactor system is isothermal. The DVODEPK integration routine (Brown et al., 1989; Byrne, 1992) was used to integrate the kinetic function in which a VLE calculation is embedded. The DFZERO routine (Dekker, 1969; Shampine & Watts, 1970) performed the Rachford-Rice flash calculations and RPOLY (Jenkins & Traub, 1970) was used to solve the cubic Peng-Robinson equations.

5.3. THERMODYNAMIC PROPERTIES ESTIMATION

In order to accurately simulate the vapour-liquid equilibrium, values are needed for the critical temperature (T_C), critical pressure (P_C), acentric factor (ω) and vapour pressure (P_{vap}). While data is available for linear paraffins very little exists in open literature for long chain paraffin isomers. Correlations are therefore used to predict the thermodynamic properties.

A large number of correlations have been proposed, however many were derived using short chained hydrocarbons and thus do not extrapolate well leading to poor property prediction at higher carbon numbers. Thus the choice of the correlations, in table 5.1, was based on their accuracy in predicting the properties of long chain linear hydrocarbons, for which data is available in the DIPPR database (Daubert et al., 1999).

It is important to note that the P_{vap} correlation relation requires T_C values and thus correlation error in T_C increases the error in the P_{vap} value. P_{vap} is not calculated for hydrogen and light hydrocarbons when they are supercritical as is $T_C>1$.

Table 5.1: Correlations selected for thermodynamic property values

Property	Correlation
T_C	Gani & Marrero, 2001 - 'group one contribution' used – figure 5.3
P_C	Ambrose, 1978, 1979 & 1980 - figure 5.4
ω	Constantinou et al., 1995 – figure 5.5
P_{vap}	Twu, Coon and Cunningham, 1994 (requires T_C values)

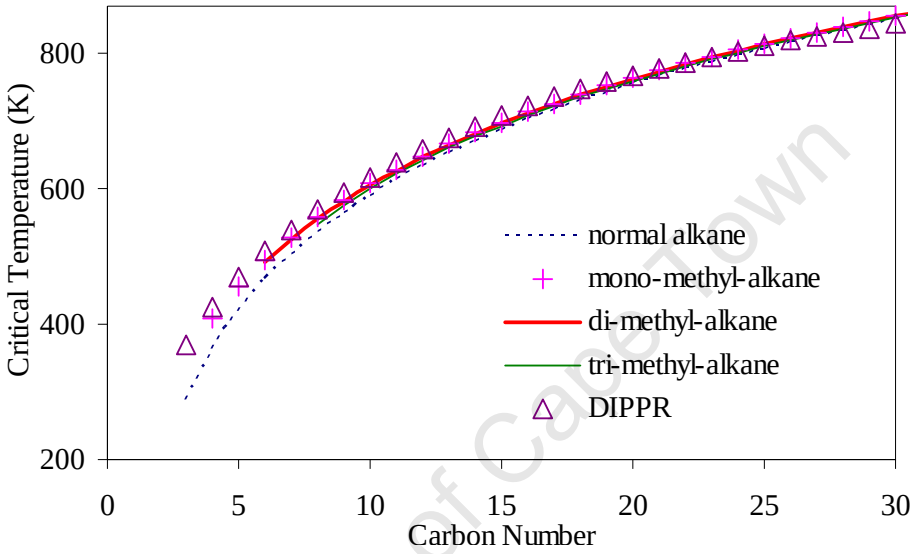

Figure 5.3: Gani and Marrero, 2001, prediction of the critical temperatures of different lumps against DIPPR data (Daubert et al., 1999) for normal paraffins

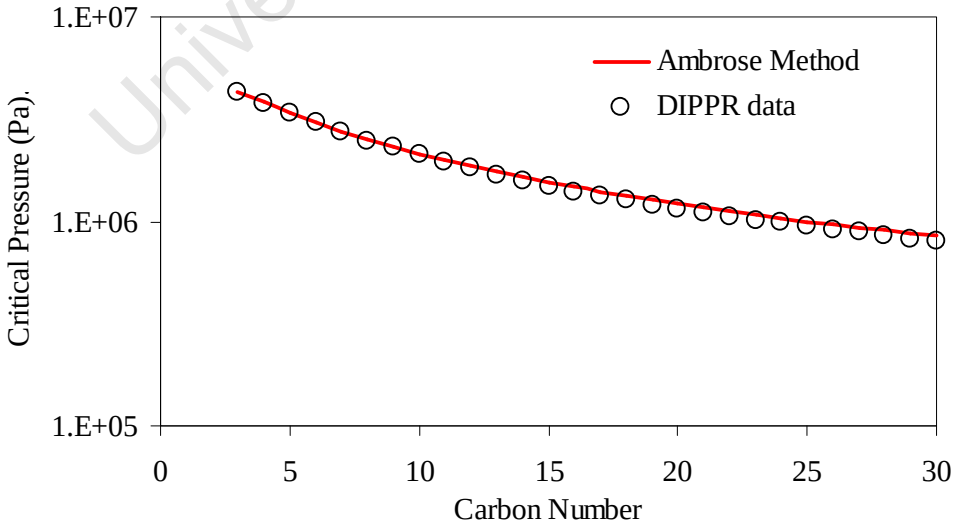

Figure 5.4: Ambrose Method critical pressure prediction vs. DIPPR databank (Daubert et al., 1999)

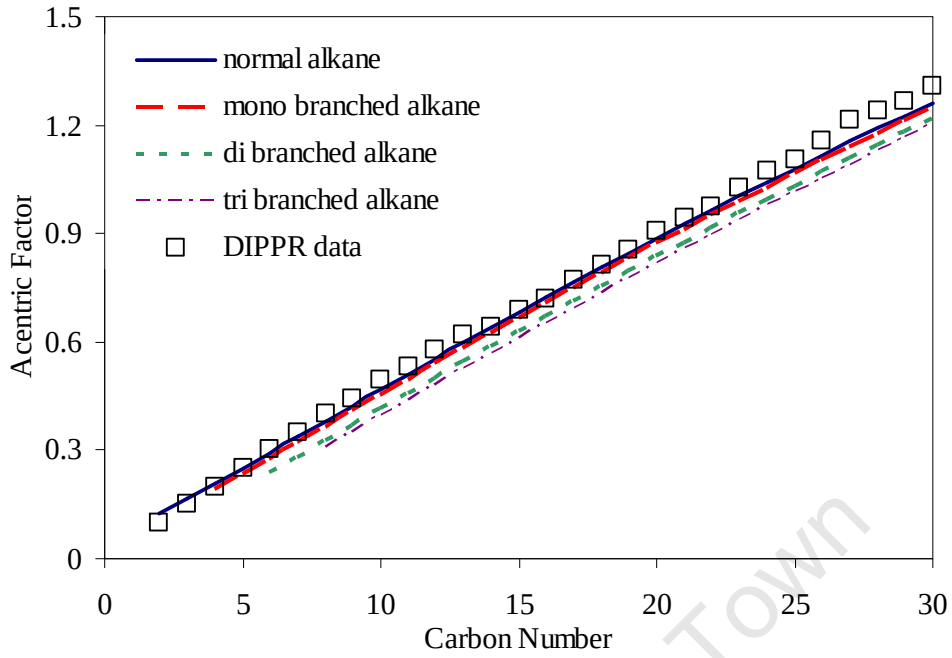

Figure 5.5: Constantinou et al., 1995, prediction of acentric factor vs. normal paraffin data from the DIPPR databank (Daubert et al., 1999)

Only minor differences between different isomer lump properties were observed, which is a result of the system species being predominantly linear (figures 5.3 & 5.5). In all correlations the 2-methyl-alkane was arbitrarily chosen to be representative of the group of mono-methyl isomers and its properties were taken to be those of the lump. Figure 5.6 shows that there is minimal difference between the properties of different mono-methyl isomers (the groups based methods do not distinguish mathematically between a 3-methyl-alkane and 4(or higher)-methyl-alkanes), thus using a representative compound to determine the properties of a lump is thought to introduce a negligible amount of error into the model. Similarly the 2,2-dimethyl alkane was used as the representative compound for the dibranched lumps with the 2,2,4-trimethyl alkane taken as being representative of the tribranched lumps.

5.4. VAPOUR LIQUID EQUILIBRIUM

The Peng-Robinson (1976) equation with the alpha function proposed by Twu, Coon and Cunningham (1995) was used, and the Rachford-Rice (1952) algorithm was used to perform all flash calculations, see sections 3.3 to 3.5.

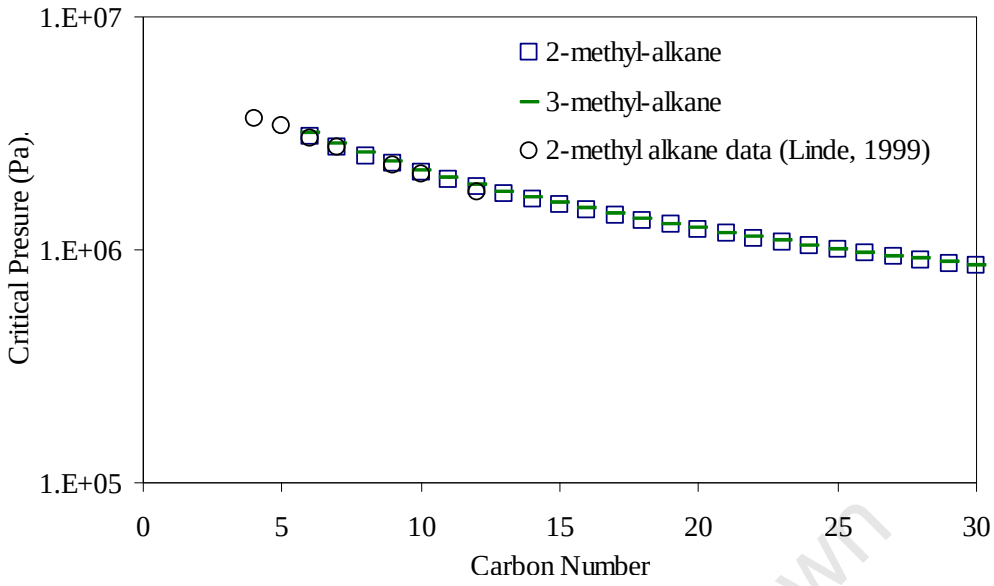

Figure 5.6: Ambrose Method simulations of different mono-methyl alkane P_C's

5.5. LUMPING

In order to reduce the number of rate equations in the reaction network to a manageable number, a lumping scheme is used whereby hydrocarbon molecules are lumped according to their number of carbon atoms and degree of branching. This allows a simple kinetic scheme, figure 5.7, to describe the complex hydrocracking process. Note that two arrows going to the same product denote that both products of a cracking reaction belong to lumps with the same degree of branching.

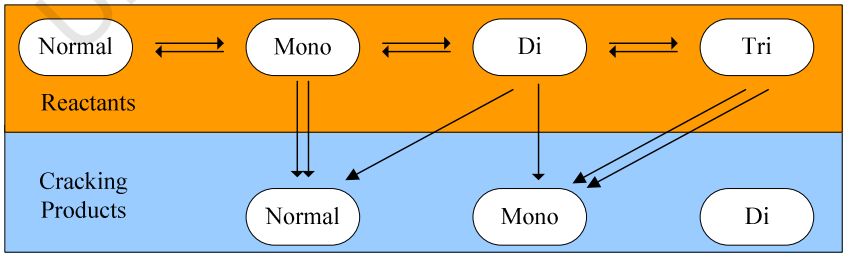

Figure 5.7: Lumped kinetic model

In this lumping scheme there are four lumps per carbon number representing the degree of isomerisation : normal, mono-branched, di-branched and tri-branched

alkanes. Due to limitations on the number of branches low carbon numbered molecules (<C8) can contain, the actual number of lumps in a system is:

$$\text{Hydrocarbon Lumps: } n_{lumps} = 4 \times C_{\max} - 13 \tag{5.1}$$

where C_{max} is the carbon number of the heaviest hydrocarbon within the system. Methane and ethane are neglected within the model, as they do not form part of the traditional hydrocracking reaction mechanism while hydrogen is required. Thus the total number of species within the model is:

$$\text{System Lumps: } n_{\text{mod\_}species} = 4 \times C_{\max} - 14 \tag{5.2}$$

5.6. CARBOCATION CONCENTRATIONS

The assumption of ideal hydrocracking implies that the dehydrogenation/ hydrogenation steps are in local equilibrium (see section 2.2.3) and hence:

$$C(i)_{olefin} = \frac{K(i)_{dehydrogenation} . C(i)_{paraffin}}{C_{H2}} \tag{5.3}$$

Martens (2000) demonstrates that the assumption of equilibrium in the protonation/deprotonation step provides a reasonable explanation of the kinetic parameters obtained by Svoboda et al. (1995) in the hydrocracking of octane. Although not conclusive evidence, it lends weight to the assumption of quasi equilibrium within these steps, thus:

$$C(i)_{Carbocation} = K_{protonation} . C(i)_{Olefin} \tag{5.4}$$

Based on the work of Laxmi-Narasimhan et al. (2006) it was assumed that there was no preferential adsorption of different hydrocarbon lumps from the liquid to the adsorbed phase and by assumption 3 for Model-C the concentration in the bulk liquid phase is equal to that on the catalyst surface.

Combining equations 5.1 and 5.2 the following expression for the carbocation concentrations on the catalyst surface are obtained:

$$C(i)_{Carbocation} = \frac{K_{protonation}.K(i)_{dehydrogenation}.C(i)_{paraffin}}{C_{H2}} \qquad (5.5)$$

Equation 5.5 shows that while the dehydrogenation equilibrium constant is dependent on carbon number, the protonation equilibrium constant is not. This is based on the idea that "the single event protonation rate coefficients only depend on the type of carbenium ion formed and are independent of the protonated olefin" (Martens, 2000). This is supported by quantum mechanical studies (Martens, 2000) that show almost no influence of olefin structure on the protonations activation energy and is in agreement with the work of Vynickier and Froment (1991) and Van Engelandt (1998).

5.7. STRUCTURAL CLASSES APPROACH

In order to accurately approximate the equilibrium between paraffins and olefins the technique of structural classes (Martens, 2000) was applied. Literature indicates that linear paraffinic isomers in the hydrocracking process with a significant presence are limited to three methyl or ethyl side chains (section 2.1.2).

Even with limitations on the number and size of branches, long chain length paraffinic hydrocarbons (e.g. $C_{100}H_{202}$) have a vast number of isomers. The Structural Classes Method places all potential isomers of a paraffin into one of ninety-five classes. Only predominantly linear paraffins with up to three ethyl and methyl sidechains are considered, significantly more classes exist for cyclic hydrocarbons.

The classes chosen are based on Bensons Group's (Benson et al., 1969) and all species within a class will have the same values of enthalpy, heat capacity and other thermodynamic properties when Benson's method is applied to them. Additionally all species within a class have a common global symmetry number.

Each paraffin class is taken to be in equilibrium with a reference olefin of the same carbon number. The overall equilibrium constant for a carbon number can thus be calculated from the formula:

$$K(i,T) = \sum_{i=1}^{n\_class} \frac{m_i}{\varsigma_i} e^{-\frac{\Delta G_{DEHYDROGENATION}}{R.T}} \qquad (5.6)$$

where m_i is the number of paraffins belonging to a class and ς_i is the symmetry number of the class.

The m_i/ς_i contribution in equation 5.6 accounts for the number of paraffins within a class that have a distinct structure but the same thermodynamic properties via Bensons group method. Hence if there are two different paraffin species with the same thermodynamic properties, according to Bensons correlations, m_i/σ_i will equal 2 accounting for both paraffins. Thus the equilibrium constant is represented as a summation of the equilibrium constants between every paraffin species (not just each class) and the reference olefin (Martens, 2000).

The series of 2-methyl-2-alkenes is chosen as a reference, with each reference olefin having the same number of carbon atoms as the lump to which it is being compared. The choice of reference olefin is unimportant as a result of two assumptions made in single event modelling of the hydrocracking kinetics:

1. *"single event protonation rate coefficients only depend on the type of carbenium ion formed and are independent of the protonated olefin."* Martens (2000)
2. *"single event rate coefficients for deprotonation depend both on the type of deprotonated carbenium ion and on the olefin formed"* Martens (2000)

The work of Martens (2000) is recommended for a detailed application of the full single events kinetics approach to hydrocracking systems as well as a proof that the nature of the reference olefin chosen is unimportant. The PhD thesis of Martens (2000) also provides detailed information necessary for the application of the Structural Classes Method, reproduced in Appendix 2.

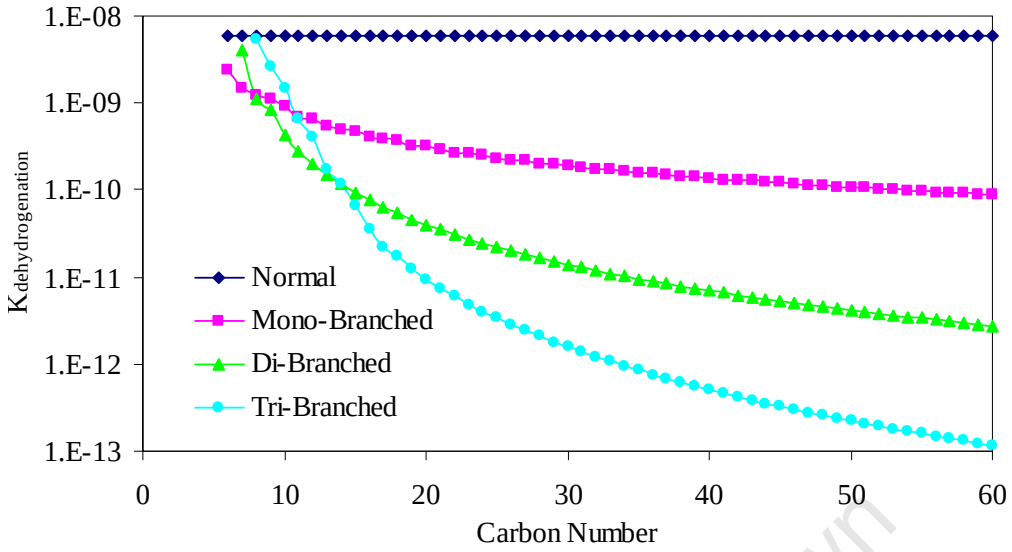

Figure 5.8: Dehydrogenation Equilibrium at 300˚C

In essence Structural Classes Method uses a second level of detailed lumping (classes) in a manner that allows the determination of the overall lumped dehydrogenation equilibrium constants which account for the dehydrogenation equilibrium of every hydrocarbon species in the system. Figure 5.8 depicts the dehydrogenation equilibrium for lumps with differing degrees of branching. The equilibrium constant for the normal paraffin lumps does not vary with carbon number.

This is confirmed in the work of van Steen and Claeys (2005) in which the difference in Gibbs free energy between n-olefins and n-parrafins of the same carbon number is shown to be approximately constant for molecules with greater than five carbon atoms. As species with less than six carbon atoms cannot undergo cracking via the mechanisms of β-scission considered in Model-C the dehydrogenation of hydrocarbons lighter than C_6 would have no impact on the model and have thus being neglected.

It was observed that the values of $K(i)_{dehydrogenation}$ decreased with increasing temperature however the quantitative trends between lumps remained constant.

5.8. RATES

5.8.1 β-scission Rates

The rate of Type-C β-scission on the acid sites was assumed to follow a linear relation with respect to the carbocation concentration:

$$r(i)_{Type-C} = (CN_i - 5).k_C.C(i)_{carbocation} \text{ where } 6 \le i \le n \quad (5.7)$$

where CN_i is the number of carbon atoms in molecule i. The rate of cracking may, using equation 5.5, be written as follows:

$$r(i)_{Type-C} = (CN_i - 5).k_C.K_{protonation}.K(i)_{dehydrogenation}.\frac{C(i)_{paraffin}}{C_{H2}} \quad (5.8)$$

the constants k_C and $K_{protonation}$ are grouped together and treated as one rate constant, $k_{C\_grouped}$:

$$r(i)_{Type-C} = (CN_i - 5).K(i)_{dehydrogenation}.k_{C\_grouped}.\frac{.C(i)_{paraffin}}{C_{H2}} \text{ for } 6 \le i \le n \quad (5.9)$$

$K(i)_{dehydrogenation}$ is determined via the structural classes method (see section 5.7). Types A and B cracking can be treated similarly:

$$r(i)_{Type-B} = (CN_i - 6).K(i)_{dehydrogenation}.k_{B\_grouped}.\frac{.C(i)_{paraffin}}{C_{H2}} \text{ for } 7 \le i \le n \quad (5.10)$$

$$r(i)_{Type-A} = (CN_i - 7).K(i)_{dehydrogenation}.k_{A\_grouped}.\frac{.C(i)_{paraffin}}{C_{H2}} \text{ for } 8 \le i \le n \quad (5.11)$$

The normalised collection of all concentration independent terms in the cracking rates (equations 5.9 to 5.11) is depicted in figures 5.9 (450˚C) and 5.10 (150˚C) and highlight some interesting trends in reactivity. Most noteworthy is the tendency of the

type C cracking constant to increase with carbon number the opposite tendency to that of the type B and type A constants. The oscillatory nature of the coefficients is due to variations in global symmetry between odd and even carbon numbered paraffins and is accounted for in dehydrogenation equilibrium constant via the Structural Classes Method. The oscillation is particularly marked for mono-branched species undergoing type C cracking as, with only one side chain, the symmetry in a large proportion of the classes used in the dehydrogenation equilibrium calculation depends on whether the carbon number is odd or even (Appendix 2).

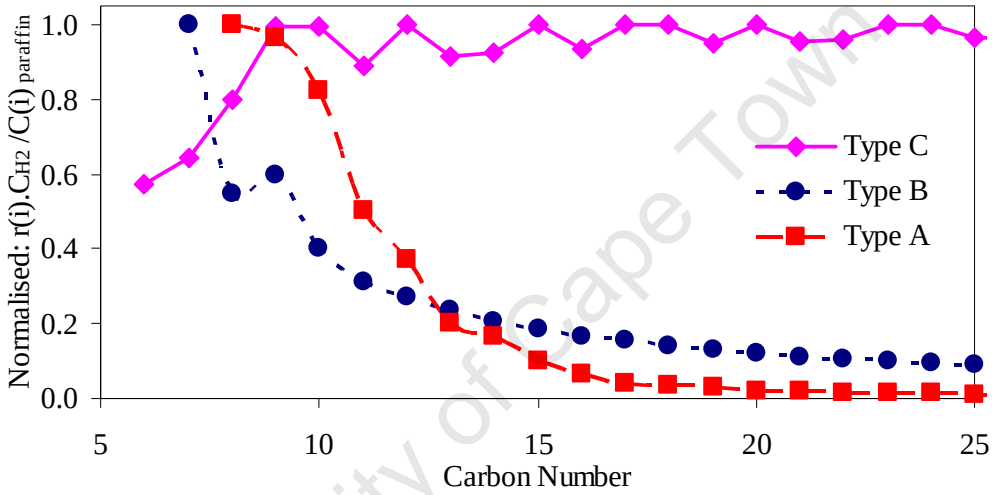

Figure 5.9: Cumulative cracking constant, 450˚C

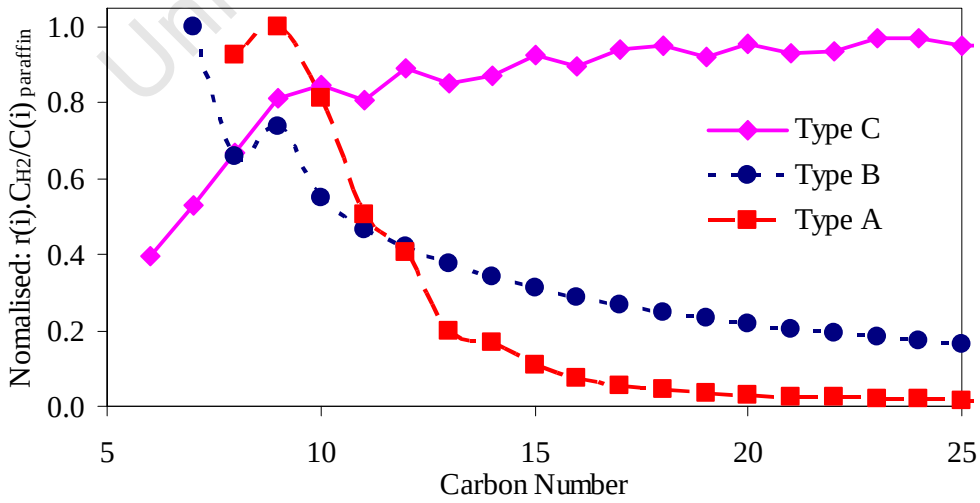

Figure 5.10: Cumulative cracking constant, 150˚C

It is clear from figures 5.9 and 5.10 that temperature has a relatively small effect on the way in which the cumulative constants vary with carbon number, with only small changes in the trends being observed over a 300˚C temperature range. One unusual change with temperature is the peak in the constants value at C_9H_{20} observed at low temperatures for type A cracking.

At all temperatures considered the value of the type B constant at C_9H_{20} does not follow the trend of other type B values. This is due to the dehydrogenation equilibrium constant and is a result of various species with ethyl side chains whose existence becomes possible at carbons numbers of nine and above.

Note that the feed distribution and isomerisation reactions will both change the way lumped cracking reactivity appears in reality.

5.8.2 Isomerisation Rates

The isomerisation between lumps was taken to be a reversible reaction. Consider the isomerisation of lump-1 (normal/linear) into lump-2 (mono branched):

$$r(i)_{isom12} = (CN_i - 4).k_{PCP1}.[C(i)_{carbocation,L1} - \frac{C(i)_{carbocation,L2}}{K_{isom12}}] \text{ for } 5 \le i \le n \qquad (5.12)$$

where k_{PCP1} and K_{isom12} are respectively the rate constant and equilibrium constant of the isomerisation reaction. K_{isom12} is calculated from the differences in Gibbs free energy of 2 reference compounds. The reaction can be written in terms of paraffin concentrations using equation 5.5:

$$r(i)_{isom12} = (CN_i - 4).k_{PCP1}.K_{prot}.[K(i)_{dehyd,L1}.C(i)_{par,L1} - \frac{K(i)_{dehyd,L2}.C(i)_{par,L2}}{K_{isom12}}].\frac{1}{C_{H2}}$$

$$\text{for } 5 \le i \le n \qquad (5.13)$$

Note that it is assumed in the above that both carbocations have the same protonation constants, i.e. both are secondary carbocations or both are tertiary carbocations. In all

groups of lumps with side chains both secondary and tertiary carbenium ion species are possible.

Both hydride and branch shift reactions are very rapid in comparison to other reactions (section 2.1.2) and thus it is reasonable to assume that within the lumps the paraffin species are in equilibrium. Hence there will always be species in both lumps isomerising that have the same protonation constant. The effect of isomerisation between species with different protonation constants is not taken into account in this model.

The rates of isomerisation between mono and di branched lumps:

Equation:

$$r(i)_{isom23} = (CN_i - 5).k_{PCP2}.K_{prot}.[K(i)_{dehyd,L2}.C(i)_{par,L2} - \frac{K(i)_{dehyd,L3}.C(i)_{par,L3}}{K_{isom23}}].\frac{1}{C_{H2}}$$

for $6 \le i \le n$ (5.14)

and the isomerisation between di and tri branched lumps :

$$r(i)_{isom34} = (CN_i - 6).k_{PCP3}.K_{prot}.[K(i)_{dehyd,L3}.C(i)_{par,L3} - \frac{K(i)_{dehyd}.C(i)_{par,L4}}{K_{isom34}}].\frac{1}{C_{H2}}$$

for $7 \le i \le n$ (5.15)

can be similarly derived. Note that lump-3 in this case refers to the di-branched isomers and lump-4 the tri-branched isomers.

6. RESULTS

6.1. MODEL TESTING

Testing of the hydrocracking model was limited by the lack of comprehensive experimental data. Open literature only reports the results of a few runs in enough detail to be of practical use in modelling. As a minimum of seven runs on the same catalyst is needed to obtain any degree of accuracy in a six constant model, traditional parameter optimisation could not be performed. In order to get a qualitative idea of the models prediction capabilities the sum of squares error in the hydrocracking product spectra was minimised.

Initially minimisation was performed using gradient based methods (Levenberg-Marquard via LMDIF routine, Garbow et al., 1980); however the numerical gradients were unstable and the model function proved too complex for solution within reasonable time. The direct optimisation simplex method of Nelder and Mead (implemented using an in-house routine) proved more successful in this regard.

The gradient of the error function with respect to parameter values was calculated by varying each parameter by 1% below and above the parameters value. This information was then used to calculate the variances in the parameters. A modification of the model program was written to perform these calculations. However, the assumption of a linear model for variance was unreasonable and the values obtained unrealistic.

In almost all of the cases regressed some information about the feeds was not published and needed to be assumed. As a result of the errors introduced by this, the model is expected to perform better if applied in an industrial situation where all information is disclosed.

Conversion was based on the reaction of hydrocarbons with 23 or more carbon atoms into hydrocarbons containing less than 23 carbon atoms, see section 4.1.

In order to test the model's internal consistency a hypothetical ASF distribution (α=0.92) was reacted to 50% conversion (figure 6.1) at typical conditions and user specified kinetic parameters (table 6.1). The optimisation routine was then used to re-determine the kinetic parameters for the data generated from variety of different starting points.

The kinetic parameters determined from regressing the data were in all cases the same as those originally used to generate the product, demonstrating that the model is internally consistent.

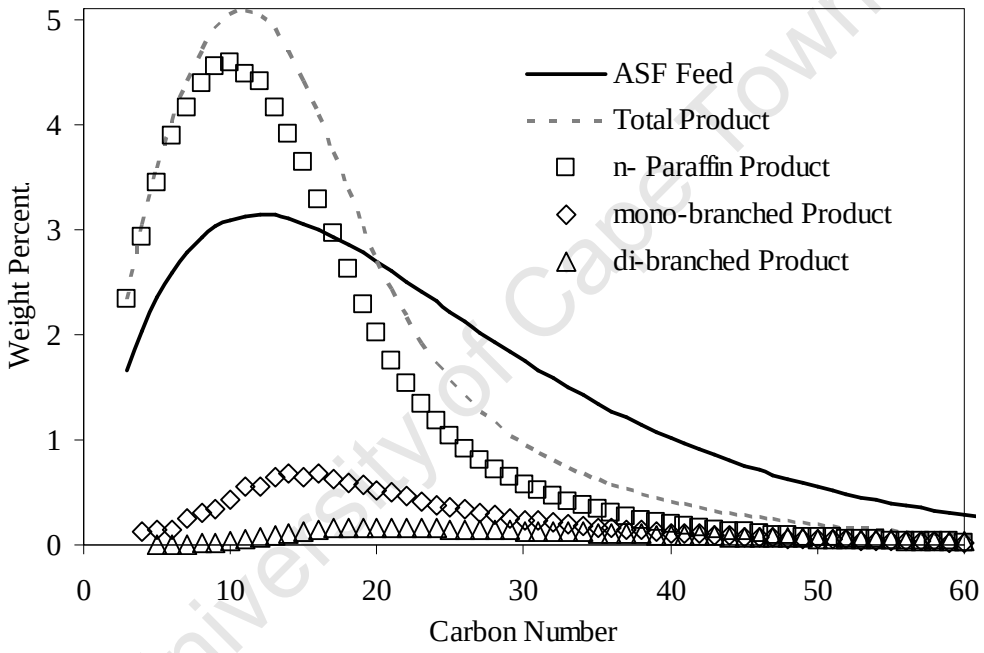

Figure 6.1: Hydrocracking of ASF (α = 0.92) feed to 50% conversion at 300˚C, 50bar, H_2/Hydrocarbon=10 (molar basis)

Figure 6.1 highlights an interesting trend in the simulated isomer carbon number distributions. As the degree of branching in an isomer increases the location of the maximum weight peak increases and the distribution broadens. This is due to differences between the isomers in critical properties and dehydrogenation equilibrium constants. Note that in figure 6.1 the tri-branched product has not been displayed as its concentration is too low (as a result of the rapid type-A β-scission) for it to be distinguished on the same scale as the total product, the C_{61}-C_{90} range is not shown for the same reason.

6.2. DATA ANALYSIS

Literature that publishes data with detailed information on the isomer product from the cracking of heavy paraffins does not exist due to limitations in current analytical techniques. As a result the parameters need to be regressed based on limit product information. Regressions were performed using the data generated from the ASF distribution discussed in section 6.1. The data used in performing the regressions was limited in order to simulate real data. In the first case only the overall product carbon number was available for regression and in the second both the overall distribution and the ratio of normal to lumped iso-paraffins for each carbon number were accessible.

Table 6.1: Parameter estimation based on limited information on the product

Parameter	Actual	Overall distribution only	Overall distribution and lumped iso/n ratio	Initial Guess
k_A	12000	11273	4055	10000
k_B	700	769	831	1000
k_C (reference)	100	100	100	100
k_{PCP1}	200	156	186	100
k_{PCP2}	200	167	192	100
k_{PCP3}	200	108	145	100

Table 6.1 reveals that for both cases in which limited information is available the rates of isomerisation decreased with the k_{PCP2} rate being significantly higher than the k_{PCP3} rate. In both cases the rate of type-B β-scission was found to be greater than its actual value and that of type-A β-scission below its actual value. In both cases the sum of squared error was minimal and of the same order of magnitude as the original parameters when they were run on the limited data sets. All of which implies that limited isomer information allows a higher rate of type-B β-scission to subsume much of type-A's influence. A decrease in accuracy with the addition of the iso/normal paraffin ratios to the overall distribution is no doubt due to lumping the paraffinic isomers together.

While the data regressions done in this thesis are not equivalent to rigorous parameter estimation (which requires data from several experiments and is not available in literature) it is very possible that the parameters obtained through rigorous optimisation on limited data could be affected similarly. From the data it also appears as if the constants are not unique and perhaps can be represented by cracking rates and a single isomer rate.

6.3. SMDS PROCESS

The data published on the SMDS process (Sie et al., 1991) was simulated, see figure 6.2. As exact process conditions were not specified a temperature of 300˚C was used for both runs in order that both runs might be determined using one set of parameters. Further a pressure of 30bar was selected for both runs, the temperature and pressure chosen are within the range of operating conditions given by Sie et al. (1991) for this process (300˚C-350˚C & 30bar-50bar).

It was further assumed (lacking more detailed information) that the molar hydrogen to hydrocarbon ratio at the inlet was 10:1 and that the feed consisted purely of n-paraffins. The feed published by Sie et al. (1991) was extrapolated from $C_{40}H_{82}$ to $C_{80}H_{162}$, by following the recursive relation observed between $C_{20}H_{42}$ and $C_{40}H_{82}$. Note that the ASF distribution did not give a good approximation (or extrapolation) to this feed at any chain growth probability. The C_{23+} conversions were calculated directly from the data presented by Sie et al. (1991) to be 0.42 and 0.74 for the medium and severe SMDS runs respectively.

Table 6.2: Model Parameters for SMDS process at 300˚C

Parameter	Relative Value
k_A	3.36E+04
k_B	1.26E+03
k_C (reference)	1.00E+00
k_{PCP1}	4.89E+00
k_{PCP2}	7.88E+01
k_{PCP3}	3.71E+01

The parameters obtained from minimising the error in these runs at the conditions discussed are presented in table 6.2. These parameters were obtained from a limited data set and from their values it appears as if the effect noted previously (section 6.2) in which type-B β-scission subsumes some of type-A's influence is at work here.

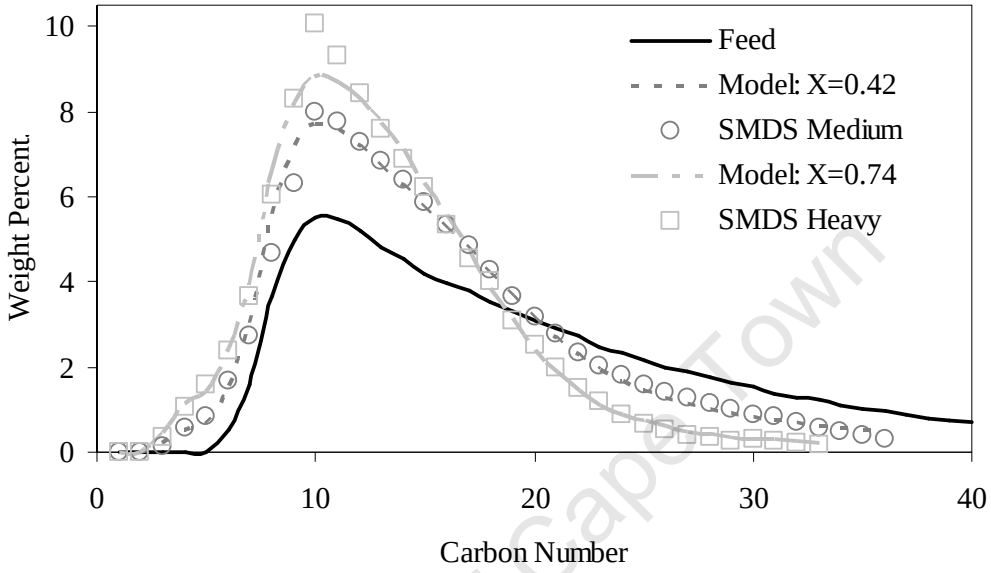

Figure 6.2: SMDS process with simulation conditions of 300˚C, 30bar and H2:Hydrocarbons ratio of 10:1 (molar)

The model gives an extremely accurate prediction of the carbon number distribution of the SMDS process with results well within the error of the stream analysis, which was performed via TBP – GLC without segmenting the feed (Sie et al., 1991). The model shows a significantly more accurate prediction, particularly for hydrocarbons with a chain length of less than twenty, than the work of Accolla (2006).

The parameters obtained in this model (table 6.2) for different β-scission types follow the trends in β-scission rate predicted in literature, see section 2.1.3. Increasing the percentage of isomers in the feed from zero to five weight percent of the same carbon numbered n-paraffin yielded minimal difference in the parameters obtained from regression or in the sum of squared error, table 6.3.

Table 6.3: Comparison of parameters and error at different isomer feed concentrations

Parameter	0% isomers in feed	5% isomers in feed
kA	3.36E+04	4.02E+04
kB	1.26E+03	1.38E+03
kC (reference)	1.00E+00	1.00E+00
kPCP1	4.89E+00	5.48E+00
kPCP2	7.88E+01	8.51E+01
kPCP3	3.71E+01	4.18E+01
Sum of Squared Error	4.81	4.80

Table 6.4: Real and simulated SMDS process middle distillate yield and selectivity

	SMDS Medium			SMDS Heavy		
	Real	Model-C	Model-A	Real	Model-C	Model-A
Yield	69	67	57	71	70	74
Selectivity	0.80	0.78	0.87	0.75	0.74	0.81

Table 6.4 shows that Model-C is able to accurately simulate the middle distillate yield and selectivity. Further Model-C demonstrates a significant improvement in prediction accuracy over Model-A, of Accolla (2006).

6.4. EXPERIMENTAL FTS WAX CRACKING WITH ISOMER DATA

Experiments performed by Pellegrini et al. (2008) in order to validate their modelling of hydrocracking reactions were adapted to test this model. The experiments used an amorphous silica-alumina catalyst in powdered form with a platinum metal function to hydrocrack a Fischer-Tropsch wax fraction in a trickle bed reactor.

The experimental product was found by Pellegrini et al. (2008) using separate GC analyses for the vapour and liquid phases. The unexpected decrease in weight percent between C_4 and C_7 is probably a result of technical issues within the analysis rather than the real physical result, see figure 6.3.

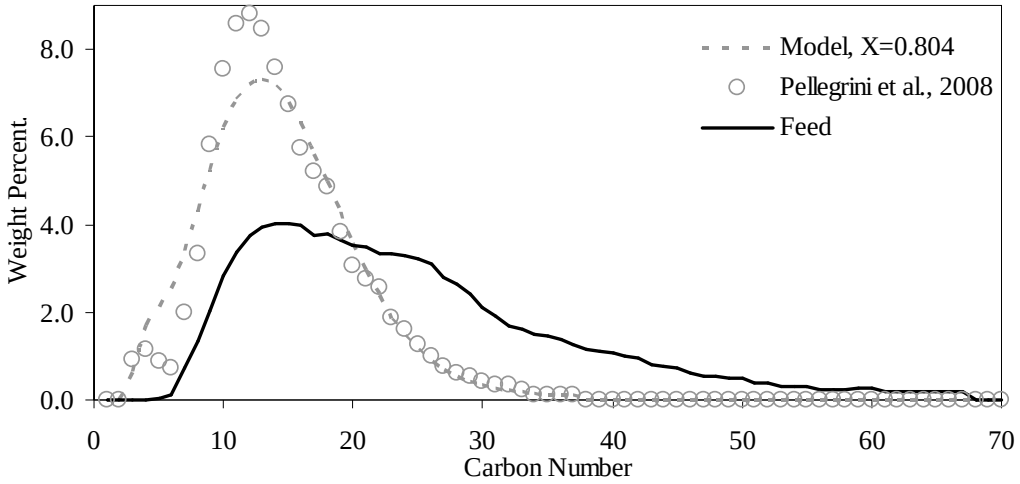

Figure 6.3: Model vs. data, 367˚C, 54bar and H2/wax = 12 (molar)

Figure 6.3 shows that the model predicts the general distribution while failing to predict the magnitude of the peak at C_{11} and the dip in reactivity between C_4 and C_7. Much of the error in this model is possibly due to errors in the technically challenging experimental product analysis. It is thus difficult to ascertain the actual error of the model in this instance. However, the model at a minimum provides a qualitative prediction of the data. Parameters with similar values and trends to the parameters predicted for the SMDS process were obtained, table 6.5.

Table 6.5: Model Parameters for data of Pellegrini et al. (2008), at 367˚C

Parameter	Relative Value
kA	1.17E+04
kB	1.56E+02
kC (reference)	1.00E+00
kPCP1	1.73E+00
kPCP2	3.81E+01
kPCP3	1.42E+00

Table 6.6: Real and simulated middle distillate yield and selectivity for data of Pellegrini et al. (2008)

	Real	Model-B	Model-C
Yield (wt%)	75.8	71.5	71.8
Selectivity	0.83	0.82	0.78

Model-C was able to accurately approximate the middle distillate yield to a slightly higher level of accuracy than Model-B however it was found to be less accurate than Model-B in its prediction of middle distillate selectivity (Table 6.6).

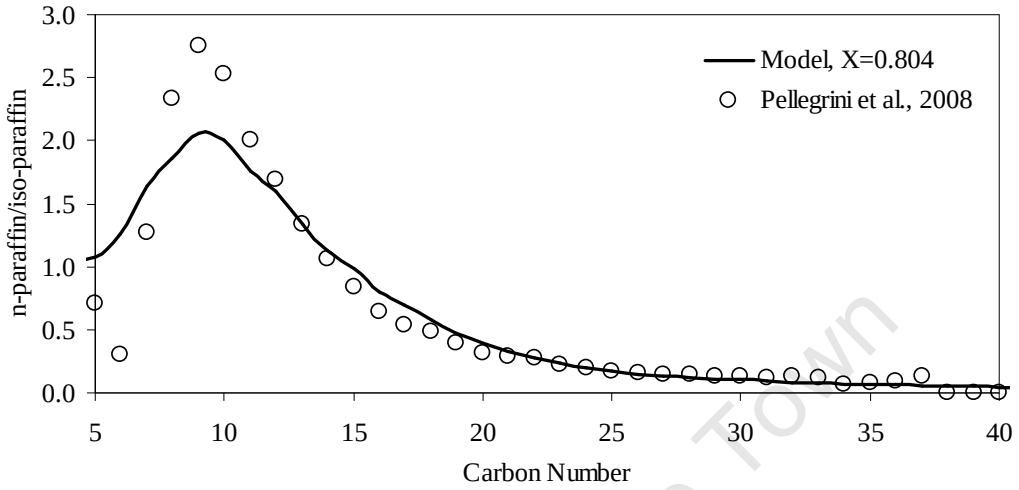

Figure 6.4: Isomer ratio-model vs. data, 367˚C, 54bar and H2/wax = 12 (molar)

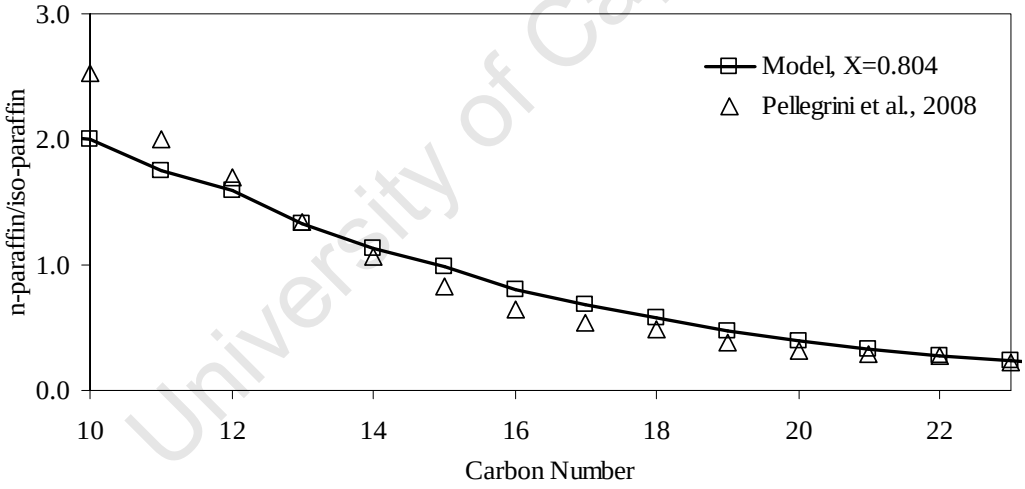

Figure 6.5: Isomer Ratio - model vs. data, 367˚C, 54bar and H2/wax = 12 (molar)

The model demonstrates good prediction of the n-paraffin/iso-paraffin ratio for all except the lowest carbon numbers (<11), figure 6.4. The difference between model prediction and data at low carbon numbers is also thought to be due to errors in the experimental product analysis. Figure 6.5 depicts the n-paraffin:iso-paraffin ratio in the middle distillate range. The prediction of the isomers in the middle distillate product (which is the primary interest in this work) is extremely accurate. This indicates that fuel properties may be successfully estimated from the model results.

6.5. SASOL M5 FTS WAX FRACTION

Leckel et al. (2006) cracked an iron based FTS wax fraction, designated M5 wax, using an unsulphided Pt on SiO_2-Al_2O_3 catalyst, modified with MoO_3. The catalyst had an average pore diameter of 10nm which implies that capillary effects within the catalyst are minimal, see figure 4.9.

At the pressures used by Leckel et al. (2006) this model was found to give a significant improvement in accuracy over that of the Model-B (section 4.2) at the same pressure, table 6.7. The model had a similar level of accuracy to the Model-B runs when they were operated at between four and eight times the pressure reported, table 4.1. This leads to the idea that higher pressures used in Model-B to simulate capillary condensation were in fact mimicking the effect of the dehydrogenation and isomerisation steps in Model-C.

Table 6.7: Sum of Squared Error for the M5 wax runs

Conditions	Sum of Squared Error
X = 0.46 & P = 70bar	13.2
X = 0.48 & P = 50bar	5.78
X = 0.81 & P = 35bar	7.48

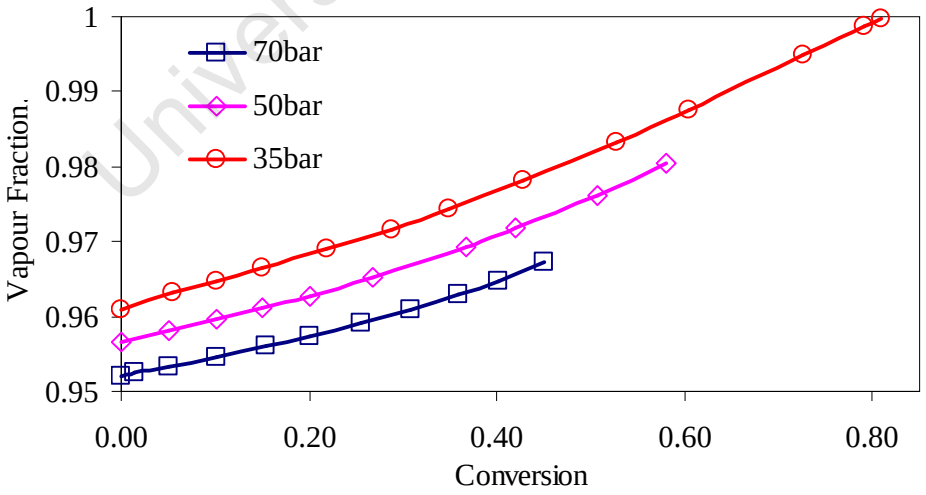

Figure 6.6: Model Predicted Vapour Fraction Evolution with Conversion

Note that in contrast to the Model-B (figure 4.6) the low pressure high conversion run does not run out of liquid during the course of the reaction (figure 6.6). This allows reaction to the full run conversion of 0.81, no doubt contributing to the much greater accuracy observed in the second model for this run. The greater model accuracy is a result of the kinetics more precisely approximating those of the real system and further highlights the strong coupling between the kinetics and the phase equilibrium in hydrocracking systems.

Figures 6.7 to 6.9 show the model predictions of the experimental results (Leckel et al., 2006). The model provides a good qualitative prediction of the result, but does not predict both the breadth and location of the peak in carbon concentrations in the C_{20} to C_{30} range. This is thought to be due to either mass transfer limitations in the system (see section 4.2) or inaccuracy in the product analysis as two fractions were joined in this region (the feed was fractionated into C_5-C_9, C_{10}–C_{22} & C_{23+} and analysed via simulated distillation).

Parameters for the results obtained are shown in table 6.8. Unlike the parameters of sections 6.3 and 6.4 there is not a sensible trend in rate between the different β-scission types. This raises the suspicion that the model may be trying to account for other effects, the most likely of which are: capillary condensation, mass transfer, non-ideal hydrocracking, error in product analysis or a combination of the aforementioned.

Table 6.8: Model Parameters for data of Leckel et al. (2006), at 370˚C

Parameter	Relative Value
kA	2.43E+02
kB	1.52E-01
kC (reference)	1.00E+00
kPCP1	2.03E+02
kPCP2	3.34E-01
kPCP3	1.84E-02

Non-ideal hydrocracking occurs when equilibrium can no longer be assumed for the dehydrogenation kinetic step (In the current terminology, ideal hydrocracking is equivalent to the (de)-hydrogenation reactions being in equilibrium). Thybaut et al. (2005) found that four conditions favour non-ideal hydrocracking:

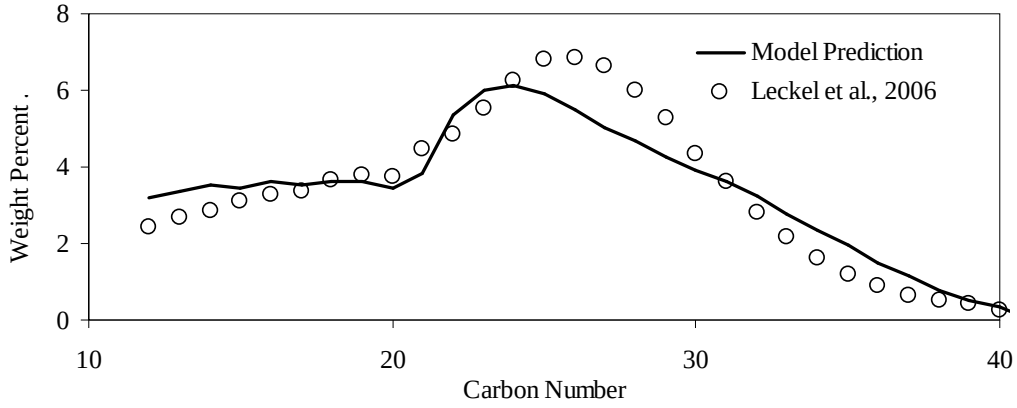

Figure 6.7: Model prediction of experimental data: X=0.46, 70bar, 370˚C, WHSV 1.0h^{-1}, H_2/Hydrocarbon =21 (molar)

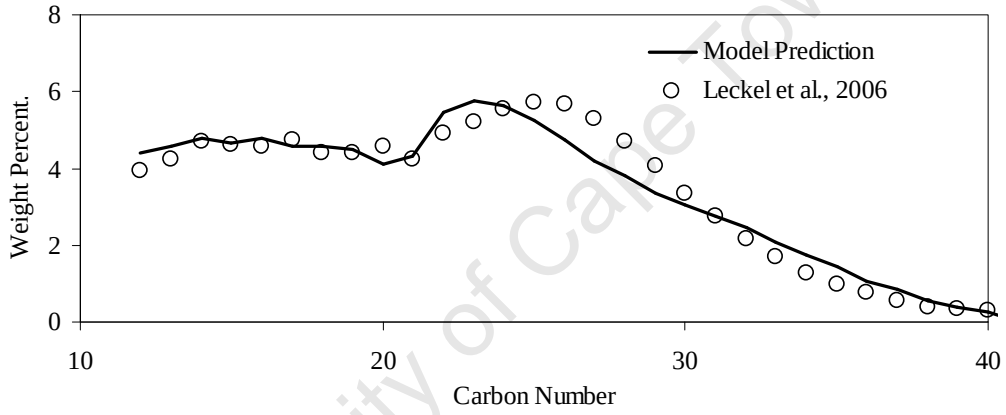

Figure 6.8: Model prediction of experimental data: X=0.58, 50bar, 370˚C, WHSV 1.0h^{-1}, H_2/Hydrocarbon =21 (molar)

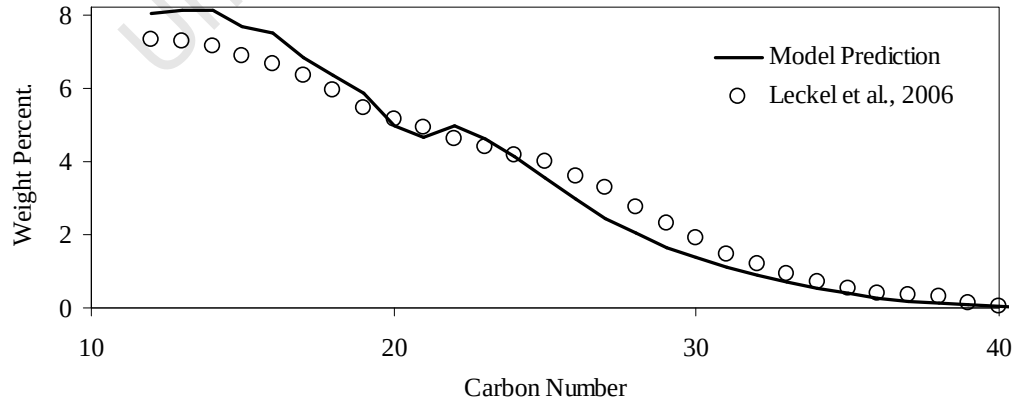

Figure 6.9: Model prediction of experimental data: X=0.81, 35bar, 370˚C, WHSV 1.0h^{-1}, H_2/Hydrocarbon =21 (molar)

1) low pressure
2) high temperature
3) high hydrogen:hydrocarbon inlet ratio
4) higher reactant carbon number

In these experiments all conditions except the first are satisfied. Model accuracy decreases with decreasing pressure which could indicate non-ideality. It is however not possible at this stage to distinguish this effect from the others mentioned.

Table 6.9 Model-C vs. Real (Leckel et al., 2006) Middle Distillate Selectivity and Yield at 370ºC, WHSV = 1.0h^{-1} and H2/Hydrocarbon= 21 (Ratio Molar)

P (MPa)	X	Yield (wt%)		Selectivity	
		Real	Model	Real	Model
3.5	81	61	58	0.75	0.71
5.0	58	46	46	0.79	0.76
7.0	46	39	39	0.84	0.78

From table 6.9 it can be seen that Model-C accurately predicts the middle distillate yield to within 3 wt%. Model prediction of product selectivity is not as accurate, and is of a similar level of accuracy to Model-B. The under-prediction of selectivity by Model-C is thought to be due to an overestimation of the light components ($<C_{10}$) in the model product. Data-points from this range were not published and hence the model parameters were regressed without reference to this region. The lack of data for the low carbon numbered species is no doubt also responsible for the unusual parameter values obtained.

6.6. SUMMARY

Model-C was successfully able to approximate the SMDS process carbon number distribution to a high degree of accuracy with the model predictions of product concentrations for lighter hydrocarbons ($<C_{20}$) showing a marked improvement over

those of Model-A (Accolla, 2006). Values of the β-scission parameters obtained were sensible in terms of the theories for hydrocracking kinetics.

Exact process conditions and the isomers distribution in the feed were unknown for the SMDS process, however values for the process conditions were chosen within the ranges given by Sie et al. (1991) and the parameters obtained to be relatively insensitive to the concentration of isomers in the feedstock, with similar parameters being obtained for both 0% and 5% mono-branched isomers in the feed. Model-C was able to accurately predict the middle distillate yield and selectivity to within 2% of their value, which was a significant improvement over Model-A of Accolla (2006).

Results from Pellegrini et al. (2006) were also successfully simulated with good predictions of both the overall carbon number distribution and the ratio of n-paraffins to iso-paraffins. The prediction of the normal to isomer ratio was particularly good within the middle distillate range, which is a promising sign that fuel properties could also be simulated using the model. The greatest error in prediction was found between C_6 to C_{10} and is thought to be due to errors in the technically challenging product analysis within this region. Model-C demonstrated a slight improvement over Model-B in predicting middle distillate yield, however it was less accurate than Model-B in its prediction of middle distillate selectivity.

Parameters obtained for the Pellegrini et al. (2008) data have very similar values to those found for the SMDS process. Both sets of parameters high values of the mono-branched to di-branched isomerisation rate and a relatively high rate of type-B β-scission. It is thought that the parameters obtained in these runs are incorrect as a result of the limited data on the product isomers (section 6.2) with which they were determined and that type-B cracking is taking the place of much the cracking done by type-A in reality.

The model was able to satisfactorily predict the outcomes of experiments done by Leckel et al. (2006) on the SASOL M5 wax fraction (figures 6.7 to 6.9 and table 6.9). Parameters obtained from the regression of this data however did not have sensible values in terms of hydrocracking kinetic theory. Possible reasons for this are mass transfer limitations in the system or the dehydrogenation kinetic step not being in

equilibrium, both of which are not accounted for in the model. The experimental product analysis was done in four fractions and also has potential for error.

It is clear that the model as a minimum can qualitatively predict the experimental results of a diverse variety of data, which may be of significant value in process optimisation. Accurate quantitative prediction of experimental parameters requires the model to be tested against a full set of experimental runs at a variety of conditions (the data for this is unavailable in open literature) in order to determine the applicability of the model and influence of other phenomena.

7. CONCLUSION

7.1. OUTCOMES

All five goals outlined in section 2.6 of this project were met.

The EOS describing the VLE was upgraded from basic Peng-Robinson (1976) (Model-A) to the modified equation described by Twu et al. (1995) (Model-B) which was developed specifically for use with heavy hydrocarbons ($>C_{30}$). On investigating the behaviour of the VLE in the M5 wax system different trends between Model-A (Accolla, 2006) and Model-B with varying temperature, pressure and conversion were observed. The different trends observed were a result of two competing kinetic effects in the hydrocracking reaction; namely the consumption of hydrogen which lowers the vapour fraction as reaction proceeds, and the reaction of heavy hydrocarbons to lighter ones which does the opposite. Thus the distribution of hydrocarbon species within the reactor, the process conditions and the way conversion is defined will determine which effect dominates the VLE in the region of interest.

Middle distillate yield and selectivity for the data of Pellegrini et al. (2008) were calculated (section 6.4). Model-B predicted selectivity was extremely close to that of the real data (within 1%) and yield was also reasonably predicted (within 4%).

Analysis of experimental data from Leckel et al. (2006) shows that product diesel selectivity, diesel yield and cloud point (a measure of the fuel quality) are functions of conversion rather than of reactor conditions. Thus the carbon number distribution of the feed has a much greater influence on the hydrocracking product fuel than the process variables for this feed. This is thought (but not proved) to be generally true in hydrocracking reactions. Model predictions of both yield and selectivity closely matched those of the experimental data (table 4.2) highlighting Model-B`s usefulness to the synthetic fuels industry.

Model-B was also used to simulate the product carbon number distributions from literature (Leckel, 2005; Leckel et al., 2006; Pellegrini et al., 2008) for the hydrocracking of three industrial F-T waxes. The iron catalysed FTS slurry wax (Leckel, 2005) product carbon number distribution was poorly predicted by the model; however this is thought to be due to inaccurate analysis of the product. The model was able to provide a better prediction of the carbon distribution of the FTS wax cracked by Pellegrini et al. (2008) but did not predict a peak of the same magnitude at $C_{12}H_{26}$.

Model-B prediction of the product carbon number distribution of experiments by Leckel et al. (2006) on the cracking of a SASOL M5 wax fraction was accurate for the low conversion, high pressure, runs. This was not the case at higher conversions as a result of the unusually high reactivity of the lighter hydrocarbons.

The unusually high reactivity of the lighter hydrocarbons in the M5 wax is potentially due to kinetic steps, dehydrogenation etc, in the hydrocracking mechanism that have not been incorporated into the kinetic scheme. A pseudo-pressure effect whereby accuracy in product distribution prediction increased on running the model at higher than specified operational pressures was observed and thought to be due to the incomplete model kinetics.

Model-C utilised a lumping scheme based on the carbon number and degree of branching of a species. A kinetic scheme which included isomerisation and dehydrogenation reactions was derived. The Structural Classes Method of Martens (2000) was implemented in order to describe the dehydrogenation equilibrium.

Model-C was able to satisfactorily predict the outcomes of experiments done by Leckel et al. (2006) on the SASOL M5 wax fraction (figures 6.7 to 6.9 and table 6.9). The kinetic scheme was accurately able to predict the carbon number distribution without the need to operate at elevated pressure. Parameters obtained from the regression of this data however did not have sensible values in terms of hydrocracking kinetic theory. The reasons for this are unclear and it seems likely that there is another phenomenon in this system (possibly mass transport) that is significantly affecting the product distribution.

The SMDS process carbon number distribution was successfully approximated with Model-C to a high degree of accuracy with the model predictions of product concentrations for lighter hydrocarbons ($<C_{20}$) showing a marked improvement over those of Model-A (Accolla, 2006). Values of the β-scission parameters obtained were sensible in terms of the theories for hydrocracking kinetics. Exact process conditions and the isomers distribution in the feed were unknown for the SMDS process. However values for the process conditions were chosen within the ranges given by Sie et al. (1991) and the parameters obtained to be insensitive to the concentration of isomers in the feedstock, with similar parameters being obtained for both 0% and 5% mono-branched isomers in the feed.

Results from Pellegrini et al. (2006) were also successfully simulated with good predictions of both the overall carbon number distribution and the ratio of n-paraffins to iso-paraffins. The prediction of the normal to isomer ratio was particularly good within the middle distillate range which is a promising sign that fuel properties could also be simulated using the model. The greatest error in prediction was found between C_6 to C_{10} and is thought to be due to errors in the technically challenging product analysis within this region.

Parameters obtained for the Pellegrini et al. (2008) data have very similar values to those found for the SMDS process. Both sets of parameters have high values of the mono-branched to di-branched isomerisation rate and a relatively high rate of type-B β-scission. It is thought that the parameters obtained in these runs are incorrect as a result of the limited data on the product isomers. In section 6.2 it was demonstrated with a typical ASF distribution (α=0.92) that regression with incomplete isomer data lead parameters which allowed higher type-B cracking to take the place of much the cracking done by type-A in reality. It is evident that this is happening for these simulations and will continue to be a problem in Model-C (and models in literature) unless detailed isomer data is available in parameter estimation and regression.

In terms of middle distillate yield and selectivity Model-C showed significant improvement over Model-A of Accolla (2006) and was able to accurately predict the middle distillate yield and selectivity to within 2% of their value. For the data of Pellegrini et al. (2008) Model-C demonstrated a slight improvement over Model-B in

predicting middle distillate yield, however it was less accurate than Model-B in its prediction of middle distillate selectivity. Similar levels of accuracy in yield and selectivity prediction of the M5 wax stream were obtained from Model-B (table 4.2) and Model-C (table 6.9).

It is clear that both Model-B and Model-C as a minimum can qualitatively predict the yield and selectivity of a diverse variety of data, which may be of significant value in process optimisation. Model-C was able to accurately reproduce the product carbon number distributions including that of the iso-paraffin to normal-paraffin ratio. However, regression was unable to produce sensible parameters for Model-C. Additionally Model-B requires only two parameters for design and control purposes as opposed to Model-C which requires six. From this it is thought that Model-B has the most potential for immediate industrial application.

7.2. MODEL IMPROVEMENTS

There are several improvements that may be made to the current models to improve their description of the hydrocracking system.

For both models:

1. Implementation of a Gibbs Excess Model in order to accurately predict the Binary Interaction Parameters for the VLE.
2. Inclusion of inter-phase mass transport limitations in the models.
3. Creation of a model interface to allow for easy use by third parties (industry/academia)
4. Use of more rigorous reactor design equations to more accurately describe the process flow dynamics.

For Model-C:

5. Examine the effect of ‘non-ideal’ hydrocracking (where the (de)hydrogenation steps are not in equilibrium) and how to distinguish this effect from transport limitations.

6. More detailed mechanistic path e.g. tri-branch isomer species undergoing type-B and type-C β-scission reactions and not just type-A.
7. Look at the impact of distinguishing between types-B1 and B2 cracking and inclusion of type-D β-scission and hydrogenolysis mechanisms.
8. Obtaining/creating correlations for the prediction of product fuel properties (Cetane Number, Pour Point and Cold Flow) from the isomer product data.

7.3. THE WAY FORWARD

A large difficulty in model testing is the lack of a complete set of experimental data from which parameter estimation can be rigorously performed and the models ability to extrapolate to different conditions and feeds can be accessed. Generation of this data or obtaining it via partnering with industry or other academic institutions is central to the continuation of this work.

The following experiments are recommended in order to test for the presence of various transport effects:

1. Test for external (inter-phase) transport limitations via varying flow velocity while keeping residence time constant.
2. Test for internal mass transport limitations with different catalyst particle sizes while ensuring that external transport limitations are no-existent or already quantified.

Note that it is important that product comparisons be made at constant equivalent conversion. It is recommended that temperature, pressure and conversion are varied in the experimental programme in order for accurate parameter estimation.

Following model validation the model could be used to optimise not just process conditions but the feed carbon number distribution as well. This could be done in conjunction with a rigorous FTS process model or by use of a simple ASF type model in order to provided valuable information for overall plant optimisation.

Further inducing inter-phase mass transfer limitations could improve product selectivity. Including this phenomenon within the model allows for investigation of this effect and the optimisation of the gas and liquid phase space velocities.

Much of the ambiguity in literature is due to the use of lumped conversion. It is thought that a new definition of conversion should be used in analysing hydrocracking data. A definition based on the consumption of carbon-carbon bonds as cracking proceeds should be investigated and may avoid the distortion of results that occurs when using a lumped measure of conversion.

In order for a model to be of practical use to industry it has to be able to accurate approximate the real system output with a minimal parameters. It is thus thought that the two-parameter (Model-B) is of potential interest to industry. It would be beneficial to look at other kinetic approximations in order to determine the optimal industrial model in terms of reliable data generated versus the number of parameters used, specifically:

1. Model-D: 1 cracking parameter and 1 isomerisation parameter
2. Model-E: 2 cracking parameters and 1 isomerisation parameter
3. Model-F: 1 cracking parameter, 1 isomerisation parameter and a parameter for dehydrogenation ('non-ideal' hydrocracking kinetics)
4. Other models with less than 5 parameters that can approximate the hydrocracking process

The hydrocracking models derived in this study (or descendants based them) are potentially a very powerful tool for optimisation of process economics. The model's accuracy in predicting product selectivity and yield coupled with its capacity to predict fuel quality (via isomer distributions) allows for prediction of the value of the product fuels. This will ultimately allow for process control that takes into account latest online fuel price indictors and optimises production accordingly, allowing refineries to respond to market trends and thus maximising profit.

REFERENCES:

Accolla C. (2006). *A Reactor model for FT wax Hydrocracking*, University of Cape Town, MSc Thesis.

Ancheyta J., Sánchez S., Rodriguez M.A. 'Kinetic modelling of hydrocracking of heavy oil fractions: A review.' *Catalysis Today* 109:76, 2005.

Anderson R.B. (1984). *The Fischer Tropsch Synthesis*, Academic Press, Orlando, pp. 100-117.

Ambrose D. (1978, 1979 & 1980). *National Physical Laboratory Reports Chem*, Middlesex, United Kingdom.

Archibald R.C., Greensfelder B.S., Holzman G., Rowe D.H. 'Catalytic Hydrocracking of alphatic hydrocarbons'. *Ind. & Eng. Chem. Res.*, 52:745, 1960.

Baltanas M.A., Froment G.F. 'Computer Generation of Reaction Networks and Calculation of Product Distributions in the Hydroisomerisation and Hydrocracking of Paraffins on Pt containing Bifunctional Catalysts.' *Comp. Chem. Eng.* 9:71, 1985.

Baltanas M.A. , Van Raemdonck K.K., Froment G.F., Mohedad S.R. 'Fundamental Kinetic Modelling of Hydroisomerisation and Hydrocracking on Noble-Metal-Loaded Faujasites. 1. Rate Parameters for Hydroisomerisation'. *Ind. Eng. Chem. Res.*, Vol. 28, No. 7:899, 1989.

Basak K., Sau M., Manna U., Verma R.P. 'Industrial hydrocracker model based on novel continuum lumping approach for optimization of petroleum refinery.' *Catalysis Today*, 98:253, 2004.

Benson S.W., Cruickshank F.R., Golden D.M., Haugen G.R., O'Neall H.E., Rodgers A.S., Shaw R., Walsh R., 'Additivity rules for the estimation of thermochemical properties,' *Chemical Review*, Vol 69.,1969, pp.279.

Böhringer W., Kotsiopoulos A., Fletcher J.C.Q. 'Selective Fischer-Tropsch Wax Hydrocracking – Opportunity for Improvement of Overall Gas-to-Liquids Processing'. *Proc. International R&D Forum on oil, Gas and Petrochemicals (IRDF), Kuala Lumpur, Malaysia, Petronas Research & Scientific Services (eds)*, 2004.

Böhringer W., Kotsiopoulos A., de Boer M., Knottenbelt C., Fletcher J.C.Q. 'Selective Fischer-Tropsch Wax Hydrocracking – Opportunity for Improvement of Overall Gas-to-Liquids Processing'. *Studies in Surface Science and Catalysis*, Vol. 163, 2007, pp.345–365.

Brouwer D.M., (1980). *Reactions of Alkylcarbenium Ions in Relation to Isomerisation and Cracking of Hydrocarbons*. In *Chemistry and Chemical Engineering of Catalytic*

Processes; Prins, R., Schuit, G. C. A., Eds.; NATO AS1 Series E; Sijthoff and Noordhoff: Alphen aan den Rijn, 1980; Vol. 39, pp.137

Brown P.N., Byrne G.D., Hindmarsh A.C. 'VODE, A Variable-Coefficient ODE Solver,' *SIAM J. Sci. Stat. Comput.*, Vol.10, 1989, pp.1038-1051.

Brown P.N., Hindmarsh A.C., 'Reduced Storage Matrix Methods in Stiff ODE Systems,' *J. Appl. Math. & Comp.*, Vol.31, 1989, pp.40-91.

Byrne G.D. (1992). *Pragmatic Experiments with Krylov Methods in the Stiff ODE Setting*, in *Computational Ordinary Differential Equations*, J. Cash and I. Gladwell, eds., Oxford Univ. Press, Oxford, 1992, pp. 323-356.

Constantinou L., Gani R., O'Connell, J.P. 'Estimation of the acentric factor and the liquid molar volume at 298 K using a new group contribution method,' *Fluid Phase Equilibria*, Vol.103, 1995, pp.11-22.

Coonradt H.L., Garwood W.E., 'Mechanism of Hydrocracking,' *Ind. Eng. Chem. Proc. Des.*, Vol.3:38, 1964.

Dahl S., Michelsen M.L., 'High-pressure Vapor-liquid Equilibrium with a UNIFAC-based Equation of State,' *AIChE J.*, Vol.36, 1990, pp.1829-1836.

Debrabandere D., Froment G.F. (1997). *Influence of the hydrocarbon chain length on the kinetics of the hydroisomerisation and hydrocracking of n-paraffins*, in: G.F. Froment, B. Delmon, P. Grange (Eds.), *Hydrotreatment and Hydrocracking of Oil Fractions*, 1997, pp.379.

Dekker T.J. (1969), *Finding a zero by means of successive linear interpolation*, *Constructive Aspects of the Fundamental Theorem of Algebra*, edited by B. Dejon and P. Henrici, Wiley-Interscience, 1969.

Denayer J.F., Refik Ocakoglu A., De Jonckheere B.A., Martens J.A., Thybaut J.W., Marin G.B., Baron G.V. 'Adsorption Competition Effects in Hydroconversion of Alkane Mixtures on Zeolites' *International Journal of Chemical Reactor Engineering*, Vol. 1, Article A36, 2003.

Daubert T.E, Danner R.P, Sibul H.M, Stebbins C.C, Rowley R.L, Wilding W.V, Oscarson J.L, Adams M.E, Marshall T.L, (1999). DDIPR (Design Institute for Physical Property Data), *Physical and thermodynamic properties of pure chemicals*, Taylor & Francis, Philadelphia, USA

DieselNet website, emission standards, http://www.dieselnet.com/standards/

Do D.D., (1998), *Adsorption Analysis: Equilibria and Kinetics*, Imperial College Press, London, pp. 115

Gani R., Marrero J., 'Group-contribution based estimation of pure component properties,' *Fluid Phase Equilibria*, Vol. 183–184, 2001, pp.183–208.

Garbow B.S., Hillstrom K.E., More J.J., (1980) M*inpack Project*, Argonne National Laboratory. march 1980.

Guillaume D., Surla K., Galtier P., 'From single events theory to molecular kinetics-application to industrial process modelling,' *Chem. Eng. Sci.* 58: 4861 (2003).

Hindmarsh A.C. (1983). *odepack, a systematized collection of ode solvers, in scientific computing*, r. s. stepleman et al. (eds.), north-holland, amsterdam, pp.55-64.

Hudson G.H., McCoubrey J.C., 'Intermolecular Forces Between Unlike Molecules A More Complete Form of the Combining Rules,' *Trans. Faraday Soc.*, Vol. 5:561-766 1960.

Jenkins M.A., Traub J.F., 'A three-stage algorithm for real polynomials using quadratic iteration,' *SIAM J. Numer. Anal. 7*, 1970, pp.545-566.

Jenkins M.A., Traub, J.F. 'Principles for testing polynomial zerofinding programs,' *ACM TOMS* 1, 1975, pp.26-34.

Krishna R., Saxena A.K., 'Use of an axial-dispersion model for kinetic description of hydrocracking,' *Chem. Eng. Sci*., Vol.41:989, 1989.

Kukard R.S. (2009). *The Effect of Zeolite Type on the Hydrocracking of Long n-Paraffins*, University of Cape Town, MSc Thesis

Laxmi Narasimhan C.S., Verma R.P., Ramachandran P.A., 'Continuous Lumping Model for Simulation of Hydrocracking,' *AIChE J*., Vol.42, 1996, pp.2645–2653.

Laxmi Narasimhan C.S., Thybaut J.W., Martens J.A., Jacobs P.A., Denayer J.F., Marin G.B., 'A Unified Single-Event Microkinetic Model for alkane hydroconversion in Different Aggregation States on Pt/H-USY-Zeolites' *J. Phys. Chem.* 110: 6750, 2006.

Lee C.C., Reichle R., Webber. U., 'Protonated cyclopropanes. X. Stuies on the deamination of n-butylamine-1-^{14}C and the decomposition of 3-(n-butyl-1-^{14}C)-1-phenyltriazene,' *Canadian Journal of Chemistry*, Vol.56:658, 1978

Leckel D., 'Hydrocracking of Iron-Catalysed Fischer-Tropsch Waxes', *Energy & Fuels*, Vol.19, 2005, pp.1795-1803.

Leckel D., Liwanga-Ehumbu M., 'Diesel-Selective Hydrocracking of an Iron-Based Fischer-Tropsch Wax Fraction (C15-C45) Using a MoO3-Modified Noble Metal Catalyst'. *Energy & Fuels*, Vol.20, 2006, pp.2330-2336.

Leckel D., 'Low Pressure Hydrocracking of Coal-Derived Fischer-Tropsch Waxes to Diesel', *Energy & Fuels*, Vol.21, 2007, pp.1425-1431.

Linde D.R. (1999), *CRC Handbook of Physics and Chemistry*, CRC Press, 79th Ed.

Martens G.G. Marin G.B., 'Kinetics for Hydrocracking based on Structural Classes: Model Development and Application' *AICHE Journal*, Vol.47 No 7: 1607, 2001.

Martens G.G. (2000). *Hydrocracking on Pt/US-Y zeolites fundamental kinetic modeling and industrial reactor simulation*, Ghent University, PhD thesis.

Martens J.A., Jacobs P.A., Weitkamp J., 'Attempts to rationalise the distribution of hydrockraced product. I. Qualatative Description of the Primary Hydrocracking Modes of Long Chain Hydrocarbons in open zeolites'. *Applied Catalysis*, Vol.20:239, 1986

Martens J.A., Jacobs P.A. (1990). *Conceptual Background for the Conversion of Hydrocarbons on Heterogeneous Acid Catalysis*. In *Theoretical Aspects of Heterogeneous Catalysis*, J.B. Moffat (Ed.), Van Nostrand Reinhold, New York, Ch2, pp.53 – 109

Martens J.A., Jacobs P.A. (1997). *Reaction Mechanisms of Acid-Catalysed Hydrocarbon Conversions in Zeolites*. In *Handbook of Heterogeneous Catalysis*, Ertl, G., Knzinger, H. and Weitkamp, J., Vol.3

Martens J.A., Jacobs P.A., 'Introduction to acid catalysis with zeolites in hydrocarbon reactions'. *Studies in Surface Science and Catalysis*, Vol.137:633, 2001.

Mathibe N., Cheang V. (2004). *Modelling of 2 phase wax hydrocracking*, University of Cape Town, 4th year project.

Mathias P.M., Naheiri T., Oh E.M, 'A density correction for the Peng-Robinson Equation of State', *Fluid Phase Equilibria*, 47, 77 (1989)

Maxwell I.E. (1983). *Hydrocracking: Current Technology and Recent Developments*, pp.52 – 58.

Michelsen M.L., 'A Method for Incorporating Excess Gibbs Energy Models in Equation of State,' *Fluid Phase Equilibria*, Vol.60, 1990a, pp.47-58

Michelsen M.L., 'A Modified Huron-Vidal Mixing Rule for Cubic Equations of State,' *Fluid Phase Equilibria*, Vol.60, 1990b, pp.213-219

Mohnty S., Saraf D.N., Kunzru D.. 'Model of a Hydrocracking Reactor,' *Fuel Process Technology*. 29: 1, 1991.

Nishiumi H., Arai T., Takeuchi K., 'Generalization of the binary interaction parameter of the Peng-Robinson equation of state by component family,' *Fluid Phase Equilibria*, Vol.42, 1988.

Orbey H., Sandler S.I, 'Reformulation of Wong-Sandler Mixing Rule for Cubic Equation of State' AICHE Journal, Vol 41(3), 1995, pp.683

Orbey H., Sandler S.I, (1998). *Modelling Vapor – Liquid Equilibria. Cubic Equations of State and Their Mixing Rules*, Cambridge University Press.

Park, K., Ihm, S., 'Comparison of Pt/zeolite Catalysts for n Hexadecane Hydroisomerization', *Applied Catalysis A: General*, volume.203, 2000 pp.201–209.

Pellegrini L.A., Gamba S., Calemma V., Bonomi S., 'Modelling of hydrocracking with vapour-liquid equilibrium', *Chemical Engineering Science*, vol.63, 2008, pp.4285 – 4291.

Peneloux A., Rauzy E.,Freze R., 'A consistant correction for Redlich-Kwong-Soave Volumes,' *Fluid Phase Equilibria*, Vol.8, 1982.

Peng D. and Robinson D.B, 'A New Two-Constant Equation of State', *Industrial & Engineering Chemistry Fundamentals*, 1976.

Pines H. (1981). *The chemistry of catalytic hydrocarbon conversions*, Academic Press, New York.

Rachford H.H., Rice J.D., 'Procedure for use of electrical digital computers in calculating flash vapourization hydrocarbon equilibrium', *JPT* No. 4, 19 – 20, *Trans.*, AIME, 195, 1952.

Rastelli H., Lok B.M., Duisman J.A, Earls D.E. , Mullhaupt J.T., 'Characterization of Zeolitic Acidity: The Cracking of 2mole% n-Butane over A Fixed Zeolite Bed', *Canadian Journal of Chemical Engineering*, Vol.60: 44, 1982.

Sandler S.I. (1989). *Chemical Engineering Thermodynamics*, 2nd Edition, John Wiley & Sons Inc, New York.

Sandler S.I. (1999). *Chemical and Engineering Thermodynamics*, 3nd Edition, John Wiley & Sons Inc, New York.

Scherzer J., Gruia A.J. (1996). *Hydrocracking Science and Technology*. Dekker, New York.

Schulz H.F., Weitkamp J.H., 'Hydrocracking and Hydroisomerisation of n-Dodecane,' *Ind. Eng. Chem. Prod. Res. Develop.*, Vol.11:46-53, 1972.

Schweitzer J.M., Galtier P., Schweich D., 'A single events kinetic model for the hydrocracking of paraffin's in a three phase reactor,' *Chemical Engineering Science*, Vol.54:2441–2452, 1999.

Shampine L.F., Watts H.A., (1970) *FZERO, a root-solving code*, Report SC-TM-70-631, Sandia Laboratories.

Sie S.T., Senden M.M.G., van Wechem H.M.H.. 'Conversion of natural gas to Transportation fuels via the Shell Middle Distillate Synthesis Process (SMDS),' *Catalysis Today*, Vol.8:371, 1991.

Steijns M., Froment G., Jacobs P., Uytterhoeven J., Weitkamp J., 'Hydro-isomerisation and hydrocracking. 2. Product distributions from n-decane and n-dodecane,' *Ind. Eng. Chem. Prod. Res. Dev.* 20: 654 (1981)

Stangeland B.E., 'A Kinetic Model for the Prediction of Hydrocracker Yields'. *Industrial and Engineering Chemistry Research, Process Development*, Vol.13:71, 1974.

Stryjek R., Vera J. H., 'An Improved Cubic Equation of State.' In *Equations of State. Theories and Applications*; Chao, K. C.,Robinson, R. L., Eds.; ACS Symposium Series 300; American Chemical Society: Washington, DC, 1986a, pp.560-570.

Stryjek R., Vera J. H., 'PRSV: An Improved Peng-Robinson Equation of State for Pure Compounds and Mixtures,' *Can. J.Chem. Eng*., Vol.64:323-333, 1986b.

Stryjek R., Vera J. H., 'PRSV2: A Cubic Equation of State for Accurate Vapor-Liquid Equilibria Calculations,' *Can. J. Chem. Eng*., Vol.64:820-826, 1986c

Svoboda G.D., Vynckier E., De Brabandere B., Froment G.F.. 'Application of a Single-Event Kinetic Model to Octane Hydrocracking on a Pt/US-Y zeolite,' *Industrial and Engineering Chemistry Research*, Vol.34:3793, 1995.

Tsonopoulos C., Dymond J. H., Szafranski A. M., 'Second virial coefficients of normal alkanes, linear 1-alkanols and their binaries', *Pure & Appl. Chem.*, Vol.61, No. 8, 1989, pp.1387-1394.

Thybaut J.W., Laxmi Narasimhan C. S., Denayer J.F., Baron G.V., Jacobs P.A., Martens J. A., Marin, G.B., 'Acid-Metal Balance of a Hydrocracking Catalyst: Ideal versus Nonideal Behavior,' *Ind. Eng. Chem. Res.*, Vol.44:5159-5169, 2005.

Thybaut J.W., Laxmi Narasimhan C.S., Marin, G.B., 'Bridging the gap between liquid and vapour phase hydrocracking,' *Catalysis Today*, Vol.111: 94, 2006.

Twu C.H, Coon J.E, Cunningham J.R., 'A generalized vapour pressure equation for heavy hydrocarbons,' *Fluid Phase Equilibria*, Vol.96:19-31, 1994.

Twu C.H, Coon J.E, Cunningham J.R., 'A new generalized alpha function for a cubic equation of state Part 1. Peng-Robinson equation,' *Fluid Phase Equilibria*, Vol.105:49-59, 1995.

Vansina H., Baltanas M.A., Froment G., 'Hydroisomerisation and hydrocracking. 4. Product distribution from n-octane and 2,2,4-trimetylpentane,' *Ind. Eng. Chem. Prod. Res. Dev.* 22:526, 1983.

van der Merwe W, Loudon D, Leckel D, 'Hydrodynamic Effects in Scaled-Down Hydrocracking of Iron Based Fischer-Tropsch Wax,' *Ind. Eng. Chem. Res.* 47: 10086-10092, 2008

van Engelandt W. (1998). *Reformuleren van Nafta door Selectieve Hydrokraking*, Gent University, PhD Thesis.

van Steen E., Claeys M. (2005). *Die Fischer-Tropsch Synthese*, In *Winnacker-Küchler Chemische Technik: Prozesse und Produkte*, 5th edition, Vol.4, *Energietrager, organische Grundstoffe*, Wiley–VCH Verlag, Weinheim pp.823–845,

Vynckier E., Froment G.F., 'Modelling the kinetics of complex processes based upon elementary steps,' *Kinetic and Thermodynamic Lumping of Multicomponent mixtures*. Elsevier Science publishers b.V., Amsterdam, 1991.

Weis P.B., 'Polyfunctional Heterogeneous Catalysis,' *Adv. Catalysis*, Vol.13:137, 1962.

Wietkamp J., 'The Influence of Chain Length in Hydrocraking and Hydro-isomerisation in of n-alkanes,' *Hydrocracking and hydrotreating (A.C.S. Symp.)*, 20:1, 1975.

Wietkamp J., Farag H., 'Methods of Heptane Isomerisation on Bifunctional Pd/H-beta Zeolites' *Acta Phys. Chem., Szeged.* 2: 327 (1978).

Wietkamp J., Jacobs P.A., Martens J.A., 'Isomerisation and Hydrocracking of C9 through C16 n-alkanes on Pt/HZSM-5 Zeolite,' *Applied Catalysis*, Vol.8:123, 1983.

Wong D.S.H., Sandler S.I., 'Theoretically Correct Mixing Rule for Cubic Equations of State', *AICHe Journal*, Vol.38(5):671, 1992.

Wojciechowski B.W., Corma A. (1986). *Catalytic cracking: Catalysts, chemistry and kinetics*, Marcel Dekker Inc., New York.

Zabaloy M.S., Vera J.H., 'The Peng-Robinson Sequel. An Analysis of the Particulars of the Second and Third Generations,' *Ind. Eng. Chem. Res.*, Vol.37:1591-1597, 1998.

APPENDIX 1: CORRELATIONS FOR N-PARAFFIN PROPERTIES

It was found that for n-Paraffin's in the temperature range of interest (400K to 700K) the impact of the final term in the vapour pressure expression:

$$P_{vap}(T) = \exp(A + B/T + C\ln(T) + DT^{E})$$

was negligible for hydrocarbons with a carbon number of more than one (see figures A1.1 and A1.2). Thus the expression:

$$P_{vap}(T) = \exp(A + B/T + C\ln(T))$$

is taken to adequately describe the vapour pressure for n-paraffin's of carbon number greater than one within the temperature region of interest.

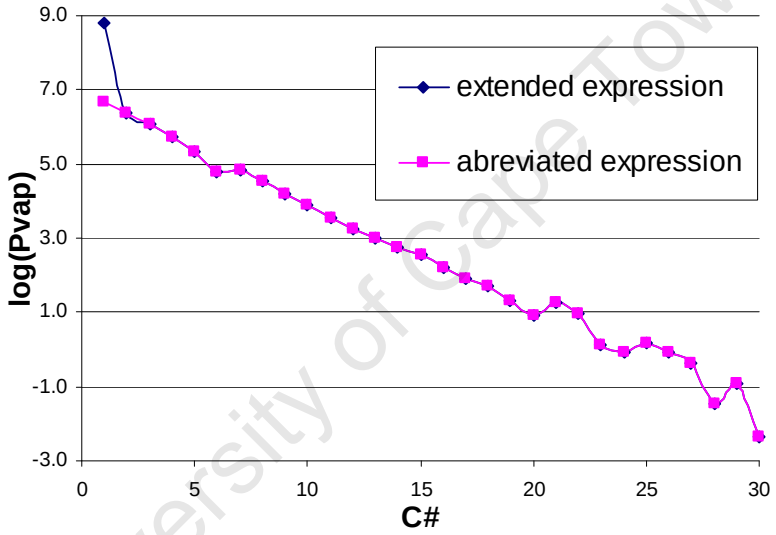

Figure A1.1: Vapour Pressure Expressions at 400K for up to C_{30}

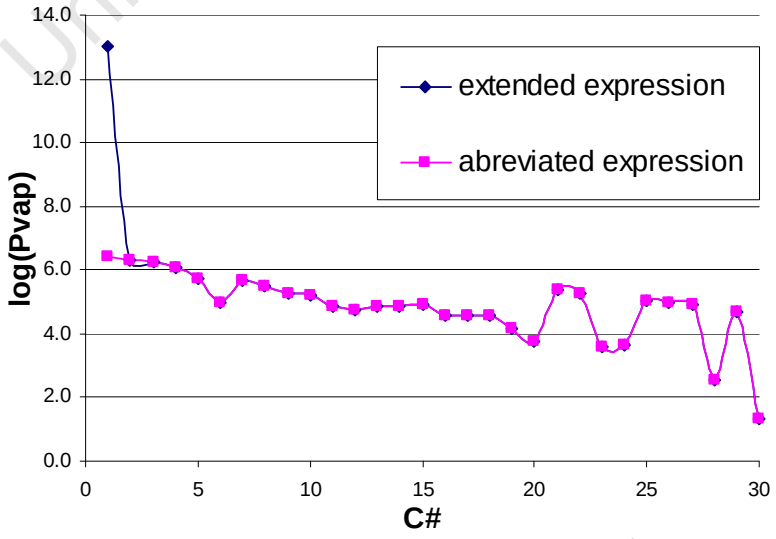

Figure A1.2: Vapour Pressure Expressions at 700K for up to C_{30}

The following correlations are proposed in order to obtain values for the constants A, B and C used in the vapour pressure expression, see figures A1.3 to A1.5. These hold from C_3 to C_{24} and can be extrapolated to predict the vapour pressure for C_{30} accurately, whether these can be extrapolated to hydrocarbons with longer chain length, for instance C_{120}, is uncertain.

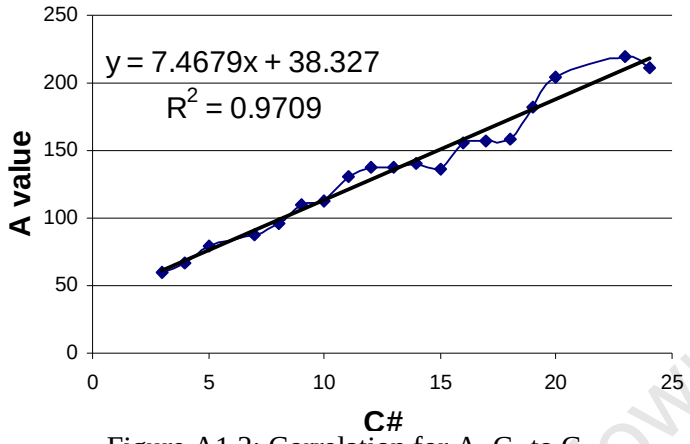

Figure A1.3: Correlation for A, C_3 to C_{24}

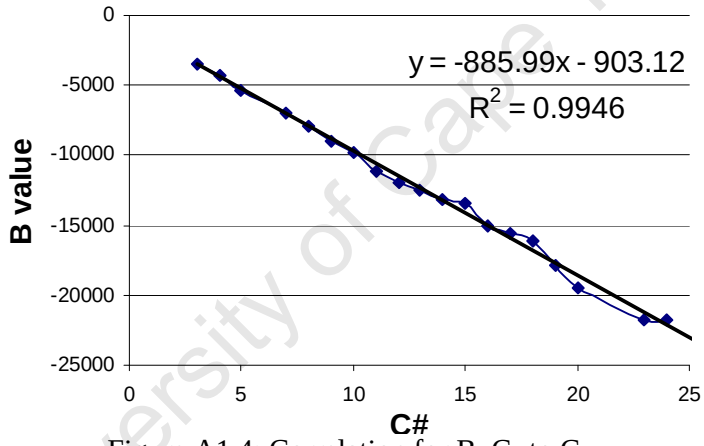

Figure A1.4: Correlation for B, C_3 to C_{24}

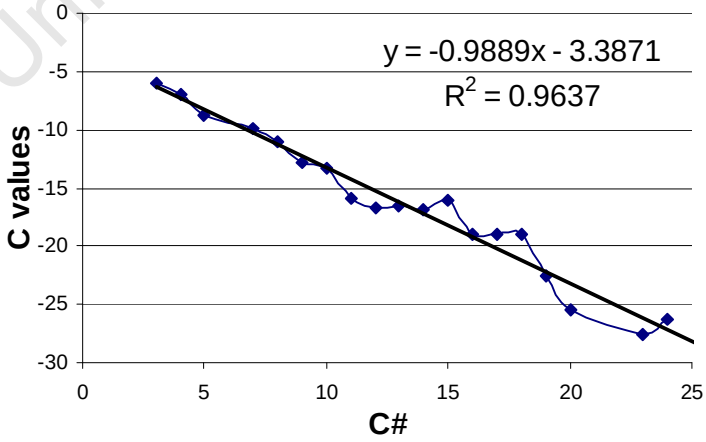

Figure A1.5: Correlation for C, C_3 to C_{24}

Correlations for the critical temperature (figure 6), critical pressure (figure 7) and accentric factor (figure 8) appear below. The initial 2, 4 and 3 linear hydrocarbons were respectively excluded from the above mentioned properties correlations. This was done in order to obtain accurate expressions for these properties.

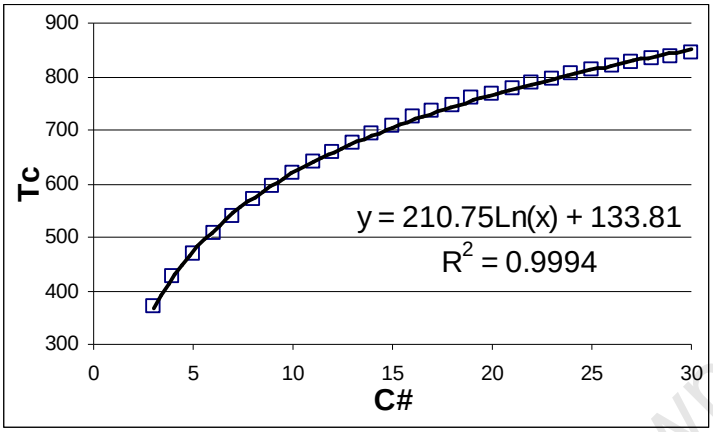

Figure A1.6: Critical Temperature Correlation, C_3 to C_{30}

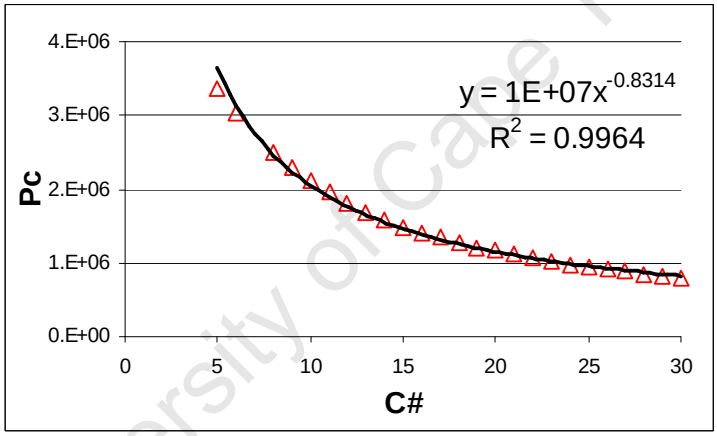

Figure A1.7: Critical Pressure Correlation, C_5 to C_{30}

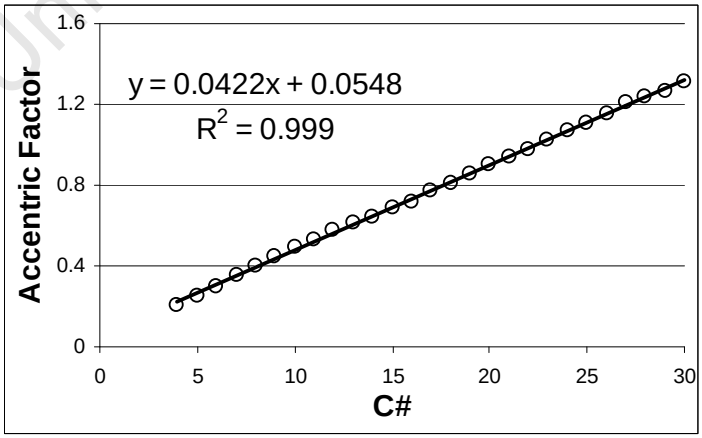

Figure A1.8: Accentric Factor Correlation, C_4 to C_{30}

APPENDIX 2: STRUCTURAL CLASSES

This appendix reproduces the Structural Classes in Gert Martens PhD thesis (2000). The data is used in performing the dehydrogenation equilibrium constant calculations of chapter 5

Table A2.1: Class of n-alkanes

Paraffin class	$n_{p,i}$	$n_{s,i}$	$n_{t,i}$	$n_{q,i}$	σ_i	$n_{gch,i}$	number of paraffins $\#_i$
	2	n-2	0	0	18	0	1

Table A2.2: Classes of single branched i-alkanes.

Paraffin class	$n_{p,i}$	$n_{s,i}$	$n_{t,i}$	$n_{q,i}$	σ_i	$n_{gch,i}$	number of paraffins $\#_i$
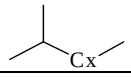	3	n-4	1	0	27	1	1
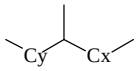	3	n-4	1	0	27/2	2	(n-6)/2 n even (n-5)/2 n odd
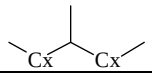	3	n-4	1	0	27	2	1 n even 0 n odd
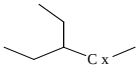	3	n-4	1	0	27	3	1
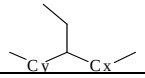	3	n-4	1	0	27/2	3	(n-8)/2 n even (n-9)/2 n odd
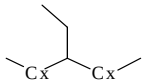	3	n-4	1	0	27	3	0 n even 1 n odd

Table A2.3: Classes of dibranched alkanes with a quaternary carbon atom.

Paraffin class	$n_{p,i}$	$n_{s,i}$	$n_{t,i}$	$n_{q,i}$	σ_i	$n_{gch,i}$	number of paraffins $\#_i$
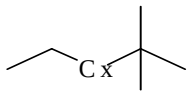	4	n-5	0	1	243	2	1
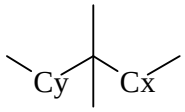	4	n-5	0	1	81	4	(n-6)/2 n even (n-5)/2 n odd
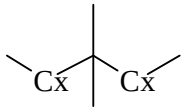	4	n-5	0	1	162	4	0 n even 1 n odd
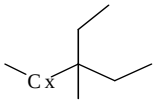	4	n-5	0	1	81	6	1
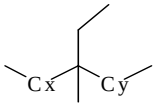	4	n-5	0	1	81/2	6	(n-10)/2 n even (n-9)/2 n odd
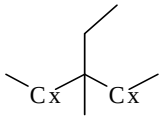	4	n-5	0	1	81	6	1 n even 0 n odd
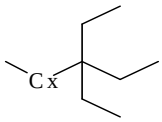	4	n-5	0	1	243	8	1
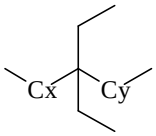	4	n-5	0	1	81	8	(n-10)/2 n even (n-11)/2 n odd
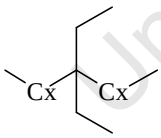	4	n-5	0	1	162	8	0 n even 1 n odd

Table A2.4: Classes of dibranched alkanes without a quaternary carbon atom

Paraffin class	$n_{p,i}$	$n_{s,i}$	$n_{t,i}$	$n_{q,i}$	σ_i	$n_{gch,i}$	number of paraffins $\#_i$
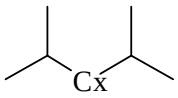	4	n-6	2	0	162	2	1
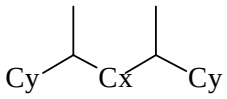	4	n-6	2	0	81/2	4	(n-6)/2 n even (n -7)/2 n odd
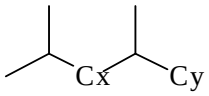	4	n-6	2	0	81/2	3	n-6
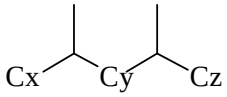	4	n-6	2	0	81/4	4	(n-6)(n-8)/4 n even (n-7)(n-7)/4 n odd
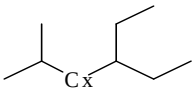	4	n-6	2	0	81	4	1
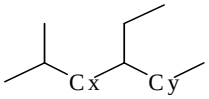	4	n-6	2	0	81/2	4	n-8
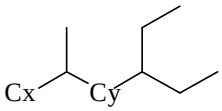	4	n-6	2	0	81/2	5	n-8
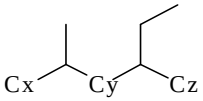	4	n-6	2	0	81/4	5	(n-8)(n-9)/2
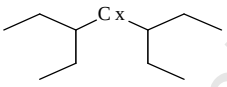	4	n-6	2	0	162	6	1
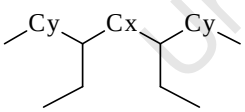	4	n-6	2	0	81/2	6	(n-10)/2 n even (n-11)/2 n odd
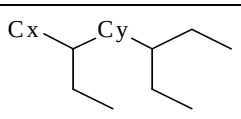	4	n-6	2	0	81/2	6	n - 10
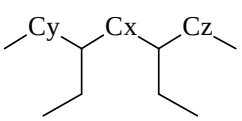	4	n-6	2	0	81/4	6	(n-10)(n-12)/4 n even (n-11)(n-11)/4 n odd

Table A2.5: Classes of trimethyl alkanes without a quaternary carbon atom

Paraffin class	$n_{p,i}$	$n_{s,i}$	$n_{t,i}$	$n_{q,i}$	σ_i	$n_{gch,i}$	number of paraffins $\#_i$
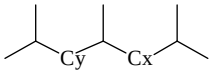	5	n-8	3	0	243/2	4	(n-8)/2 n even (n-7)/2 n odd
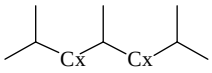	5	n-8	3	0	243	4	1 n even 0 n odd
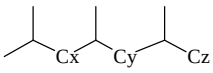	5	n-8	3	0	243/4	5	(n-7)(n-8)/2
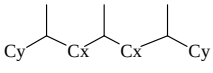	5	n-8	3	0	243/4	6	(n-8)/2 n even 0 n odd
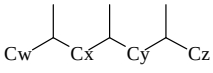	5	n-8	3	0	243/8	6	(n-6)(n-8)(n-10)/12 n even (n-7)(n-8)(n-9)/12 n odd

Table A2.6: Classes of trimethyl alkanes with a quaternary carbon atom

Paraffin class	$n_{p,i}$	$n_{s,i}$	$n_{t,i}$	$n_{q,i}$	σ_i	$n_{gch,i}$	number of paraffins $\#_i$
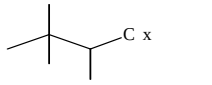	5	n-7	1	1	729/2	5	1
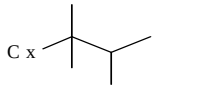	5	n-7	1	1	243	6	1
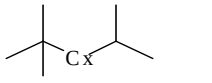	5	n-7	1	1	729	3	1
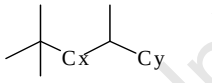	5	n-7	1	1	729/2	4	n-8
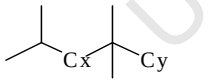	5	n-7	1	1	243	5	n-8
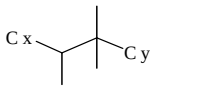	5	n-7	1	1	243/2	7	n-8
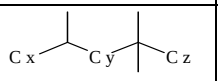	5	n-7	1	1	243/2	6	(n-8)(n-9)/2

Table A2.7: Classes of ethyl-dimethyl alkanes with a quaternary carbon atom

Paraffin class	$n_{p,i}$	$n_{s,i}$	$n_{t,i}$	$n_{q,i}$	σ_i	$n_{gch,i}$	number of paraffins $\#_i$
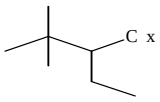	5	n-7	1	1	729/2	6	1
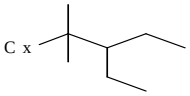	5	n-7	1	1	243	8	1
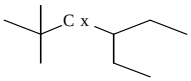	5	n-7	1	1	729	5	1
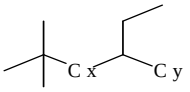	5	n-7	1	1	729/2	5	n-10
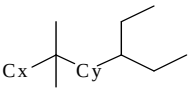	5	n-7	1	1	243	7	n-10
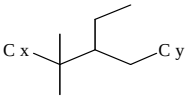	5	n-7	1	1	243/2	8	n-10
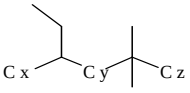	5	n-7	1	1	243/2	7	(n-10)(n-11)/2
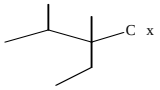	5	n-7	1	1	243/2	8	1
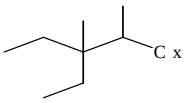	5	n-7	1	1	243/2	9	1
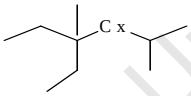	5	n-7	1	1	243	7	1
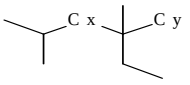	5	n-7	1	1	243/2	7	n-10
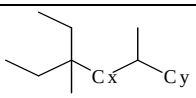	5	n-7	1	1	243/2	8	n-10
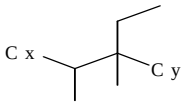	5	n-7	1	1	243/4	9	n-10
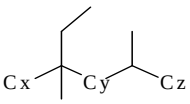	5	n-7	1	1	243/4	8	(n-10)(n-11)/2

Table A2.8: Classes of ethyl-dimethyl alkanes without a quaternary carbon atom

Paraffin class	$n_{p,i}$	$n_{s,i}$	$n_{t,i}$	$n_{q,i}$	σ_i	$n_{gch,i}$	number of paraffins $\#_i$
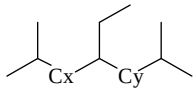	5	n-8	3	0	243/2	5	(n-8)/2 n even (n-9)/2 n odd
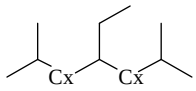	5	n-8	3	0	243	5	0 n even 1 n odd
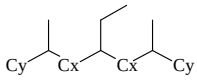	5	n-8	3	0	243/4	7	0 n even (n-9)/2 n odd
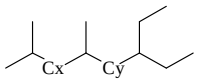	5	n-8	3	0	243/2	6	n- 9
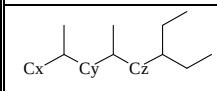	5	n-8	3	0	243/4	7	(n-9)(n-10)/2
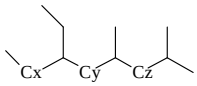	5	n-8	3	0	243/4	6	$(n-9)^2$
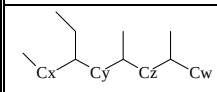	5	n-8	3	0	243/8	7	$(n-9)(n-10)^2/4$

Table A2.9: Classes of diethyl-methyl alkanes without a quaternary carbon atom

Paraffin class	$n_{p,i}$	$n_{s,i}$	$n_{t,i}$	$n_{q,i}$	σ_i	$n_{gch,i}$	number of paraffins $\#_i$
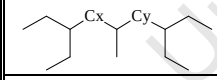	5	n-8	3	0	243/2	8	(n-12)/2 n even (n-11)/2 n odd
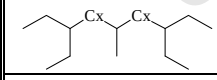	5	n-8	3	0	243	8	1 n even 0 n odd
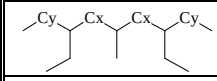	5	n-8	3	0	243/4	8	(n-12)/2 n even 0 n odd
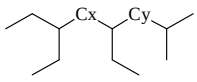	5	n-8	3	0	243/2	7	n - 10
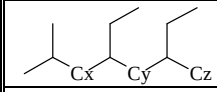	5	n-8	3	0	243/4	7	(n-10)(n-11)/2
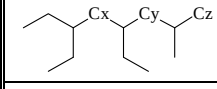	5	n-8	3	0	243/4	8	$(n-11)^2$
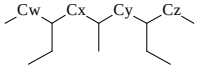	5	n-8	3	0	243/8	8	$(n-10)(n-12)^2/4$

Table A2.10: Classes of diethyl-methyl alkanes with a quaternary carbon atom

Paraffin class	$n_{p,i}$	$n_{s,i}$	$n_{t,i}$	$n_{q,i}$	σ_i	$n_{gch,i}$	number of paraffins $\#_i$
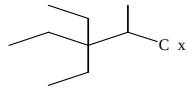	5	n-7	1	1	729/2	11	1
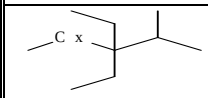	5	n-7	1	1	243	10	1
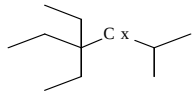	5	n-7	1	1	729	9	1
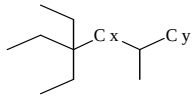	5	n-7	1	1	729/2	10	n-11
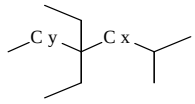	5	n-7	1	1	243	9	n-11
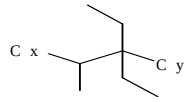	5	n-7	1	1	243/2	11	n-11
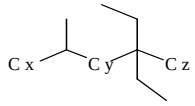	5	n-7	1	1	243/2	10	(n-11)(n-12)/2
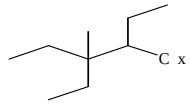	5	n-7	1	1	243/2	10	1
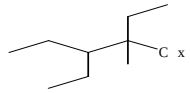	5	n-7	1	1	243/2	10	1
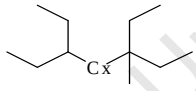	5	n-7	1	1	243	9	1
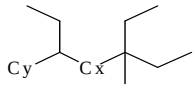	5	n-7	1	1	243/2	9	n-12
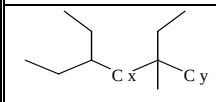	5	n-7	1	1	243/2	9	n-12
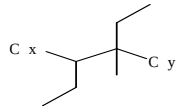	5	n-7	1	1	243/4	10	n-12
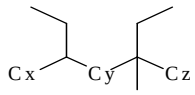	5	n-7	1	1	243/4	9	(n-12)(n-13)/2

Table A2.11: Classes of triethyl alkanes with a quaternary carbon atom

Paraffin class	$n_{p,i}$	$n_{s,i}$	$n_{t,i}$	$n_{q,i}$	σ_i	$n_{gch,i}$	number of paraffins $\#_i$
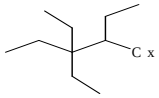	5	n-7	1	1	729/2	12	1
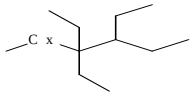	5	n-7	1	1	243	12	1
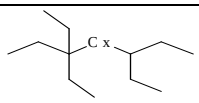	5	n-7	1	1	729	11	1
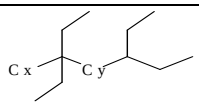	5	n-7	1	1	243	11	n-13
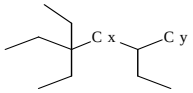	5	n-7	1	1	729/2	11	n-13
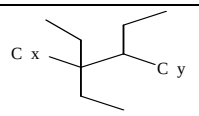	5	n-7	1	1	243/2	12	n-13
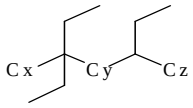	5	n-7	1	1	243/2	11	(n-13)(n-14)/2

Table A2.12: Classes of triethyl alkanes without a quaternary carbon atom

Paraffin class	$n_{p,i}$	$n_{s,i}$	$n_{t,i}$	$n_{q,i}$	σ_i	$n_{gch,i}$	number of paraffins $\#_i$
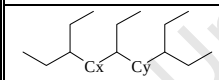	5	n-8	3	0	243/2	9	(n-12)/2 n even (n-13)/2 n odd
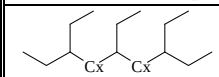	5	n-8	3	0	243	9	0 n even 1 n odd
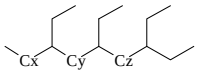	5	n-8	3	0	243/4	9	(n-12)(n-13)/2
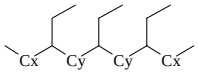	5	n-8	3	0	243/4	9	0 n even (n-13)/2 n odd
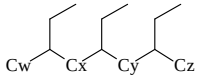	5	n-8	3	0	243/8	9	(n-12)(n-13)(n-14)/12 n even (n-11)(n-13)(n-15)/12 n odd